HEAT TRANSFER FROM ELECTRICALLY HEATED THIN METAL FILMS TO WATER IN POOL BOILING

A THESIS

Presented to

The Faculty of the Graduate Division

by

Steve Herren Bomar, Jr.

In Partial Fulfillment

of the Requirements for the Degree

Doctor of Philosophy in the School

of Chemical Engineering

Georgia Institute of Technology

June, 1967

HEAT TRANSFER FROM ELECTRICALLY HEATED THIN METAL FILMS TO WATER IN POOL BOILING

Approved:

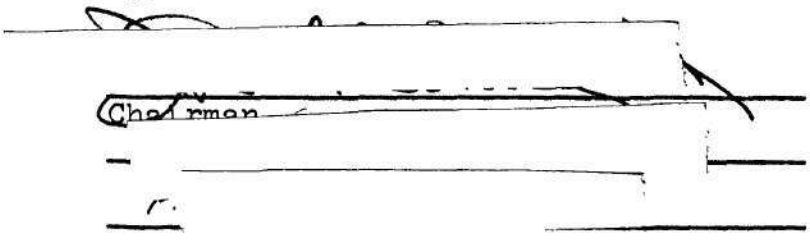

Chairman

Date approved by Chairman: May 24, 1967

In presenting the dissertation as a partial fulfillment of the requirements for an advanced degree from the Georgia Institute of Technology, I agree that the Library of the Institute shall make it available for inspection and circulation in accordance with its regulations governing materials of this type. I agree that permission to copy from, or to publish from, this dissertation may be granted by the professor under whose direction it was written, or, in his absence, by the Dean of the Graduate Division when such copying or publication is solely for scholarly purposes and does not involve potential financial gain. It is understood that any copying from, or publication of, this dissertation which involves potential financial gain will not be allowed without written permission.

3/17/65
b

ACKNOWLEDGMENTS

The author wishes to express his sincere gratitude to Dr. J. D. Fleming, Jr., for his inspiration, assistance and friendship. Without Dr. Fleming's encouragement and aid, this thesis and the lengthy course of study leading to it would not have been completed.

The author is indebted to many others whose generous help contributed greatly to this work: Messrs. J. D. Walton and N. E. Poulos, who made experimental facilities available; Messrs. J. W. Johnson and R. R. Swank, Jr., who gave technical advice and assistance; Drs. Frederick Bellinger and Clyde Orr, Jr., who read the thesis and provided helpful guidance; and Dr. H. V. Grubb whose cooperation and guidance have been invaluable.

The author is deeply grateful to his wife, for her patience, understanding and help; to his parents and his two daughters for their inspiration and interest.

The Engineering Experiment Station of the Georgia Institute of Technology provided employment which made graduate study practical, and deserves the author's sincere thanks.

TABLE OF CONTENTS

TABLE OF CONTENTS

LIST OF TABLES

LIST OF FIGURES

Figure Page

SUMMARY

This thesis reports an investigation of transient boiling of subcooled water at atmospheric pressure using thin nickel films simultaneously as heaters and resistance thermometers. High-speed instrumentation was used to record film currents and voltages, and from these data instantaneous values of film temperature and heat generation rate were calculated.

Previous research by others had demonstrated that thin metal films could be useful in studies of heat transfer to liquids. The electrical resistance of thin films can be made high enough to give substantial power dissipation with currents that are easily manageable in the laboratory. However, thin films have extremely small masses and negligible effective heat capacities, so that they respond very rapidly to changes in power level. They must be deposited on substrates because they do not have sufficient mechanical strength to be self supporting. These characteristics indicate the use of high speed instrumentation in thin film heat transfer studies to permit adequate observation of the heat transfer parameters associated with metal films.

The purpose of this investigation was the adaptation of high-speed data recording techniques to the study of boiling heat transfer from thin metal films, and exploration of

the behavior of metal films used in this manner. Pool boiling in subcooled water was investigated because experimental data are available in the literature for comparison. The heat transfer test elements were thin nickel films (1500 to 2500 Å thick) deposited on polished clear fused quartz slides one inch wide and three inches long. Electrical connections to the film were made by fired conductive paints applied to the substrates and soldered copper connection blocks. Nickel films were deposited by vacuum evaporation and calibrated as resistance thermometers.

Test sections were immersed in distilled water and the power level was increased until burnout occurred. Test duration ranged from 0.67 to 23.15 seconds. Film voltage and current were recorded by a high-speed tape recorder, and played back into a dual-beam oscilloscope at 1/200th of the recording speed. Photographs of the oscilloscope traces were made on 35 millimeter film and electrical parameters were read from the photographs. Then instantaneous temperatures and heat-generation rates in the metal film were determined.

A technique was devised for estimating heat flux to the substrates, which accounted for a significant fraction of the energy dissipated in the film.

Heat-flux curves were plotted and the tests grouped into four types, depending on experimental conditions. Films were heated with direct current, 60 cycle per second alternating current, and half-wave rectified direct current.

Typical transient boiling phenomena were observed but maximum apparent burnout heat fluxes were 500,000 to 600,000 Btu/hr-ft^2, much lower than those reported in the literature for conventional systems in subcooled boiling.

Metal film temperatures were observed to fluctuate during individual power pulses when ac and half-wave dc heating were used. Although its thermal conductivity is much lower than that of a metal, the substrate strongly damps the film temperature's fluctuation. A mathematical description of this fluctuation with ac heating was developed.

A study of film thickness uniformity by an x-ray fluorescence technique is described. The thickness of evaporated nickel films varied considerably over the substrate surface. This variation in thickness was caused by the tendency of nickel to alloy with refractory metal filaments when it is evaporated in vacuo, leading to uneven deposition.

The results of this investigation indicate that heat transfer studies are practical using thin metal films simultaneously as heaters and thermometers with data recorded by high-speed instrumentation. The most significant experimental problem was determination of film temperature. A metal film for this application should have uniform thickness and high temperature coefficient of resistance.

CHAPTER I

INTRODUCTION

The advance of modern technology has resulted in steadily increasing interest in heat transfer in boiling of liquids. Although this process has been in common use for hundreds of years, it is still not understood well enough to permit accurate prediction of system performance under the severe conditions imposed in many modern applications.

Several years ago Fleming (1) used thin gold films simultaneously as resistance thermometers and heaters in the study of heat transfer to water in swirling flow. He suggested that high-speed instrumentation for data recording would greatly improve the investigator's ability to measure heat transfer parameters. His investigation raised questions concerning the behavior of thin metal films in studies of this kind, in particular how the film temperature varied with time during alternating current (ac) heating. Since the heat capacity of a thin (1000 to 2000 Å thick) film is negligible in comparison to other parts of the system, its temperature can respond very quickly to changes in energy input. The few investigators who had used metal films for temperature measurement assumed no thermal interaction with their insulating substrates. This led to the conclusion that film temperatures

could vary with cycling power inputs. Several related questions concerning the behavior of thin metal films in heat transfer to water were considered worthy of study: What is the magnitude of the temperature fluctuation with cycling power input? Does this fluctuation lead to increase in heat flux at a particular average film temperature? Do the peculiar characteristics of thin films cause increase or decrease in the maximum boiling heat flux?

The present investigation describes the application of high-speed instrumentation to thin film heat transfer studies. Pool boiling in subcooled water was investigated because it is a relatively simple system and experimental data, though rather sparse, are available in the literature for comparison.

Historical Background

The first study of boiling to include detailed and quantitative data is considered to be that published in 1756 by Johann Gottlob Leidenfrost, a German physician. His work, A Tract About Some Qualities of Common Water, has recently been translated from the original Latin (2) and includes observations on the boiling of small liquid masses on a hot surface. Leidenfrost's data permit rough calculations of heat transfer rates.

Recent research on the phenomena of boiling began in the 1920's when Mosciki and Broder made studies of electri-

cally heated wires in cool water and heated water. They found that "subcooled" boiling results in greater heat fluxes than can be obtained with the liquid at its boiling point. While studying boiling of water at 212°F on a submerged electrically heated platinum wire, Nukiyama observed that the heat flux increased steadily with wire temperature until the wire reached about 300°F. Then the wire temperature jumped suddenly to about 1800°F. Further increase in temperature resulted in a smooth increase in heat flux. His experiments led to the "boiling curve" which is discussed below. These and other advances up to the early 1960's are described in excellent reviews of boiling by McAdams (3), Jakob (4)(5), Kreith (6), Westwater (7)(8), and Rohsenow (9).

The boiling curve is of such fundamental importance to the understanding of boiling phenomena that it will be described briefly here. Farber and Scorah (10) published a study of water boiling at its saturation temperature (boiling point) on horizontal electrically heated wires, in which they were able to observe heat transfer characteristics in the several boiling regimes. Their data at atmospheric pressure for a typical test wire are shown in Figure 1. This process, when there is no external agitation and the liquid is at its saturation temperature, is usually called pool boiling.

For small differences in temperature between the wire and liquid, heat is transferred by conduction and free con-

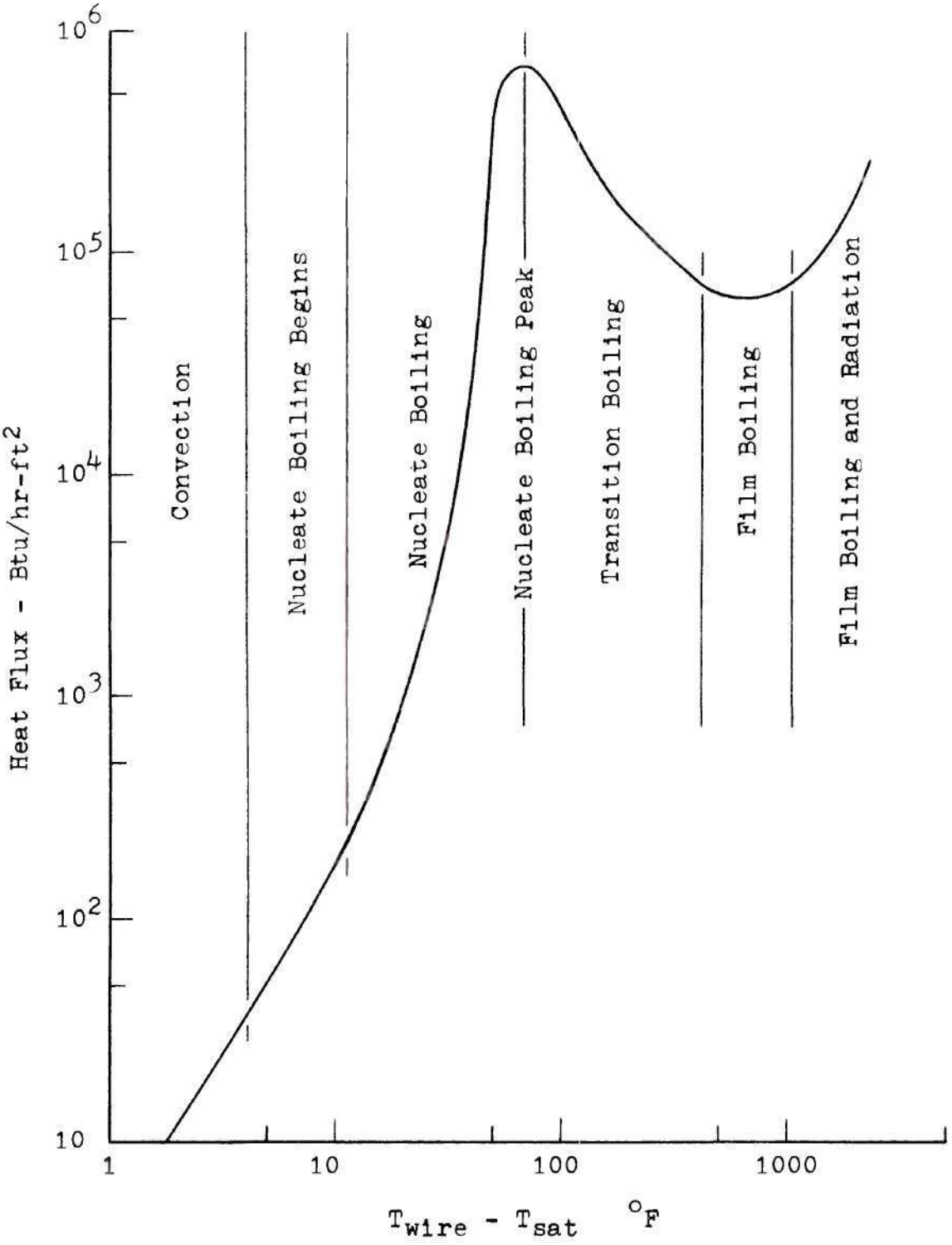

Figure 1. Typical Boiling Curve for Heat Transfer from Wire to Saturated Water at Atmospheric Pressure.

vection. Evaporation occurs at the liquid-vapor (liquid-air) interface and an upward current of superheated liquid is established.

As the temperature difference is increased above about 4°F in "pool boiling" experiments, molecules of water begin to form bubbles at favored spots on the metal surface. At first the bubbles are unstable and collapse before reaching the liquid-vapor interface, but as the temperature difference is increased above about 11°F the bubbles become more numerous and larger until they finally rise to the free surface. This is the nucleate boiling regime, which exists until the temperature difference reaches about 65°F, for boiling water at atmospheric pressure. This regime derives its name from the tendency of bubbles to originate at favored spots, or nuclei, on the heating surface *. In the nucleate regime the heat flux increases very rapidly with increasing temperature of the heating surface; partly because of the intense turbulence caused by moving bubbles and partly because the bubbles transport their latent heat from the heating surface

---

* Jakob (11) shows that bubbles cannot form spontaneously in a saturated liquid. This would require the latent heat of vaporization to be taken from the surrounding medium which would become cooler, a violation of the second law of thermodynamics. Further, he and others found that in boiling water the bubble vapor is exactly at saturation temperature, and the liquid at a higher temperature. In practical systems nuclei consist of foreign particles or pockets of dissolved gas.

and the superheated liquid adjacent to the surface.

At the boiling curve's maximum, bubbling is so vigorous that the heating surface is largely covered with vapor. An unstable steam film forms and provides a high resistance to heat flow. The result is a reduction of heat flux with increasing temperature, until the temperature difference is about 400°F. This is called the transition region from nucleate to stable film boiling.

From about 400 to 1000°F--the film boiling region--a stable vapor film covers the heating surface and large bubbles separate from the film and float away. Since the thermal conductivity of vapor is much lower than that of the liquid, the heating surface is effectively insulated and very high temperature differences are found.

When the temperature differences exceeds 1000°F, heat transfer by radiation becomes important, and heat flux again increases with temperature.

"Subcooled boiling" or "surface boiling" occurs when the bulk temperature of the liquid is below the boiling point but the temperature of the heating surface and liquid layer adjacent to it are above the boiling point. Bubbles form in the superheated layer and behave much the same as in saturated boiling, except that they condense in the cold liquid. In subcooled boiling bubbles increase in number while their size and average lifetimes decrease, as compared with saturated

boiling. The extremely high bubble population causes vigorous agitation near the heating surface, and contributes to higher peak heat fluxes than can be attained in saturated boiling.

The primary variables controlling boiling phonemena are the surface condition and the temperature of the liquid layer adjacent to the heating surface. In the nucleate boiling regime, variation of the liquid layer temperature is relatively small over a wide range of heat fluxes, irrespective of the fluid bulk temperature. For design purposes, the conventional heat transfer coefficient, based on the temperature difference between the bulk fluid and the heating surface, is only of secondary interest compared to the maximum heat flux obtainable in nucleate boiling and the surface temperature at which boiling begins.

From the boiling curve one can easily see a major reason for the intense interest in boiling during the last few years. Heat release of 40,000 to 50,000 Btu/hr-ft^2 is considered high in an ordinary boiler, but the introduction of more sophisticated equipment such as nuclear reactors and rockets has placed greater demand on heat removal systems. A characteristic common to the newer equipment is that the rate of heat generation is essentially constant; if the heat flux passes beyond the nucleate boiling maximum, the heat transfer surface temperature will rise sharply and catastrophic melting or "burnout" will occur.

Nucleate boiling is receiving most of the current

research effort, because it offers the promise of attaining very high heat fluxes if systems can be operated near the peak heat flux and burnout prevented. Because of the high temperature differences required in film boiling there is little commercial interest in this boiling regime, except in the area of quenching of solids at high temperature.

The use of electrical systems to simulate operating conditions in boiling research has been common practice for many years. Early investigators usually employed wires as heating elements. McAdams (12) found that the diameter of heating wires used in boiling studies could influence the results, but correlations of boiling data have generally ignored this effect (13). Investigators of boiling have used resistance heated tubes, wires, plates, and ribbons to provide desired geometrical conditions. The low electrical resistance of metals often demands the use of very high current power supplies to obtain the required levels of heat flux, with accompanying experimental difficulties and high cost.

In 1955 and 1956 Winding and coworkers (14)(15) suggested the use of thin metal films as resistance thermometers and heaters. This technique offered the advantages of heat transfer surfaces with significant surface area and high electrical resistance, so that large amounts of power could be dissipated with relatively low currents. Fleming (1) demonstrated the utility of thin metal films for research on heat

transfer to water and found that high-speed instrumentation would greatly facilitate experimental measurements. The method apparently has not been widely adopted by other investigators. Kirby and Westwater (16) studied bubble and vapor behavior in nucleate boiling on a horizontal glass plate heated by a thin conductive coating on its surface. The plate was photographed from below; its unidentified conductive coating could not be used as a resistance thermometer, because its resistance did not appear to be a function of temperature.

Purpose of This Research

This investigation was designed to adapt high-speed instrumentation techniques to the study of boiling heat transfer from thin metal films and to explore in some detail the behavior of thin metal films used for this purpose.

The significance of the extremely low heat capacity of thin metal films was of special interest. The expectation that film temperature might vary with cycling power input offered the possibility that unusual boiling phenomena might be observed. With the equipment available for this study, phase relationships among applied voltage, current, temperature, and heat flux could be measured.

Since Fleming's work dealt with heat transfer in swirling flow--a system not extensively explored--comparison of his results with those of other investigators was difficult. Subcooled pool boiling was chosen for the present study

to permit comparison with results of other investigations, thereby establishing whether heat transfer data from thin films is representative of that from other metal surfaces.

The film's relatively large area and the experimental system's ability to change power level rapidly suggested that transient studies in pool boiling would be a promising area of investigation. Johnson et al. (17) have published a study of transient pool boiling undertaken for the purpose of investigating the behavior of a nuclear reactor during a power excursion. This latter work, performed with metal ribbon heating elements, provided a good comparison for the present investigation.

Related Literature

Thin Films

Thin metal films have been used for a wide variety of purposes ranging from the decoration of inexpensive parts to the preparation of reflective surfaces in optics and the manufacture of electronic circuit components. Holland (18) has reviewed the uses and technology of thin films.

As mentioned earlier, Winding and coworkers studied the use of thin films as resistance thermometers (14)(15). The negligible heat capacity associated with films led these investigators to suggest their use in measuring temperature transients. Several investigations have employed thin-film, resistance thermometers in shock-tube experiments to measure

detonation velocities and shock and flame velocities (19)(20). Thin-film thermometers have been used in measurements of aerodynamic heating (21) and heat transfer coefficients for condensing films (14). Electrical pulsing techniques have been developed for calibration of thin-film thermometers (22)(23).

Simpson and Winding (15), and Belser and Hicklin (24) have investigated the characteristics of films of a number of metals. Their data suggest that nickel has the most desirable combination of properties for a study of this kind: high positive temperature coefficient of resistance, stability as a resistance thermometer, and suitability for use in water. For these reasons nickel films were chosen for this investigation.

Evaporated metal films show a permanent change in resistance when heated to a temperature above the highest in their history. This characteristic is due to annealing of the highly strained metal structure obtained by vacuum evaporation (24). Stable thermometric calibrations can be obtained by depositing on a heated substrate or annealing the film before calibration.

Subcooled Boiling

Heat transfer by subcooled, or surface, boiling has been studied by many investigators for a variety of experimental conditions. This area of investigation should be distinguished from nucleate boiling, in which the liquid is at its saturation temperature, and which has received even more experimental and theoretical attention than subcooled boiling.

Gunther and Kreith (25) studied subcooled pool boiling from a heated metal strip at atmospheric pressure. They found that heat flux versus temperature data for subcooled boiling were somewhat different from data for nucleate boiling: the slope of the curve was steeper, and the burnout heat flux much higher. The temperature of the heating surface was not a function of subcooling and approached a limit of 280°F at high heat fluxes. The important characteristics of the bubbles formed were their small size, large numbers and rapid collapse. They observed that the rapid growth and collapse of small bubbles in subcooled water causes strong convection near the hot surface.

Kreith, Summerfield, and Gunther (26)(27) published two papers describing experiments in which they found that the wall temperature during forced convection subcooled boiling is sensitive only to fluid conditions adjacent to the heating surface (fluid properties and pressure) and relatively insensitive to fluid velocity, heat flux and bulk temperature. The burnout heat flux increased as subcooling of the liquid increased, but the critical wall temperature at burnout was not a function of subcooling. The temperature difference corresponding to driving force in heat transfer by surface boiling was found to be $T_{wall} - T_{saturation}$. With increasing heat flux, bubble size and lifetime decreased moderately, whereas bubble population and bubble coverage of the heating surface increased. Decrease

in liquid temperature (increase in subcooling) caused bubble size and lifetime to decrease sharply, and bubble population to increase.

McAdams and coworkers (28) obtained results substantially in agreement with the above; they found, for example, that boiling and burnout heat fluxes were very weak functions of pressure in the range 30 to 90 psia. The idea that $T_{wall} - T_{saturation}$ is the driving force in subcooled boiling was reinforced by these investigators' correlation of a large collection of data with the temperature difference defined in this way.

Rohsenow and Clark (29) studied photographs by McAdams and concluded that latent heat transport by bubbles is negligible compared with convection caused by their growth and collapse.

This latter conclusion, also reached by Gunther and Kreith (25), has been disputed by Moore and Mesler (30), Bankoff (31), Gaertner (32), and others (33). Bankoff estimates that several bubble volumes of steam flow through a bubble during its lifetime, vapor being formed at the hot surface and simultaneously condensing at the cool surface.

Many investigators have proposed semi-theoretical correlations of boiling data based on various mechanisms (13) (34-39). Gaertner (32) points out that several "regions", or discrete mechanisms, are observed in nucleate boiling

(discrete bubble region, transition from discrete bubbles to vapor columns and mushrooms, vapor column and mushroom region) and any overall correlation based on a single region must be in serious error. This conclusion applies, in principle, to subcooled boiling as well.

Bankoff (40) proposed a "sequential rate process" to account for the mechanism of subcooled nucleate boiling. His work is an important contribution toward understanding the process, but it is not useful for design purposes since the expressions involve local bubble parameters. Most of the previous mechanism concepts can be incorporated in Bankoff's model.

Bergles and Rohsenow (41) noted that no general correlation of boiling data is presently possible because of the unpredictable influence of fluid and surface conditions. However, an empirical equation

$$\frac{q}{A} = C(T_{wall} - T_{sat})^n$$

expresses the data of many investigators. The constant n is in the vicinity of four for most surfaces and C depends on the pressure and fluid-surface combination. The degree of subcooling affects pool boiling far more strongly than forced convection boiling, so that it is generally not possible to predict subcooled pool boiling from forced convection boiling data. At higher heat fluxes, however, the rela-

tive importance of bulk liquid flow compared to bubble agitation decreases, and forced convection and pool boiling data for similar fluid and surface combinations agree quite well.

Heat transfer data in the literature on subcooled pool boiling are not as plentiful as might be expected. Gunther and Kreith (25), Bergles and Rohsenow (41), Duke and Schrock (42), and Grassmann and Hauser (43) have given steady-state experimental data. Rosenthal (44), Johnson, et al. (17), and Lurie and Johnson (45) have studied transient pool boiling of water at atmospheric pressure.

Numerous attempts have been made to predict burnout heat flux as a function of fluid properties, system geometry, flow conditions, pressure and subcooling. These are discussed in extensive reviews by Rohsenow (9) and Bernath (46).

Rohsenow (47) presents a graph of burnout heat flux for water at atmospheric pressure as a function of subcooling and liquid velocity. The curve at zero velocity (pool boiling) is extrapolated by a theoretical relation from forced convection boiling data. Kreith (48) presents a similar plot from data by Ellion. Gunther and Kreith (25) show burnout fluxes for subcooled pool boiling; their results, however, are uncertain in the range of subcooling covered by the present study.

Zuber, Tribus and Westwater (49) developed theoretically a relation to predict burnout heat fluxes from fluid properties alone. Bernath (46) published an empirical correlation based on hydraulic diameters.

CHAPTER II

INSTRUMENTATION AND EQUIPMENT

One of the major objectives of this study was the adaptation of high-speed instrumentation to heat transfer studies. A tape recorder capable of recording electrical signals at a tape speed of 60 inches per second and playing back the signals at 0.3 inches per second was available for this purpose. The data were thereby played back at 1/200th of the original speed, greatly facilitating observation and subsequent calculation. Since this basic equipment was already in existence, the experimental system was necessarily set up to be compatible with it.

Data Recording System

The tape recorder, built by Minneapolis-Honeywell and pictured in Figure 2, consisted of a tape transport mechanism, two frequency modulated (fm) recording oscillators, two fm signal discriminators, a signal attenuator and a signal preamplifier. A brief outline of the operation of the instrument is necessary to understand its uses and limitations.

A schematic diagram of the data recording system is shown in Figure 3. The two recording oscillators, one for each of two channels of information recorded simultaneously,

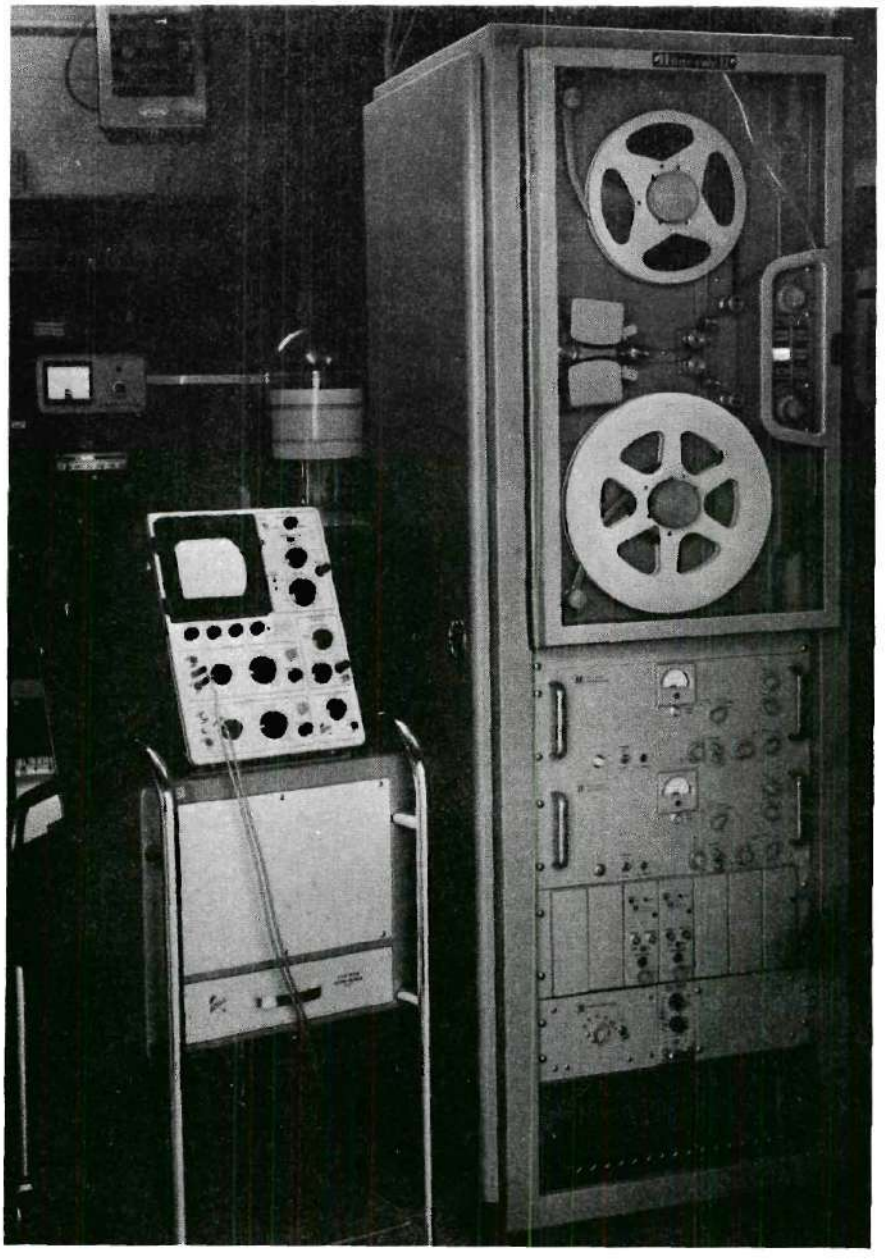

Figure 2. Tape Recording System and Oscilloscope.

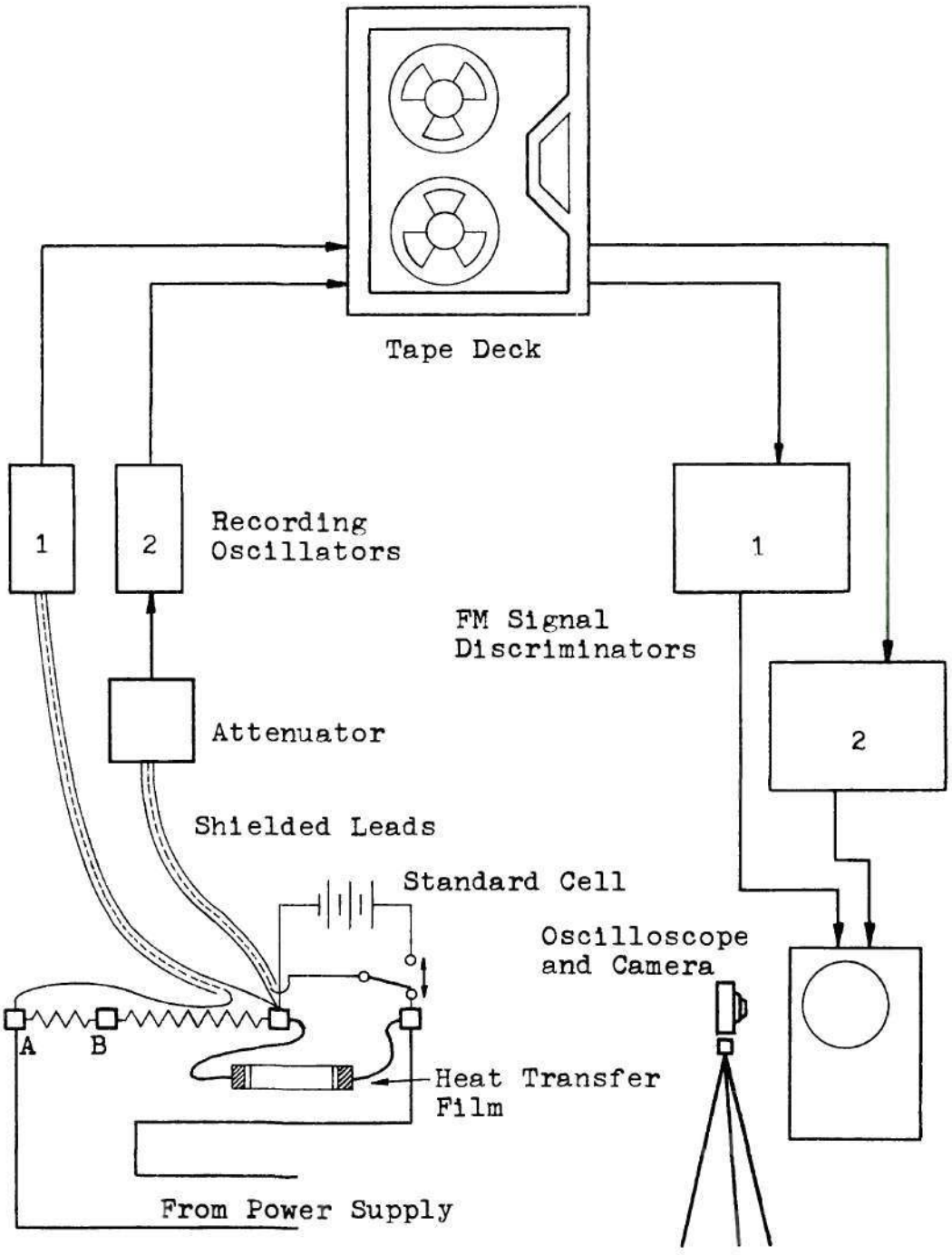

Figure 3. Schematic Diagram of Data Recording System.

generated a "center frequency" of 54 kilocycles per second when no signals were applied to their input terminals. The information to be recorded was applied to an oscillator in the form of a voltage, the maximum recordable signal being 1.2 volts. An applied positive voltage of 1.2 volts caused the oscillator output frequency to be reduced by 40 per cent, and conversely, the same negative voltage gave a 40 per cent increase in frequency. The oscillator output frequency, impressed on the magnetic tape, deviated from the center frequency by an amount proportional to the voltage applied to the input of the recording oscillator.

Since a maximum of 1.2 volts could be applied to the oscillators, a signal attenuator, consisting of a rotary switch and a set of precision resistors, was required for the channel used to record voltage across the heat transfer film. The resistors were arranged in a simple voltage divider circuit, so that 5-, 10-, 25-, 50-, or 100-volt inputs could be selected. A 200-volt input step was later added.

It had been anticipated that currents would be measured by recording the voltage drop across a standard shunt resistor in series with the heating element load. Shunt resistors of this type are ordinarily chosen to have low voltage drops, 50 millivolts or so. For this reason a preamplifier was supplied for the current channel of the tape recording system to amplify the shunt voltage to a recordable level. Difficulties were experienced with the amplifier, and a high resistance shunt

(0.02 ohms) was installed instead. This shunt was connected directly to the recording oscillator for the current channel and the preamplifier was no longer used.

As stated earlier, when the recorded data were played back the tape was run at 1/200th of the recording speed. The center frequency of the playback signal from the tape transport was therefore 270 cycles per second, and this was sent to the fm signal discriminators. These units, one for each channel, converted the tape signal to a voltage proportional to the deviation from the center frequency. Thus the output from the discriminators, which might more accurately be called demodulators, was proportional to the original signal.

Without modification to either the oscillators or discriminators, only one combination of record and playback speed was possible. The ratio of these speeds was fixed by the ratio of center frequencies. This modification could have been accomplished easily by changing plug-in component assemblies in the oscillators or discriminators. The required assemblies were available from the equipment manufacturer, and the tape transport was already capable of operating at several tape speeds.

The discriminator output was a voltage which required conversion to a graphical display before processing of the data was possible. A Tektronix, Model 502, dual-beam oscilloscope was used for this purpose. Its scanning rate was set

so that about two seconds were required for the two spots to pass across the screen, giving ample time to photograph them without special equipment.

A Tektronix camera was available for photographing the screen on Polaroid, Type 47, roll film or on conventional four inch by five inch cut film. Because a large number of photographs were required for this study (up to 80 for a single experimental run) it was found far more convenient to record data graphically with a 35 mm camera. A Kodak Retinette camera with a plus 3 close-up lens was used for this. The camera was mounted on a tripod and focused with a piece of ground glass held at the film plane. Then a masonite template was cut to position the camera for each set of photographs and the same settings were used for each test. A cable release was needed to prevent camera motion during the long exposures and the lens was stopped down to f:8 to assure good depth of field. A slow film, Kodak Panatomic-X, gave proper exposures with the oscilloscope's spot and grid intensity set at normal viewing levels. The room was darkened during photographic exposures. Figure 4 shows typical recordings of alternating and direct current and voltage traces.

In view of the data recording system complexity, direct calibration was necessary for each test. The potentiometer taps, marked A and B in Figure 3, and a standard voltage cell were used for calibration; the procedure is described in Chapter III.

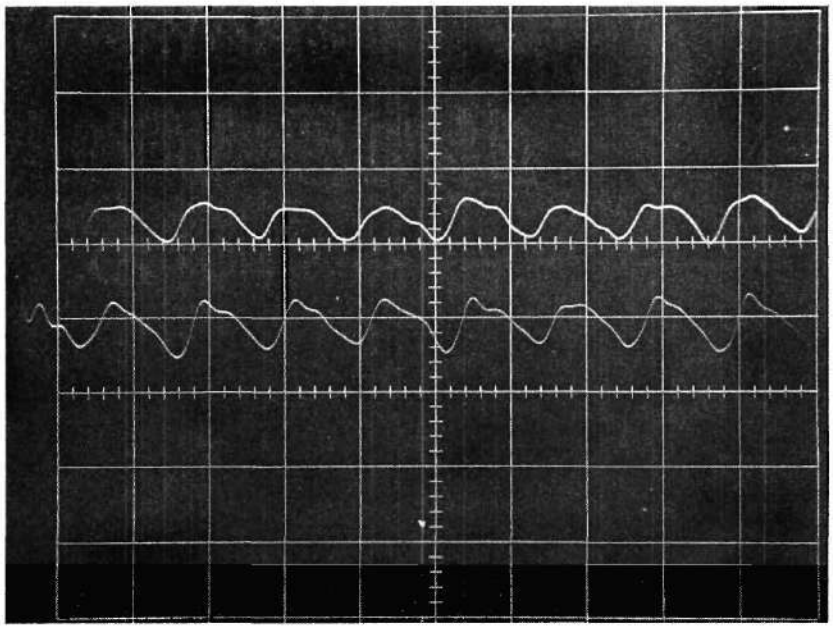

Base Line →

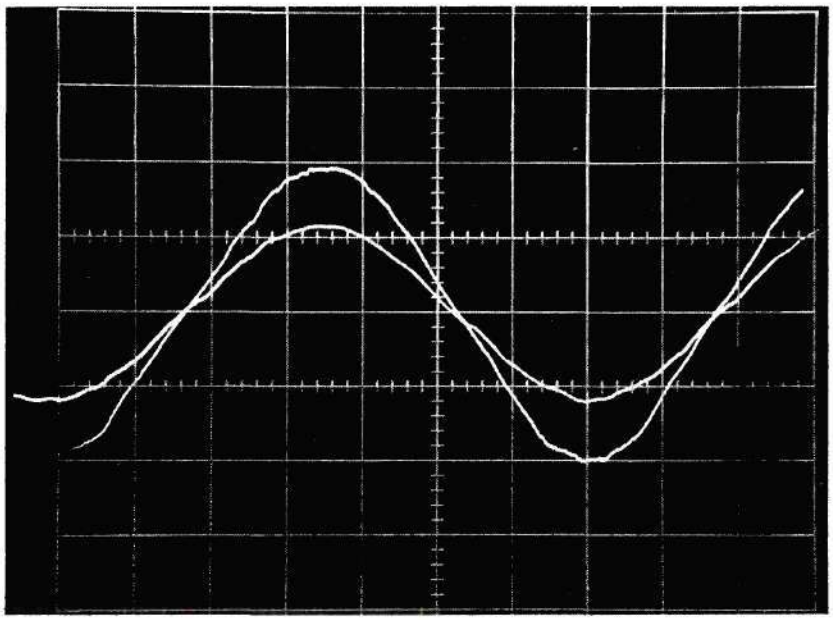

Base Line →

Figure 4. Typical Recordings of Direct and Alternating Currents and Voltages.

Power Supply

It was estimated that an adjustable source of about 100 amperes at 100 volts ac and a comparible source of direct current (dc) would be required for the heat transfer studies. Variable transformers were chosen as the most suitable method of meeting the ac requirements in order to avoid the sine-wave distortion characteristic of operation with a saturable core reactor. Since full-wave rectified dc is equivalent to ac in a resistive circuit, the dc power had to be smoother than full-wave or there would be no advantage in using it. Electrical filters perform well only under constant loads, and batteries or motor-generator sets seemed an awkward way to supply dc because these sources are expensive, bulky, and difficult to control. A three-phase rectifier bridge was selected as the best compromise between smoothness and simplicity.

The power supply was capable of furnishing ample electrical energy for heat transfer experiments of this kind, in several different modes of operation. Three-phase rectified dc, single-phase ac, and half-wave rectified dc were used in these experiments. It would have been possible to supply three-phase ac and full-wave rectified dc as well, had the experiments called for these types of power.

Three-Phase Rectified Direct Current

Figure 5 shows a schematic of the power supply connection for three-phase rectified current. The power was fed

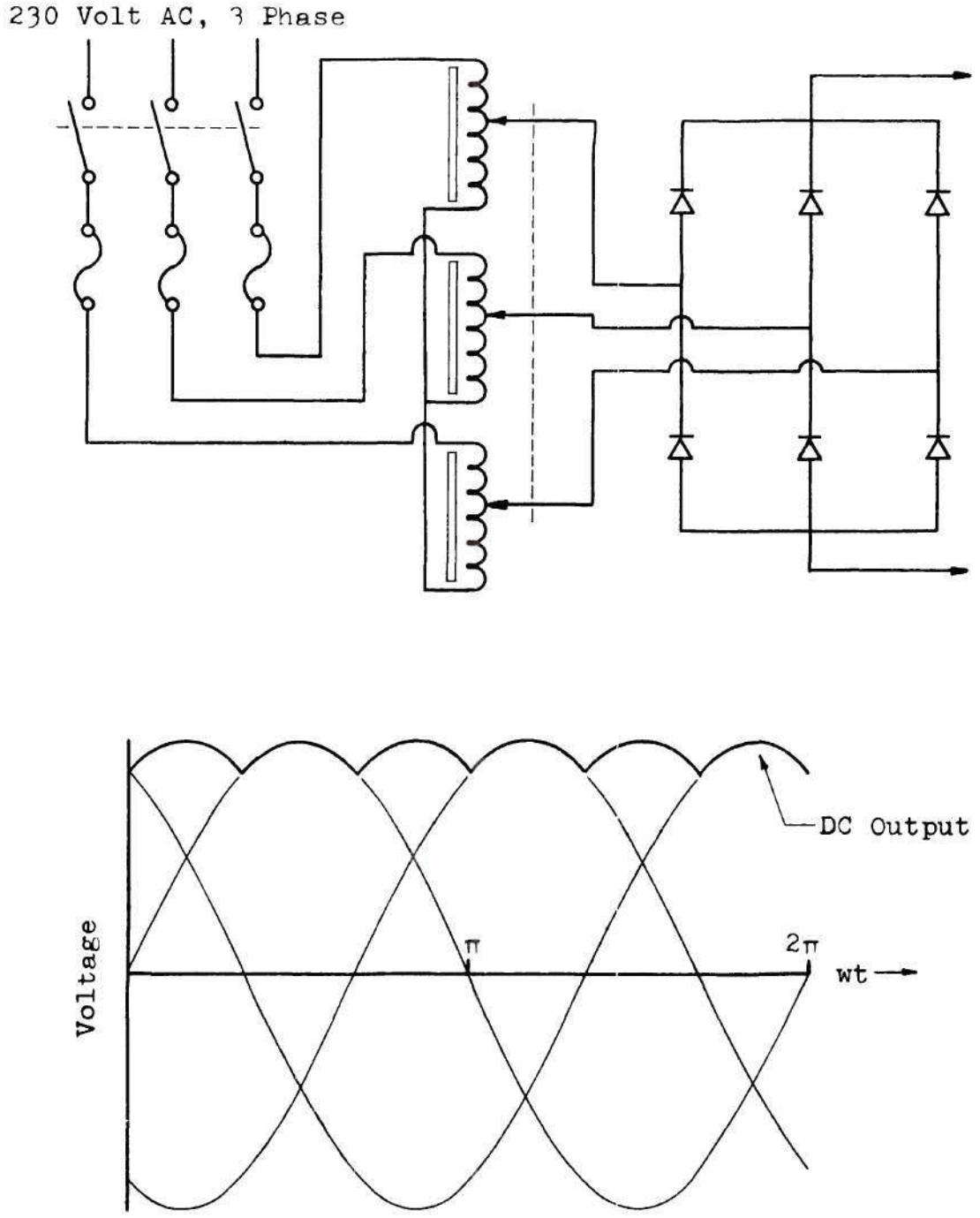

Figure 5. Power Supply Connection and Voltage Waveform for Three-Phase Rectified Direct Current.

from a master switch to a Superior Electric Company "Powerstat" variable transformer assembly, Model 1156D-6Y. This is a stack of six transformers, one on top of another, with a common control shaft and manual control wheel. Two transformers and a load matching device are connected to each of the three power legs in a three-phase wye connection. Nominal maximum output of this unit is 230 volts, 90 amperes.

The transformer output was fed to a bridge rectifier composed of six 100-ampere Sarkes-Tarzian silicon rectifiers, mounted on 1/2-inch aluminum plate heat sinks and installed in a box with a small electric blower for cooling. Direct current from the bridge was fed to the heat transfer film and measuring shunts as shown in Figure 3. The rectifier bridge could supply about 100 amperes at 140 volts without exceeding current and peak inverse voltage ratings of the rectifiers. The ripple frequency in a three-phase bridge rectifier is six times the supply frequency and the output voltage does not become zero during any portion of the cycle as with single-phase rectifiers. The output voltage as a function of time is shown as a heavy line in the lower part of Figure 5.

Single-Phase Alternating Current

The connection of the power supply for single-phase current is shown in the upper part of Figure 6. The fuse in one leg of the transformer supply was removed, and power was taken directly from the transformer after disconnecting the rectifiers.

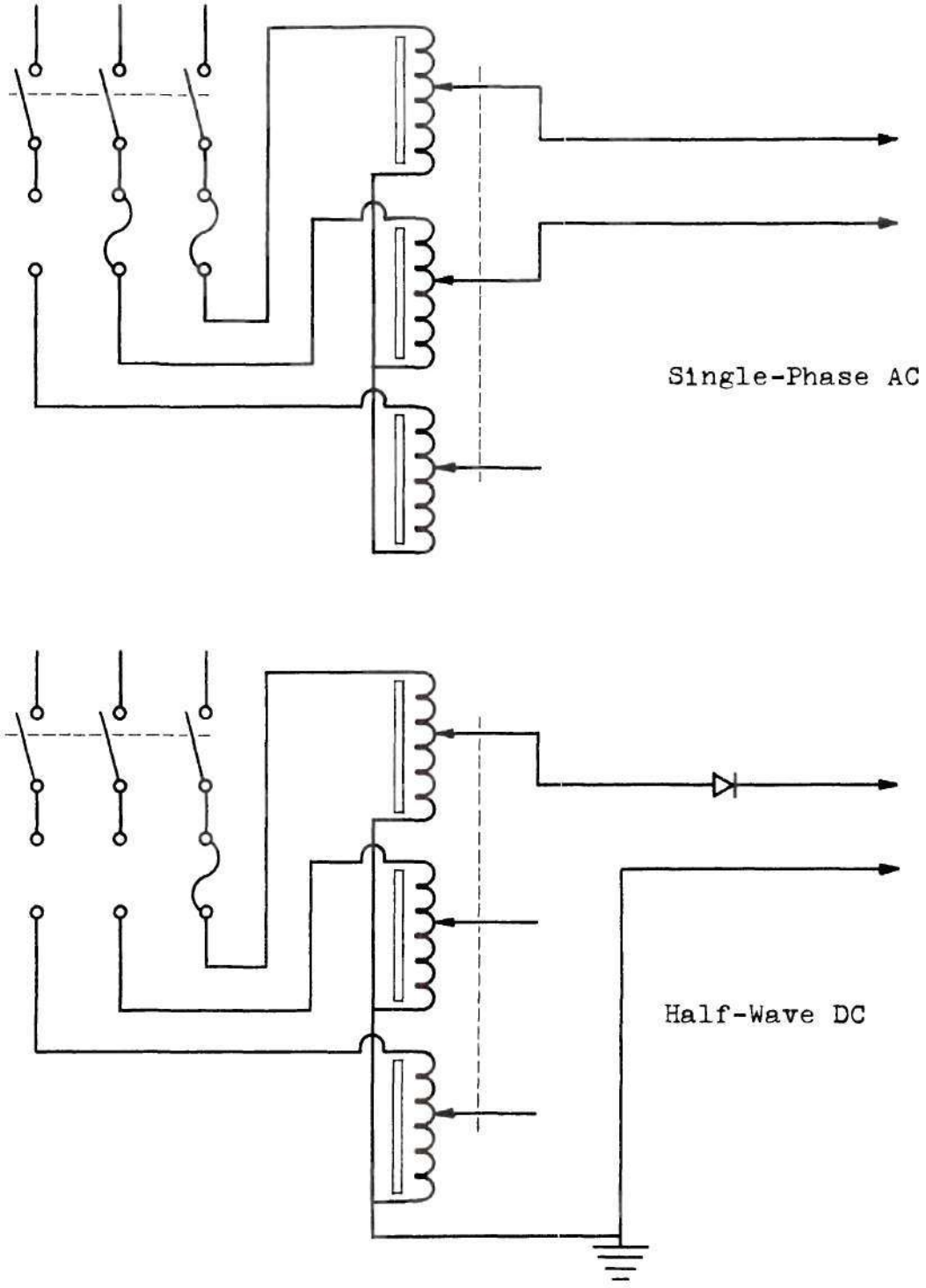

Figure 6. Power Supply Connections for Single-Phase Alternating Current and Half-Wave Direct Current.

Half-Wave Rectified Direct Current

The connection of the power supply for half-wave rectified current is shown in the lower part of Figure 6. Only one leg of the power supply and one rectifier were employed. The return leg was grounded.

Film Calibration Equipment

The equipment used to calibrate heat transfer films as resistance thermometers is shown in Figure 7. Films were deposited on one inch by three inch quartz microscope slides and copper connection blocks were soldered to the ends of the slides. For calibration, the film assembly was supported on a brass stand and placed in a furnace enclosed under a vacuum bell jar.

The furnace was made of fused-silica foam and heated by 0.040-inch Kanthal A-1 resistance wire wrapped around 1/4-inch diameter by four-inch long alumina rods. There were eight heating rods, standing vertical and equally spaced around the perimeter of the furnace chamber. Furnace heating current was supplied by a three kilovolt-ampere variable transformer and the temperature was controlled by a Wheelco temperature controller operating a relay in the transformer power line. By proper adjustment of the furnace voltage, temperature fluctuations caused by cycling of the controller could be kept very small.

The film resistance was measured by a Honeywell

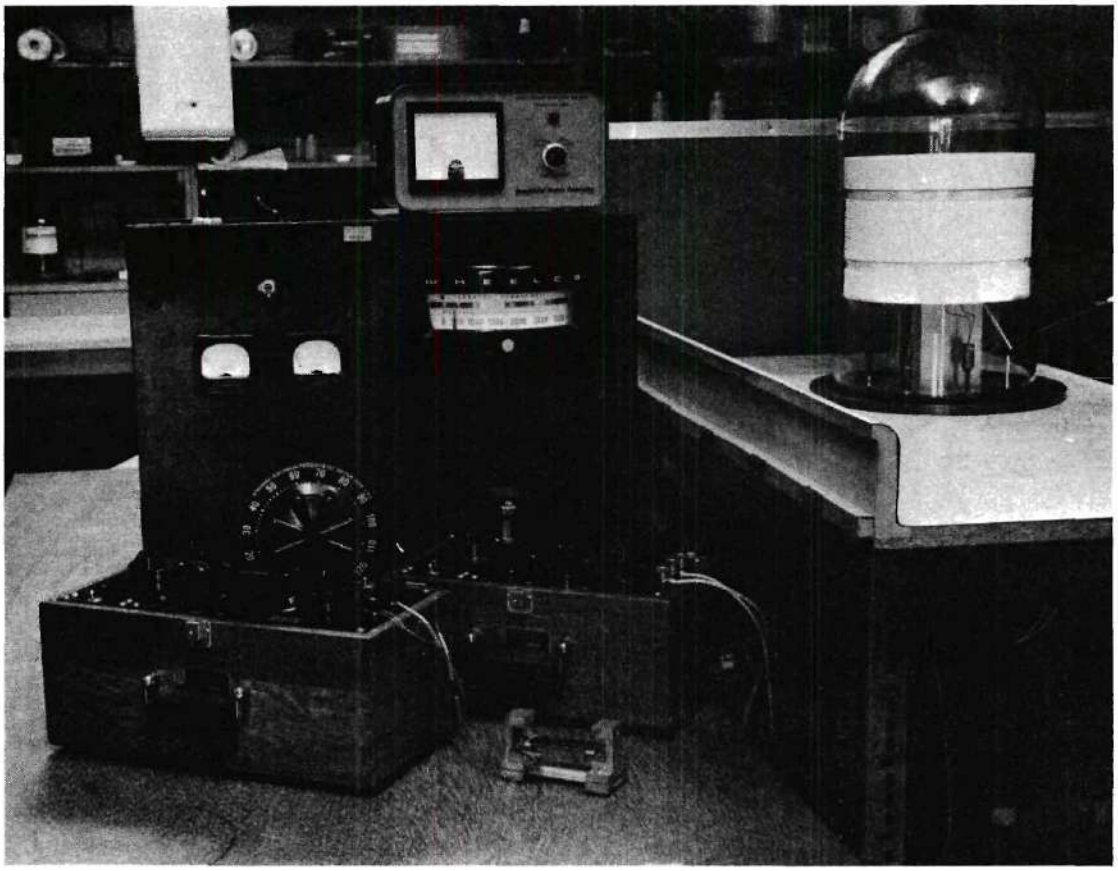

Figure 7. Film Thermal Calibration Apparatus.

Wheatstone bridge; its temperature was determined by two platinum:platinum-13% rhodium thermocouples, the output voltage of which was read from a Honeywell Rubicon potentiometer.

Calibration was carried out at a pressure of about 0.05 Torr to reduce the danger of film oxidation. Thermometric calibration required about eight hours, and the temperature reached a maximum of about 450°F during this period. The thermal calibration procedure is described in Chapter III.

Miscellaneous Equipment

Nickel heat transfer films were prepared by vacuum evaporation of nickel from 0.020-inch diameter tungsten wire filaments onto clear fused quartz substrates. Satisfactory films could be made only after nickel had been electroplated onto the tungsten filament.

A photograph of the vacuum deposition vessel and details of the fixtures are shown in Figure 8. The vacuum vessel was a six inch diameter by six inch long section of Pyrex pipe. It was closed at one end by the base plate and pumps and at the opposite end by a brass plate on which two Conax vacuum feed-throughs were mounted. The nickel-plated tungsten filament was supported by the feed-throughs, and arranged in the configuration shown to minimize sagging caused by thermal expansion.

The quartz substrate rested on a substrate heater made of copper and nickel. The heater temperature was controlled

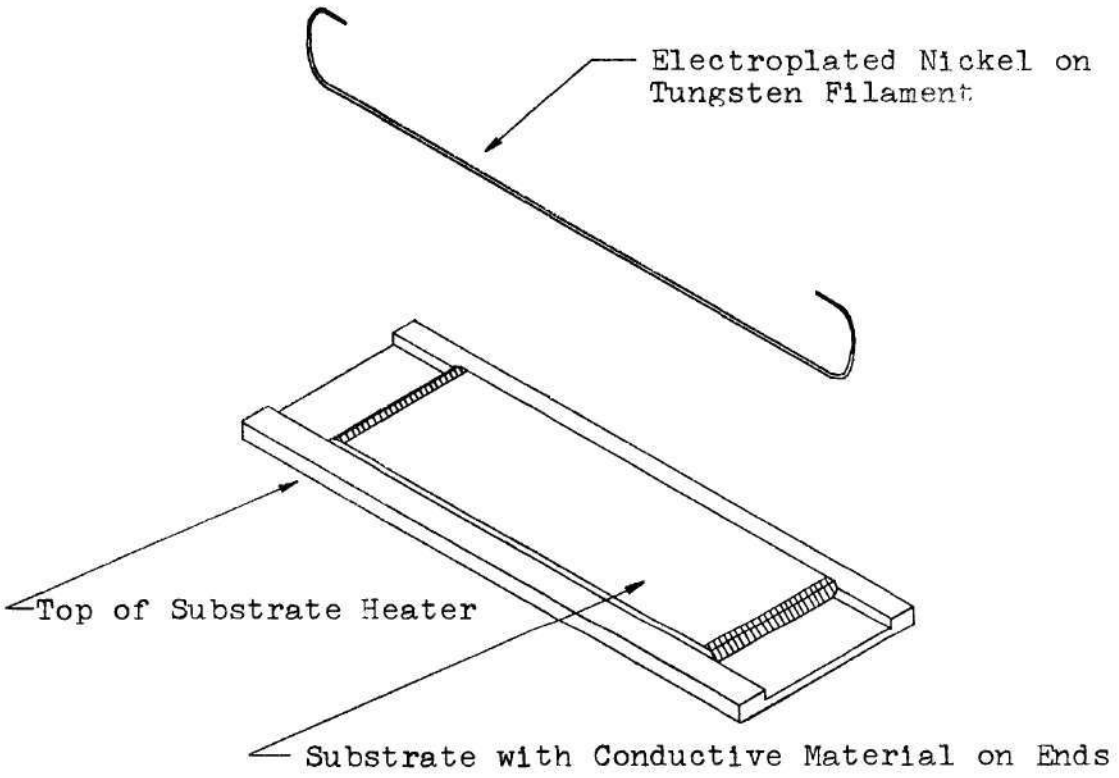

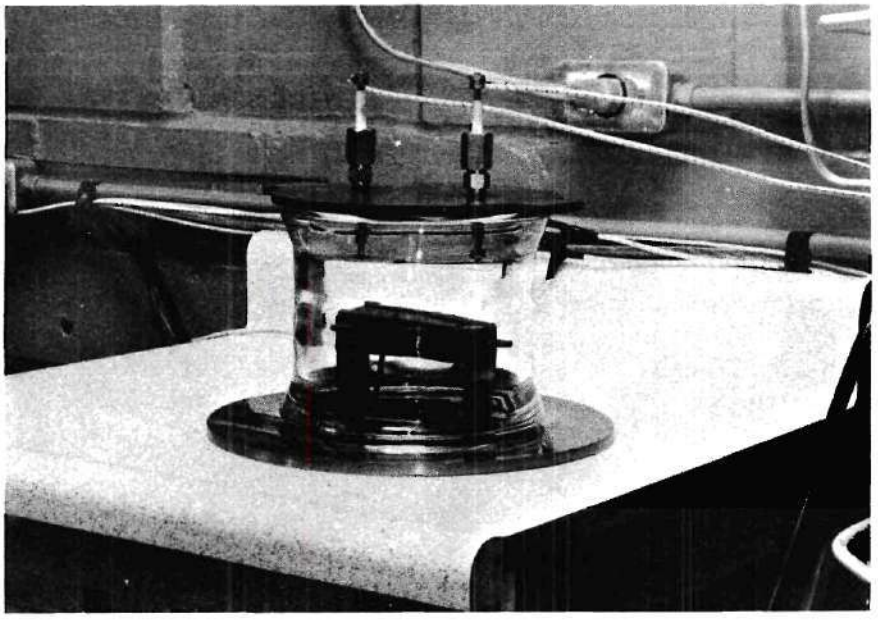

Figure 8. Vacuum Deposition Vessel and Detail of Deposition Fixtures.

by a thermocouple leading to a temperature controller, variable transformer, and relay arrangement similar to that used for the film calibration furnace. Heat was supplied by an electrical heater of tungsten wire supported by alumina rods. It was necessary to exclude high vapor pressure metals, such as zinc, from the heater assembly to prevent unwanted deposition of these metals within the vacuum vessel.

The vacuum system was evacuated by a two-inch, National Research Corporation water-cooled diffusion pump, backed by a two-stage mechanical pump. Pressure was determined with a thermocouple gauge and a Penning-type discharge gauge.

Figure 9 shows an overall view of the vacuum evaporation vessel, power supply transformers, rectifiers, and a heat transfer film set up for an experiment.

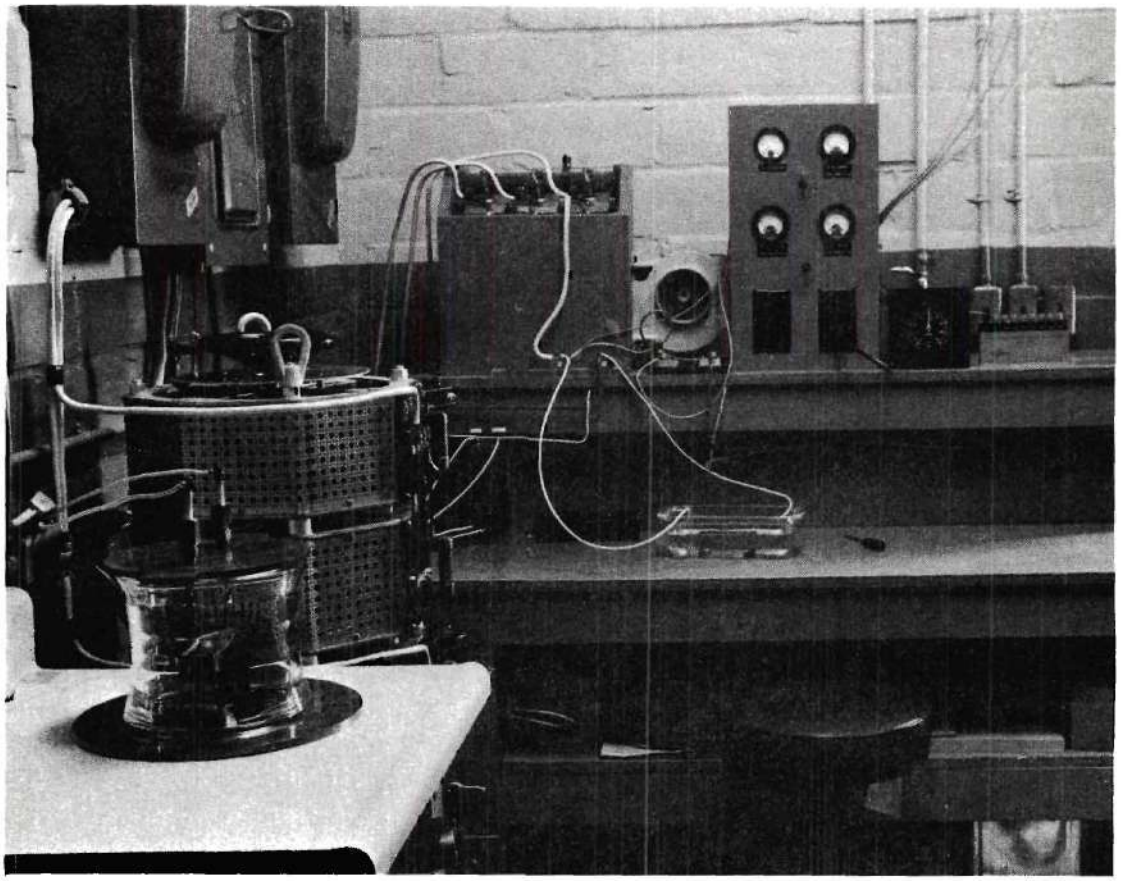

Figure 9. Film Deposition Vessel and Power Supply with Heat Transfer Film Prepared for Experiment.

CHAPTER III

EXPERIMENTAL PROCEDURE

The maximum duration of the experiments in this study was less than one-half minute, but a considerable expenditure of time was required to complete the preparation, execution, and data reduction for each experiment. The techniques of employing thin metal films involve art as well as science, and each investigator must develop methods that work for his particular application. In this chapter the experimental processing of a heat transfer film is described, but it should be understood that the procedure finally selected was the result of an evolution of technique. In planning an experimental program which employs other than conventional methods, it is impossible to anticipate every difficulty. The several steps described here were chosen to meet the requirements of this study, but future related studies are certain to demand their own modifications.

Production of Heat Transfer Films

One of the reasons for employing thin metal films in heat transfer studies is that their electrical resistance can be made high enough to give substantial power dissipation with easily manageable currents while affording large surface areas.

However, films with these properties are too thin to support themselves during handling and need a substrate for support. The substrates for this study were required to be electrical non-conductors, capable of immersion in water without damage, capable of withstanding the thermal shock of rapid temperature transients, and compatible with the vacuum film deposition system. Since thin metal deposits follow the contours of the supporting surface, smooth substrate surfaces were desired.

Crown glass substrates were tried, but proved unable to stand the thermal shock imposed by the heat transfer experiments. Clear, polished, fused-quartz, microscope slides, one inch by three inches by one-eighth inch thick, were then chosen for substrates. Figure 10 shows an exploded view of a heat transfer film assembly.

A method for making low resistance contacts to the nickel film was necessary. A strongly adhering, thin, gold film could be formed on the ends of the slides with Hanovia Liquid Bright Gold, No. 5154, a gold resin material used in the ceramics industry for decorating china and similar purposes. The gold resin was applied by painting onto the substrate and allowed to dry at room temperature. After drying, the piece was fired to about 1200°F in air to burn out the organic material and leave a gold film. Gold films applied in this manner gave satisfactory connections to the nickel films, but were too thin to permit soldering of end blocks for connection of leads.

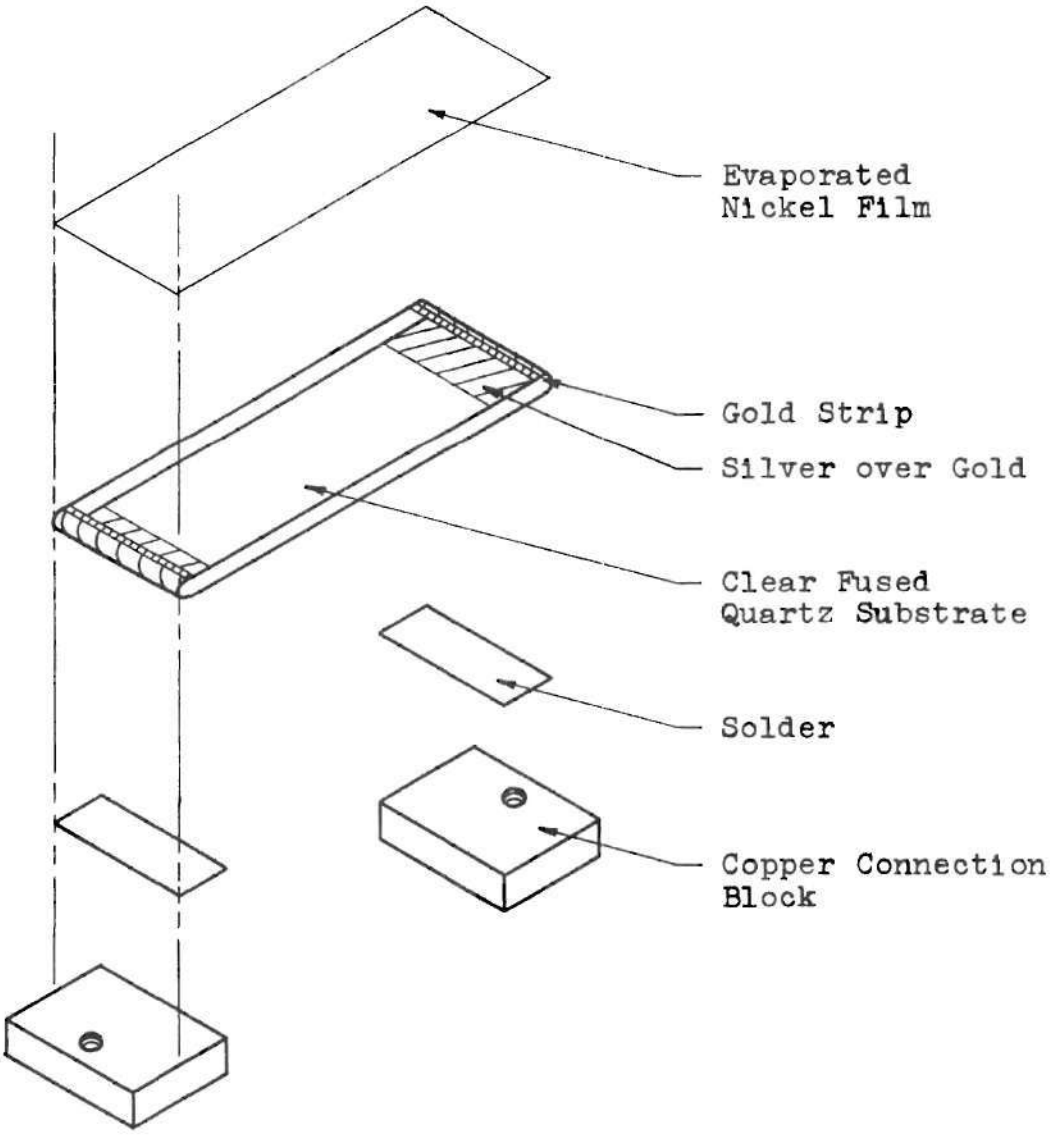

Figure 10. Exploded View of Thin Film Heat Transfer Element.

Hanovia Flexible Silver Coating, a material consisting of finely divided silver in a liquid vehicle, could be applied like Liquid Bright Gold and fired to give a silver film much thicker than the gold films. The silver films produced in this manner did not adhere well to glass, however.

End connections were made by using both materials according to the following steps:

(1) Ends of the quartz slides were rounded and polished to prevent failure of the painted and fired contacts at sharp corners.

(2) Slides were cleaned in hot aqua regia and rinsed.

(3) Slides were brought to a boil in a solution of Fisher RBS-25, a laboratory detergent, and rinsed.

(4) Slides were brought to a boil in distilled water, then removed while hot and dried in air.

(5) Liquid Bright Gold was painted on the ends of the slides in the desired pattern.

(6) Slides were dried 48 hours at room temperature.

(7) Slides were fired to 1200°F for two hours in an electric furnace with the door partially open to admit air.

(8) After cooling, Flexible Silver Coating was painted over the gold except for a thin strip of gold which was left for contact with the nickel film.

(9) Slides were dried 24 hours at room temperature.

(10) A second coat of Flexible Silver Coating was

applied, as in step 8.

(11) Slides were dried 24 hours at room temperature.

(12) Slides were fired for 72 hours, as in step 7.

The above procedure gave sound end connections to which solid end blocks could be soldered after deposition of the nickel film. It is a lengthy operation, but shortcuts led to subsequent difficulties in obtaining reliable soldered connections.

The next step in making a heat transfer film was deposition of the film onto the prepared substrate. Nickel is a very difficult metal to deposit by vacuum evaporation, but for reasons listed earlier, nickel films were used. The need to have films with thickness as uniform as possible coupled with the requirement that a short source-to-substrate distance be used to achieve a reasonably high deposition rate, led to selection of an extended wire source. After the filaments had been cleaned with abrasive paper and bent to the desired shape they were electroplated with about 100 milligrams of nickel from a conventional sulfate plating bath, rinsed, and dried with compressed air.

The nickel plated filament was installed in the deposition vessel, and a substrate was cleaned with hot detergent solution and rinsed. It was brought to a boil in distilled water, then removed while hot and dried in air. Dust particles were blown off with a gentle stream of clean compressed

air, and the slide was placed on the substrate heater. The vacuum system was closed, evacuated to about 10^{-5} Torr and the heater temperature raised to 800°F. Substrate heating served two purposes. First, film adherence was improved by more thoroughly driving off air and water vapor that had been adsorbed on the substrate surface. Second, most metal films, including nickel, show irreversible changes in resistance on heating if they have been deposited on cool substrates. These irreversible changes are caused by recrystallization of the strained metal structure inherent in thin films and destroy a film's thermal calibration if it is heated above the maximum temperature in its history. Deposition on a hot substrate eliminated the need for thermal recrystallization before the film's calibration as a resistance thermometer. During this evacuation period the filament was outgassed several times by heating it to a dull red color, well below the evaporation temperature of nickel.

After about an hour of outgassing, the substrate heater temperature was reduced to 700°F and nickel was evaporated from the tungsten filament. The filament current was controlled by a variable transformer and step-down transformer which allowed the voltage to be varied from zero to sixteen volts. Control was too coarse when the variable transformer alone was employed. The behavior of nickel evaporated in this manner is discussed further in Chapter IV.

After the film had been deposited and cooled to room temperature, copper connection blocks were soldered to the ends of the substrate. Since it was desired that the film thermometric calibration be carried to at least 400°F, conventional lead-tin solders with melting ranges of about 350 to 370°F were unsuitable, but the films could not be heated to the temperatures required to melt silver solders. A soldering alloy of 5 per cent silver-95 per cent lead with melting range near 500°F was prepared and hammered into sheets about 0.010 inch thick. These solder leaves were cleaned with fine abrasive paper, fluxed lightly with a commercial rosin paste flux, and placed between the substrate and clean end block.

Soldering was accomplished by applying heat to the metal blocks with a small natural gas-oxygen torch, taking care to avoid letting the flame touch the nickel film or substrate. Copper blocks were used because their high conductivity facilitated melting of the solder without overheating the nickel film to the point of causing oxidation.

With care, bright metallic films without pinholes or visible flaws could be produced by this method. The end connections were capable of carrying high enough currents that burnout occurred on the evaporated nickel film, an obvious requirement for meaningful heat transfer data. The soldered joints had good mechanical strength; attempts to break the copper blocks off the substrates often resulted in break-

ing the quartz substrate.

One of the most common, though qualitative, tests for adhesion of evaporated metal films is the "Scotch tape test". For this test a piece of gummed cellulose tape is pressed firmly onto the metal film (50). The tape is removed; some sources state that removal should be done rapidly, and others stipulate slowly. The evaporated film is then examined to see if metal has been removed by the tape. Failure of metal to be removed is an indication of good film adherence.

The nickel films employed for this study passed the "Scotch tape test" with only an occasional removal of bits of metal. In no test was an appreciable part of the film stripped off if substrate heating had been used during film deposition. Generally, the films remained continuous and opaque, although a few tiny flakes of metal could be seen on the tape after stripping. Both rapid and slow stripping were tried, with no noticeable difference in results.

Calibration of Films as Resistance Thermometers

The final operation in the production of a heat transfer test element was calibration of the film as a resistance thermometer. This was accomplished after the end blocks had been soldered in place for two reasons: electrically sound connections to the film would be available for resistance measurements, and disturbance of the thermal calibration caused by soldering would be avoided.

For calibration a loop of stranded 14-gauge copper wire was fastened to each copper end block and the heat transfer element placed on a brass holder and positioned in the center of the calibration furnace. The stranded loops were clamped to leads connecting the Wheatstone Bridge for resistance measurement. Film resistances, about two to five ohms, were within the range of the bridge and correction for lead resistance was made.

A thermocouple was used to control furnace temperature, and two additional thermocouples were positioned to measure the film temperature. One was fastened to the brass holder and one connected to the center of an exposed edge of the substrate.

After installation of the heat transfer element, the calibration furnace was covered by a glass bell jar and evacuated to a pressure of about 0.05 Torr. Thermometric calibration was carried out in vacuum to reduce the danger of film oxidation and to reduce temperature gradients caused by convection currents.

To establish a calibration point, the furnace temperature was manipulated so that the two thermocouples measuring film temperature indicated identical values. The film resistance was taken at this time. Calibration points were determined at several temperatures up to about 450^{o}F, then at several points as the temperature decreased. Differences between

these two sets of points never exceeded 5°F. To check calibration permanence, this cycle was repeated for several films with good agreement. A typical temperature calibration plot is shown in Figure 11.

Calibration of Data Recording System

Calibration of the data recording system was accomplished before and after each experiment. A known voltage and current were recorded on a few feet of tape and these recordings were used to establish scale factors relating the photographed data to volts and amperes. Figure 12 shows a schematic diagram of the connections employed for calibration. The standard mercury reference battery was connected to the voltage recording channel by a switch. Current was determined by measurement of the voltage drop across a precision, shunt resistor.

To record the calibration signal, a length of Kanthal A-1 resistance heating wire was connected in place of the heat transfer film as shown in Figure 12. The power supply, wired for three-phase rectified direct current, was turned on and a current flow established. When the current measured by the potentiometer was constant, the channel recording voltage was switched to the standard cell for about ten seconds, then the recorder was stopped.

No provision for scanning the tape signal was available, so that there was no way to identify the measured signals on

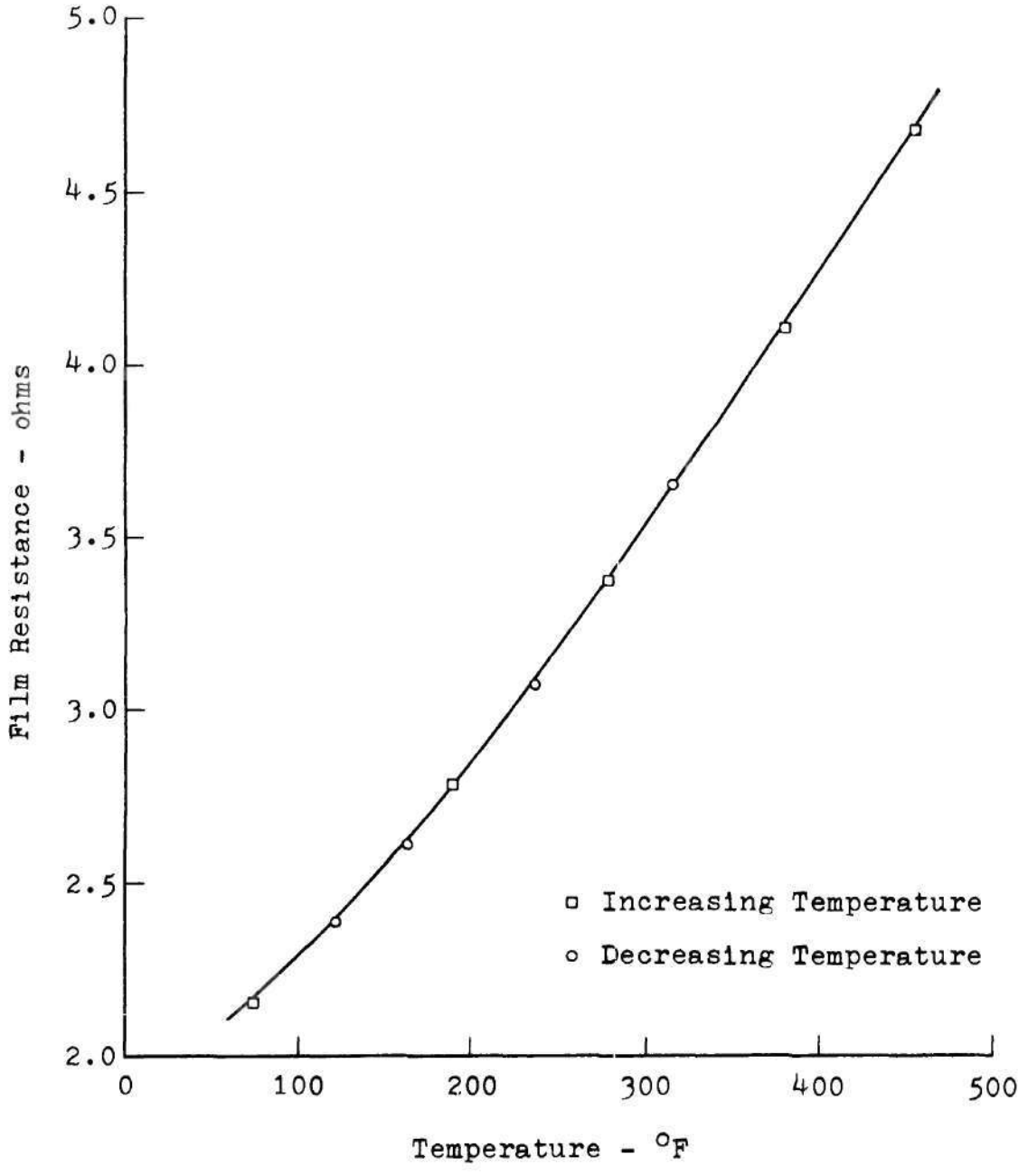

Figure 11. Typical Temperature Calibration Plot.

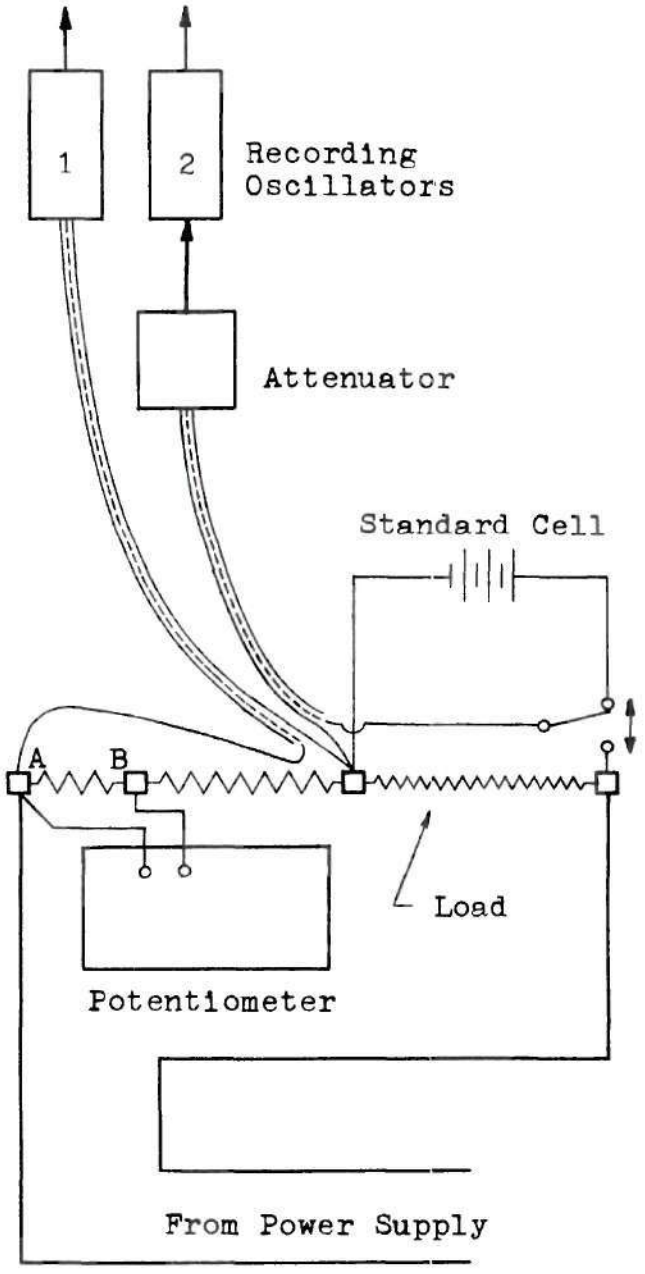

Figure 12. Connections for Calibration of Data Recording System.

replay except by visual observation of waveforms. However, the voltage from the standard cell had no ripple and was readily identifiable. When the above sequence of steps had been followed, the recorded current was known to correspond to the value determined by the potentiometer when the voltage showed no ripple.

As described later, a degree of judgment was required to read the photographed data after replay. Recording of calibration signals before and after each test permitted the resolution of small errors in scale factors arising from drift of the equipment or errors in interpreting data. Thus when two calibrations were made, more confidence could be placed in the experimental measurements, particularly film temperatures which were ultimately derived from the quotient of the two recorded signals.

Experimental Tests

To conduct an experiment, the heat transfer element was connected as shown in Figure 3 and submerged in a one-quart Pyrex dish filled with distilled water at room temperature. With the power supply transformer turned low, the master switch was closed, then the tape transport started. The power supply voltage was increased at the desired rate until the heat transfer film burned out.

After the second calibration, the tape transport was rewound to the beginning of the first calibration and replayed

without stopping while photographs of the oscilloscope screen were made at the desired intervals. Runs were timed during replay by an electric clock and the time of each photographic frame was calculated from the ratio of the recording and playback tape speeds.

After development of the photographic film, currents and voltages could be read in units of length on the oscilloscope grid. Direct current runs were usually read from an image of the negative projected by a photographic enlarger. Power supply ripple from the three-phase bridge rectifier required that a measure of individual judgment be exercised in determining direct currents and voltages. A hairline was placed through the recorded trace and positioned so that areas defined by the trace under the line were as nearly equal as possible to areas above the line. The straight hairline then represented the average voltage or current on the photographic frame.

Photographic prints of the data were made when it was desired that wave-forms be studied in more detail than was possible by projection of the negative. This was the case with alternating and half-wave direct current runs. Reading of voltages and currents at several places on the recorded wave of these traces quickly proved to be a tedious task and it was observed that the necessary data could be determined from peak values if the traces had a true sine-wave form.

Careful measurement showed this assumption to be satisfactory in alternating current tests and a reasonable approximation in the half-wave direct current test.

Reduction of Data to Heat Transfer Parameters

Using the scale factors determined by calibration, film currents and voltages read from photographs were converted to engineering units: amperes and volts. Film resistance was calculated and temperatures were determined from the individual film thermometric calibration. The rate of heat generation in dc operation was given by the power dissipation in the metal film using the formula

$$\left(\frac{q}{A}\right)_f \left(\frac{\text{Btu}}{\text{hr-ft}^2}\right) = 172.4 \text{ E(volts) I(amperes).} \qquad (1)$$

Slight modification of this formula is required for ac and half-wave dc operation. The power factor of the ac supply was measured on several days and found to range from 0.975 to 0.995; so this was taken as unity in all calculations. Then the instantaneous ac voltage and current, respectively, are:

$$E_i = E_p \sin wt \quad \text{and} \quad I_i = I_p \sin wt$$

where E_p and I_p are peak values. The instantaneous rate of power dissipation is

$$P_i = E_i I_i = E_p I_p \sin^2 wt$$

and the effective power is

$$P = \frac{1}{2\pi} \int_0^{2\pi} E_p I_p \sin^2 wt \, d(wt) = \frac{E_p I_p}{2}.$$

For ac power, equation (1) with the same units becomes

$$\left(\frac{q}{A}\right)_f = 86.2 \, E_p I_p \qquad (2)$$

and, with half-wave dc power, half the power pulses are eliminated and

$$\left(\frac{q}{A}\right)_f = 43.1 \, E_p I_p. \qquad (3)$$

Since the effective single-phase alternating voltage and current are

$$E = \frac{E_p}{\sqrt{2}} \quad \text{and} \quad I = \frac{I_p}{\sqrt{2}}$$

film resistance for an ac or half-wave dc test is

$$R = \frac{E}{I} = \frac{E_p}{I_p} \qquad (4)$$

if the voltage and current follow a sine-wave form.

There was considerable scatter in the film temperature determinations at low power levels. This occurred because the error in a voltage or current measurement was approximately constant regardless of the magnitude of the measured quantity. As the quantity became larger, the per cent error was reduced. The effect was more noticeable in film temperatures than in heat dissipation rates since temperatures were derived from the quotient of voltage:current, and a small error in either term of this quotient had a substantial effect on the measured temperature.

CHAPTER IV

FILM THICKNESS UNIFORMITY STUDIES

In the heat transfer experiments described in this study, electrical resistance of the films was used as a measure of temperature. In such an application, it is desirable that resistance be uniform over the area of the film so that temperature measurements will be representative of the entire film surface. The heat generation rate is equivelent to $P = E^2/R$, and the measured value of this too should represent the conditions over the whole film. If uniform properties of the film material are assumed, then the film resistance will be a function of thickness, and the obvious requirement is that film thickness should be as uniform as possible for measured heat transfer parameters to give an accurate picture of the experimental conditions. The purpose of this chapter is to describe a series of experiments undertaken to ascertain the thickness uniformity of nickel films prepared under conditions identical to those under which the heat transfer elements were made.

Experimental Procedure

Film thickness as a function of position on the substrate was measured by x-ray fluorescence. The K-alpha emission for nickel was used to determine the quantity of metal

present in an area of the sample defined by a mask having dimensions of 1/4 by 3/8 inch. This was compared to the K-alpha emission of a thick sample of the same area, and the ratio A_f/A_∞ taken as a measure of film thickness, where A_f is the area under the recorded x-ray peak for a thin film, and A_∞ is the area under the recorded x-ray peak for a thick sample.

The equipment employed was a Siemens x-ray unit with tungsten tube operated at 50 kilovolts and 14 milliamperes. The "white" tungsten radiation was directed onto the specimen held by a steel mask in which the specified aperture had been cut. The specimen, excited by this radiation, emitted its own characteristic x-rays and the desired nickel K-alpha radiation was selected by diffraction through a lithium fluoride standard crystal and detected by a proportional counter. The proportional counter was operated on its plateau and an appropriate counter window was set up to discriminate against all energies except that corresponding to the nickel radiation.

The counter and standard crystal were mounted on a Siemens goniometer which scanned slowly across the desired peak. The counter output was plotted on a strip chart recorder, and areas under the recorded peaks were taken as proportional to the quantity of metal present. A "blank" with no sample in the holder and a "thick" sample of 1/4 inch nickel plate were run before, after, and periodically during each set of film measurements. The x-ray peak area for a blank was 2 to 6 per cent of the area for a specimen, and the area for a

thick piece was 10 to 20 times the area for a specimen. Corrections for these quantities were made during subsequent calculations. Strip chart peak areas were measured by a polar planimeter, with a minimum of three readings which agreed within 0.02 square inches for each peak.

Calibration

An unpublished study by a member of the Engineering Experiment Station staff (51) indicated that for nickel films under about 10,000 Å thick the ratio A_f/A_∞ is a linear function of film thickness. Calibration showed this to be a good approximation for films used in this study.

To calibrate the measurement system, ordinary one inch by three inch glass microscope slides were cut into six 1/2-inch by one inch segments as shown in Figure 13. The slides were cleaned in the customary manner described in Chapter III, then placed in the vacuum system and evacuated for a few minutes to allow adsorbed water to equilibrate. The system was opened and each segment immediately weighed to the nearest 0.01 milligram on a Mettler, Model B6, analytical balance. They were returned to the vacuum system and placed in the same position for plating as substrates used for heat transfer experiments. The evaporation procedure was carried out exactly as with heat transfer films, and the segments were removed and weighed again.

The average film thickness on each segment was calcu-

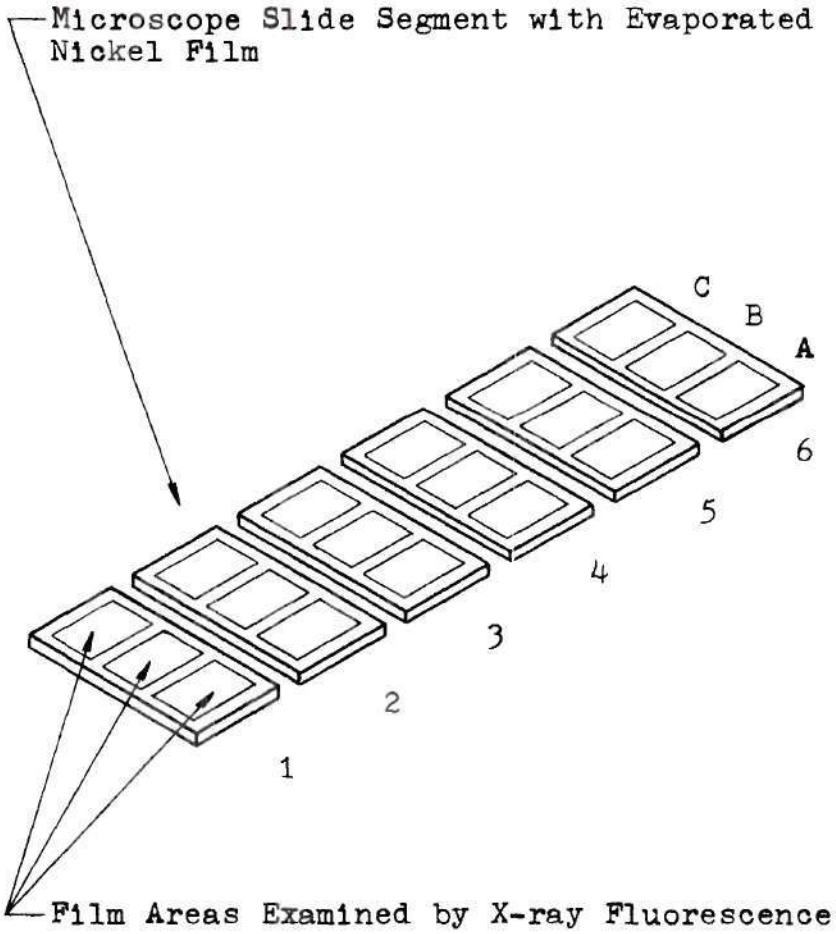

Figure 13. Nickel Uniformity Film Showing Sample Area Designations.

lated from the weight gained in plating, assuming the density of the film equal to the bulk density of nickel. The area of each segment was taken as the total slide area multiplied by the ratio of the segment weight to the slide weight.

X-ray fluorescence measurements were made on three 1/4-inch by 3/8-inch areas of each segment, as shown in Figure 13. The A_f/A_∞ ratios were averaged for each segment, and the data were plotted against the segment film thickness calculated from weight gain. A calibration line was drawn, based on the data from four complete slides. This plot is shown in Figure 14, and the calculations are tabulated in Appendix IV.

Other techniques, such as those of Talysurf or interferometer, are capable of thickness measurement, and might have been used for calibration. The procedure described was considered most suitable for this study, however, because equipment was readily available and the method tended to give average thicknesses over areas significantly smaller than that of a heat transfer film. Measurement of thickness uniformity on a macroscopic scale permitted data to be compiled over a whole microscope slide, and gave a useful picture of thickness profiles.

The points shown in Figure 14 give a rather good straight line plot when it is noted that an error of 0.05 milligram in determining film weight will move a point about 250 Å in the vertical direction. Exceptional care was re-

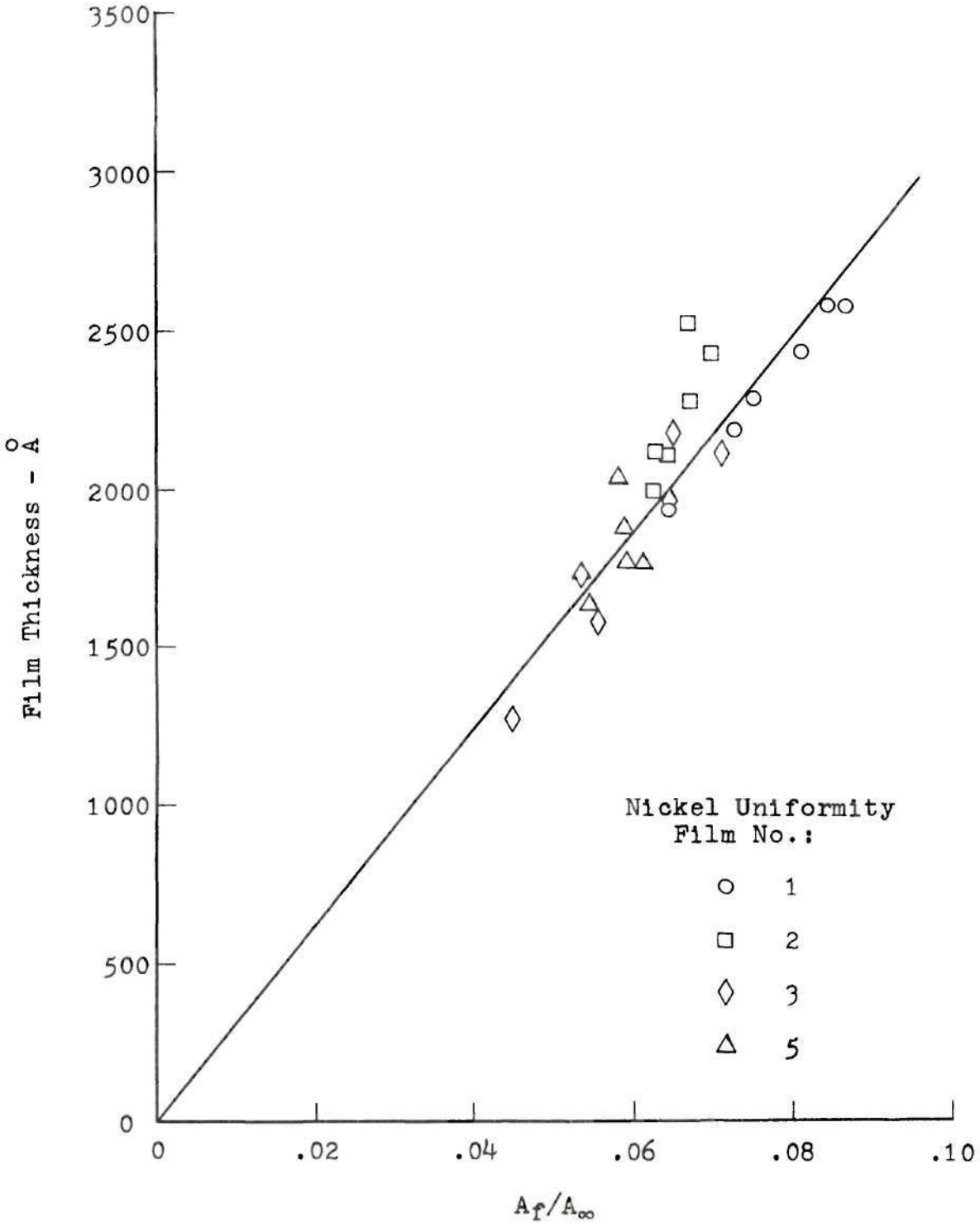

Figure 14. Film Thickness Calibration for Thickness Uniformity Studies.

quired in weighing films because this operation was performed near the limit of the sensitivity of the analytical balance. Film weights in the calibrations ranged from 0.35 to 0.75 milligram.

Results of Thickness Uniformity Measurements

The film thickness at each fluorescence measurement area was determined from the calibration plot using the measured A_f/A_∞ ratio. These data are shown in Figures 15 and 16. The heavy vertical lines are proportional in length to film thickness, and contour lines form a profile of thickness as a function of position on the substrate.

For comparison, a similar drawing in Figure 17 shows the theoretically predicted thickness distribution for a film evaporated under the same geometry from a filament substantially the same as a wire source. The filament model used in this calculation was a thin ribbon with material evaporating from its underside, but it is a close approximation to a wire filament in the present case. Further mention of this point will follow.

The data displayed in Figures 15, 16, and 17 are tabulated in Appendix IV.

Calculation of the predicted thickness distribution was accomplished by adaptation of the evaporation equations published by Holland (52). It was assumed that evaporation took place according to Knudsen's cosine law, the equivalent

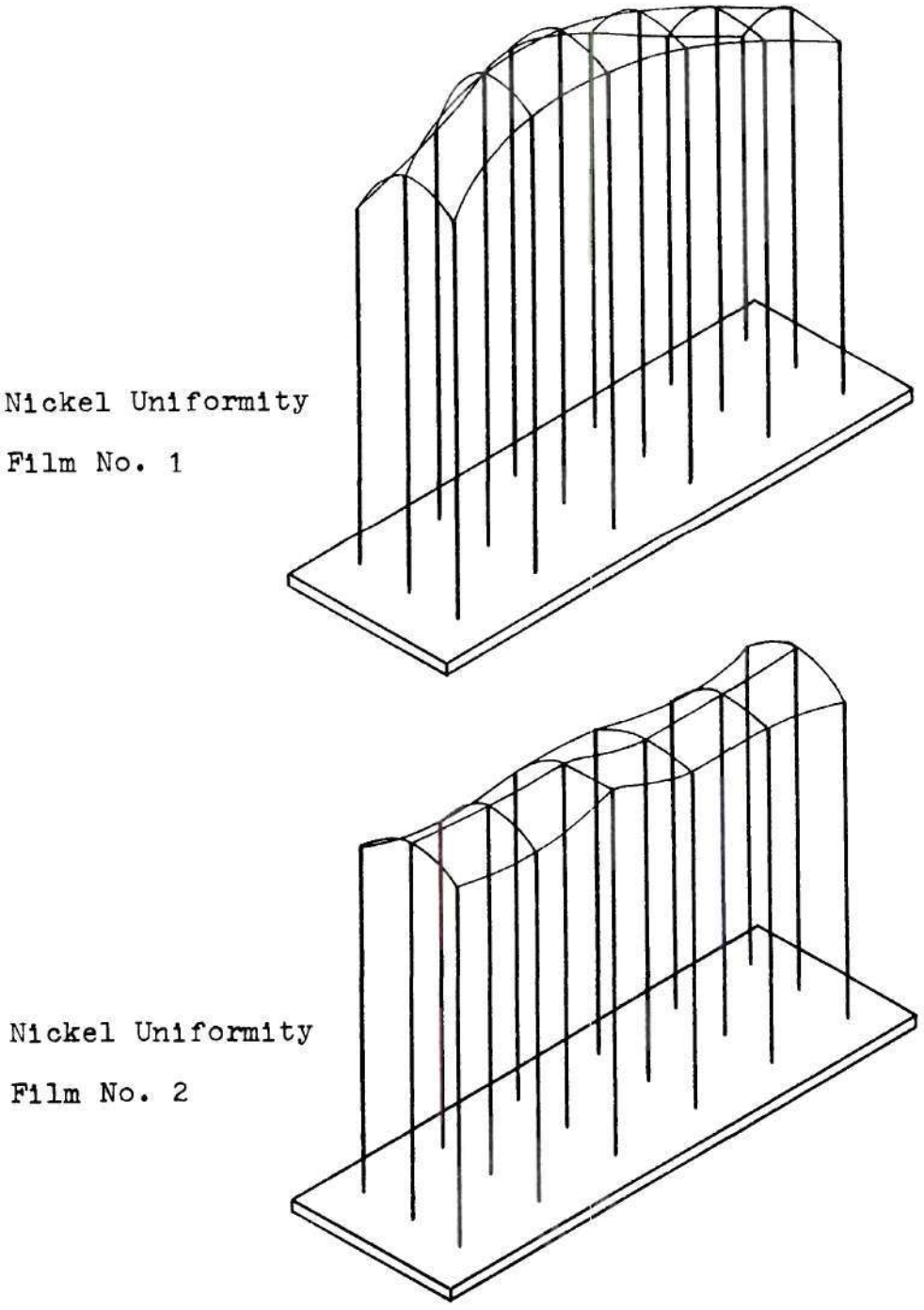

Figure 15. Thickness Profiles for Nickel Uniformity Films 1 and 2.

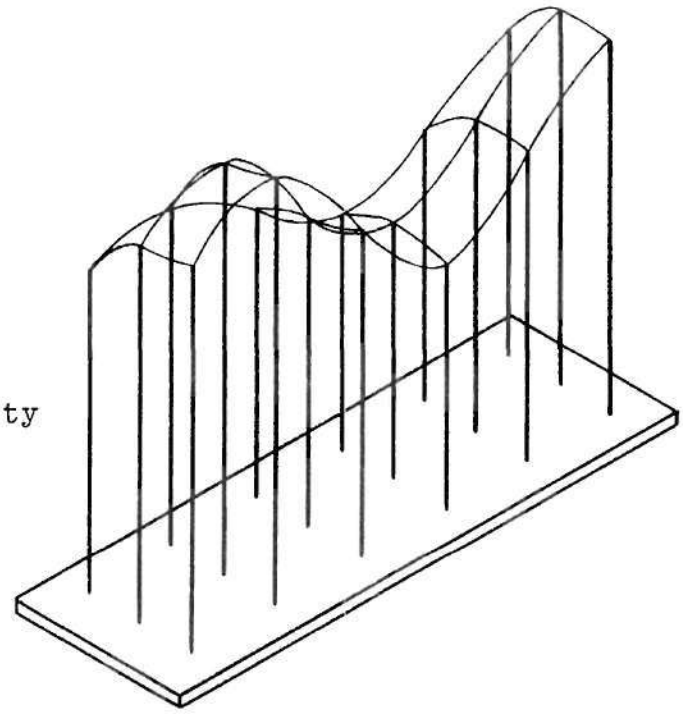

Nickel Uniformity

Film No. 3

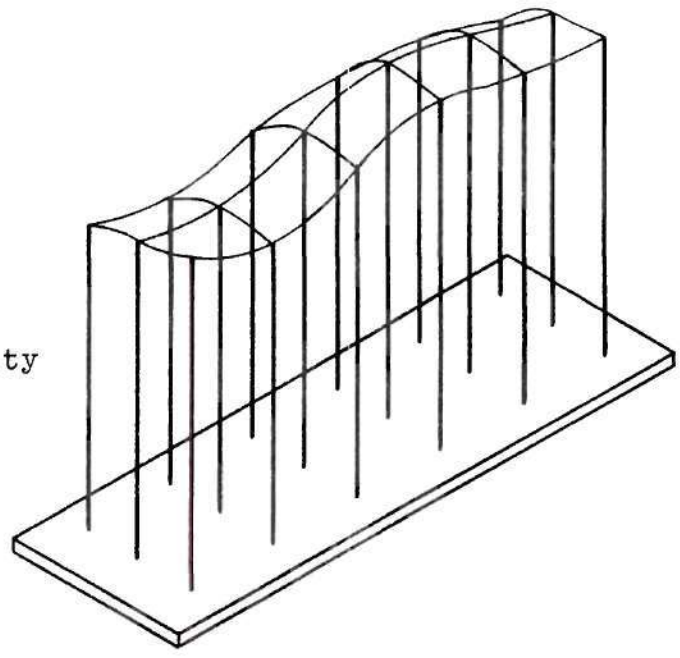

Nickel Uniformity

Film No. 5

Figure 16. Thickness Profiles for Nickel Uniformity Films 3 and 5.

Theoretical

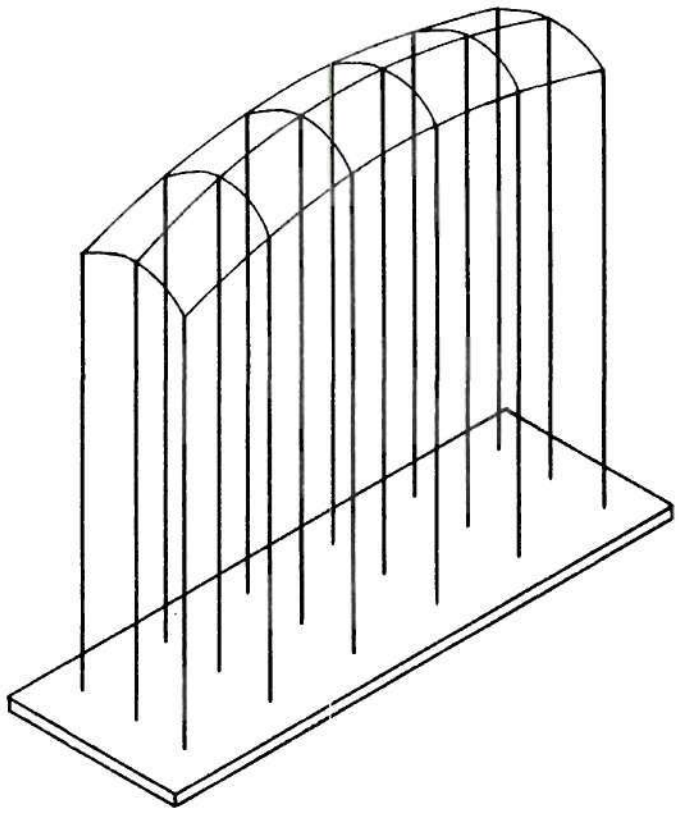

Figure 17. Calculated Thickness Profile for Nickel Uniformity Films.

of Lambert's law in the transfer of radiant energy. This assumption is justified if:

(1) The evaporation is carried out at sufficiently low pressures and evaporation rates for collisions between metal vapor molecules and gas molecules and collisions among metal vapor molecules to be negligible.

(2) Metal vapor molecules striking the receiving surface condense on first impact.

These assumptions are generally valid for metals deposited by vacuum evaporation onto clean glass substrates at pressures below 10^{-4} Torr.

Consider a differential area dS_1 of a source, radiating material from one side at a rate of m grams per second as shown in the upper part of Figure 18. The amount of material passing through the solid angle $d\sigma$ in a direction forming an angle γ with the normal to the surface in a unit time is given by:

$$dm = \frac{m}{\pi} \cos \gamma \, d\sigma. \tag{5}$$

If the material arrives at an area dS_2 on a surface inclined at an angle θ to the direction of the vapor stream, then

$$d\sigma = \frac{\cos \theta}{r^2} dS_2 \tag{6}$$

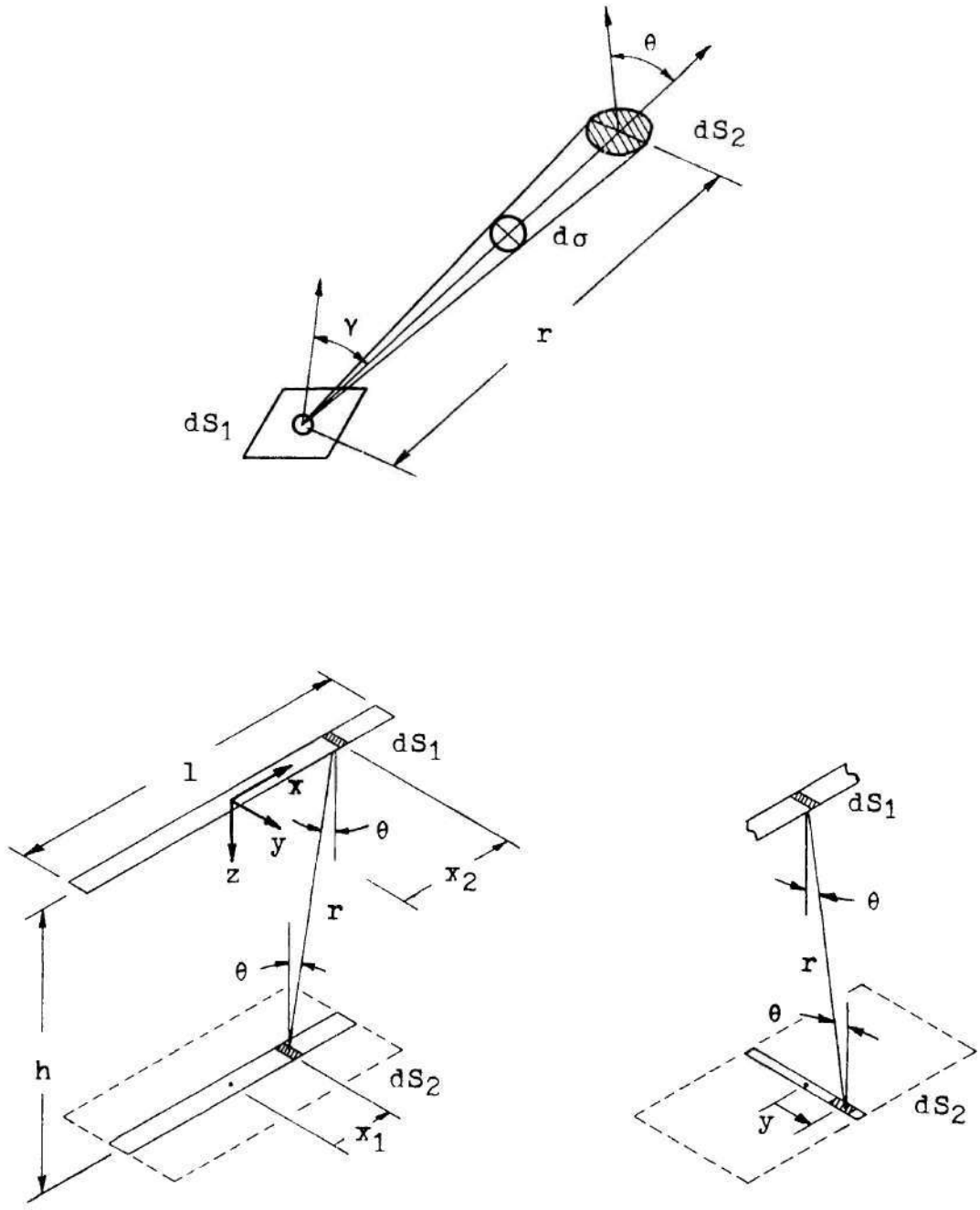

Figure 18. Geometric Arrangements for Prediction of Film Thickness Showing Small Area Sources dS_1 and Receiving Surfaces dS_2.

so that material arrives on dS_2 at the rate

$$dm = \frac{m}{\pi} \frac{\cos \gamma \cos \theta}{r^2} dS_2. \tag{7}$$

If the material has a density d grams per cubic centimeter and the thickness of the film condensed per unit time is t centimeters per second, then the volume of material deposited is $t\, dS_2$ and

$$dm = d\ t\ dS_2. \tag{8}$$

Combining (7) and (8), the thickness of the deposit on dS_2 is

$$t = \frac{m}{\pi d} \frac{\cos \gamma \cos \theta}{r^2}. \tag{9}$$

The time element can be eliminated by taking m to be the total mass and t the total thickness of metal deposited rather than the corresponding rates.

To calculate the thickness distribution along the longitudinal axis of the slide, consider a narrow strip source of length l arranged symmetrically and parallel to a narrow strip receiving surface as shown in the lower left part of Figure 18. The evaporation area $dS_1 = dx$ and $\gamma = \theta$. Note also that $r^2 = (x_2 - x_1)^2 + h^2$, and

$$\cos \theta = \frac{h}{r} = \frac{h}{\sqrt{(x_2 - x_1)^2 + h^2}}.$$

Then

$$\frac{dm}{dx_2} = \frac{m}{l}$$

and from equation (9)

$$dt = \frac{\cos^2 \theta}{\pi\, d\, r^2}\, dm = \frac{m\, h^2}{l\, \pi\, d\, ((x_2 - x_1)^2 + h^2)^2}\, dx_2. \qquad (10)$$

Integration of this latter expression gives

$$\left[t \right]_0^t = \frac{m}{2\, l\, \pi\, d} \left[\frac{x_2 - x_1}{(x_2 - x_1)^2 + h^2} + \frac{1}{h} \arctan \frac{x_2 - x_1}{h} \right]_{x_2 = -\frac{l}{2}}^{x_2 = \frac{l}{2}}. \qquad (11)$$

After application of limits, the film thickness along the longitudinal axis of the slide is given by

$$t\ (x=x_1, y=0) = \frac{m}{2\ l\ \pi\ d}\left[\frac{\frac{l}{2} - x_1}{(\frac{l}{2} - x_1)^2 + h^2} + \right. \qquad (12)$$

$$\left. \frac{1}{h} \arctan \frac{\frac{l}{2} - x_1}{h} + \frac{\frac{l}{2} + x_1}{(\frac{l}{2} + x_1)^2 + h^2} + \frac{1}{h} \arctan \frac{\frac{l}{2} + x_1}{h}\right].$$

Film thicknesses along the axis of a slide were calculated from the above equation using values of the constants measured from the vacuum system in which the films were made. The constants were:

l = 12.6 centimeters,

h = 4.73 centimeters,

d = density of nickel (8.90 grams per cubic centimeter), and

m = 0.060 grams (half the mass of metal evaporated from a wire filament).

The variation in film thickness across a slide in a direction perpendicular to the strip source was roughly estimated by assuming the same source model, as shown in the lower right part of Figure 18. From equation (9) the film thicknesses at the center of the slide (y=0) and at a point off center (y=y) are given respectively by

$$t_o = \frac{m}{\pi d} \frac{1}{r_o^2} \quad \text{and} \quad t = \frac{m}{\pi d} \frac{\cos^2 \theta}{r^2}.$$

From the figure it is clear that $r^2 = y^2 + h^2 = y^2 + r_o^2$, and

$$\cos^2 \theta = \frac{r_o^2}{r^2}.$$

Combining this with the two expressions for thickness gives

$$\frac{t}{t_o} = \cos^2 \theta \frac{r_o^2}{r^2} = \frac{r_o^4}{r^4}.$$

Evaluation of film thickness at a value of y corresponding to the off-axis positions shown in Figures 15, 16, and 17 reveals that thickness should be reduced by only 6 per cent from its value along the axis. Therefore the strip-source model is sufficient to show that film thickness is not likely to vary greatly in a direction perpendicular to the axis of the slide in the plating system used for these films. A wire source model would have led to still less expected variation.

Discussion of Thickness Uniformity Measurements

The film thickness profiles show that thickness uniformity was good in some cases and poor in others. This irregularity was caused by the peculiar behavior of nickel when it is evaporated in vacuum. Under these conditions nickel tends to alloy with filament materials such as tungsten,

molybdenum, and tantalum, leading to disintegration and breaking of the filament. Holland (53) and Sloan (54) recommend evaporation of nickel from heavy tungsten wire filaments, and Holland states that rapid disintegration of the filament can be prevented only if the weight of evaporant is less than 30 per cent of the filament weight. This condition was met in these experiments, but difficulty in obtaining useable nickel films was still encountered.

In the usual thin-film deposition system, nickel evaporates at a useful rate just above its melting point (about 1500°C). When the melting point is reached, however, nickel does not uniformly wet the filament, but flows along its surface and collects into small globules, randomly spaced about 1/4 to 3/4 inch apart. As the filament temperature is slowly increased, the globules evaporate to form a film on the substrate, the thickness uniformity of which is a function of the size and distribution of nickel globules on the filament. Too rapid an increase in filament temperature results in small beads of molten metal flying off the globules, damaging the film if they strike it and reducing the amount of nickel available for deposition. Nickel forms partial liquid phases with tungsten at all temperatures above 1500°C, so that the evaporation rate must be fast enough to give the required deposit thickness before alloying destroys the filament. Thus, the correct evaporation rate for a particular

deposition system is seen to be a compromise among several factors, and experience is needed before good quality films can be made.

The evaporant must be uniformly distributed over the filament so that the maximum permissible nickel concentration will not be locally exceeded. Satisfactory films could be made only with filaments on which nickel had been electroplated, and even then the tendency of nickel to collect into globules led to films which did not have the predicted thickness distribution. Thickness non-uniformity in evaporated nickel films is principally caused by the inability of nickel to wet uniformly the filament from which it is evaporated.

The use of nickel films in spite of these problems was continued because nickel is reported to give stable and sensitive thin film resistance thermometers, as mentioned in Chapter I.

The resistance of a heat transfer film as a function of thickness can be estimated from Figure 19. Two curves are shown, one based on the bulk resistivity of nickel and a second based on a resistivity twice that of bulk nickel as reported for evaporated nickel films 500 to 1500 Å thick by Simpson and Winding (15). Resistivity has been reported for nickel films up to about 1500 Å thick, but no reports of measurements in the range of 1500 to 2500 Å were found in the literature. Most heat transfer films in this study had room

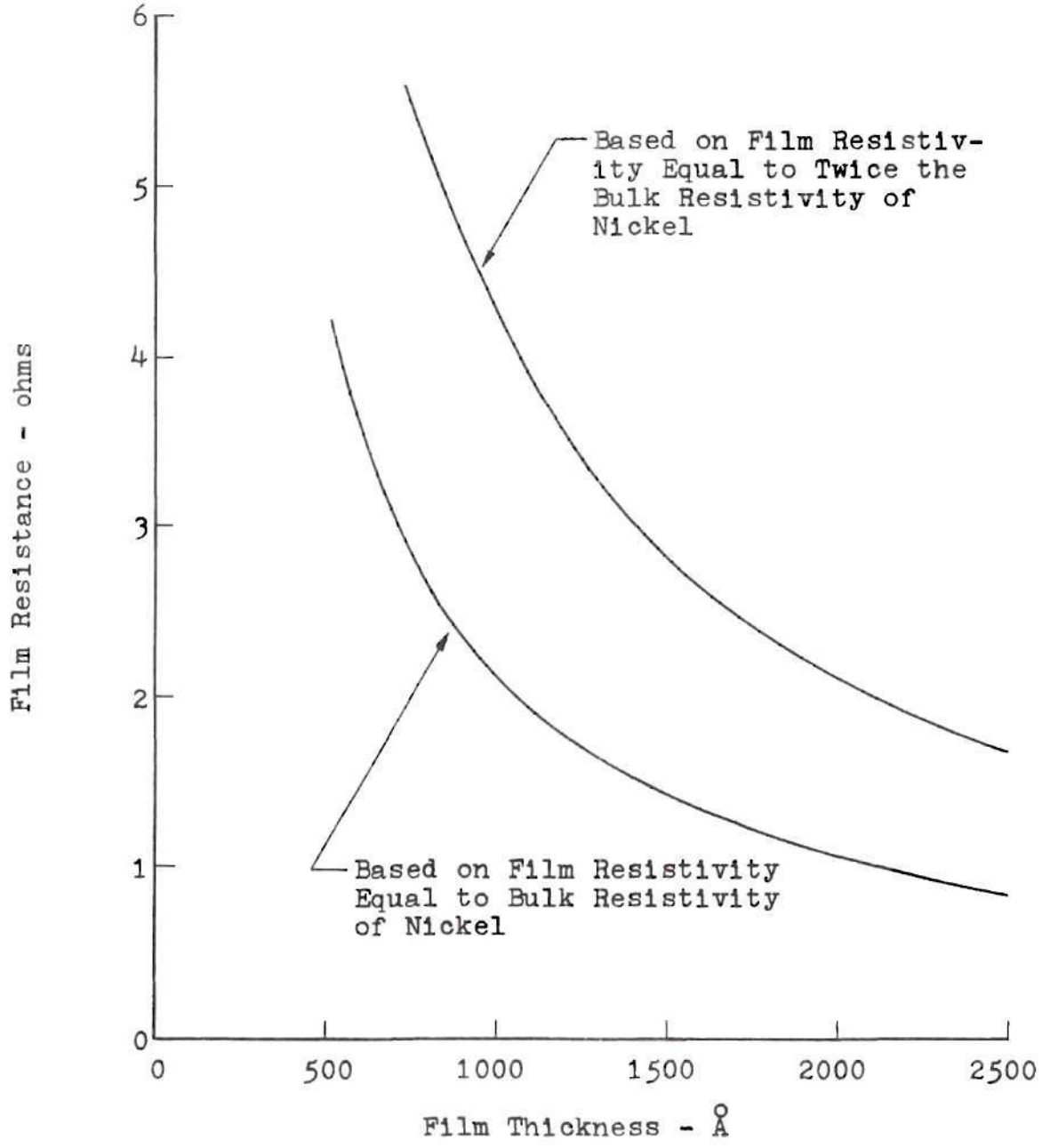

Figure 19. Estimated Resistance of a One-Inch by Three-Inch Heat Transfer Film as a Function of Thickness.

temperature resistances of 1.8 to 2.5 ohms and probable thicknesses of about 2000 Å. This points to the conclusion that the upper curve in Figure 19 best represents the resistance as a function of thickness for these films.

Exact determination of the effect of film thickness non-uniformity on the heat transfer data is difficult. The largest variations in thickness occurred along the longitudinal axis of the heat transfer element. If thickness variation along this axis is considered, the film can be pictured as a group of narrow strips side by side and connected in series. It is evident that the current across each strip is constant, and, since $P = I^2R$, the thinner sections of the film will dissipate more power and operate at higher temperatures than the thicker sections. The increase in resistance associated with heating can be largely attributed to the thinner parts of the film. Then measured temperatures and heat fluxes would be lower than true values for thinner parts of the film. Conversely these parameters would be higher than the true values on the thicker parts of the film. The average heat flux and temperature and the measured heat flux and temperature, lie between the extremes associated with thin and thick areas.

Films with unusually low burnout heat fluxes are suspected of having large variations in thickness. Films with substantial thickness variations and holes visible to the eye

when the film was held up to a bright light were of course discarded, but thickness monitoring of each film was not possible because of limitations on the size of sample that could be put into the x-ray fluorescence apparatus.

Three of the four nickel uniformity films showed thickness variations not drastically different from that predicted by theory. If this average held throughout the heat transfer films, the heat transfer data, except for films with abnormally low burnout heat fluxes, should closely represent the actual conditions of temperature and heat generation rate.

CHAPTER V

RESULTS AND DISCUSSION OF HEAT TRANSFER MEASUREMENTS

The experimental techniques used for collecting heat transfer data have been explained in detail in Chapters II and III. This was considered important because many of the methods employed in this investigation have not been described before, and a sizeable part of the total effort was directed toward coordinating the separate parts of the procedure. At the present stage, experimental data have been obtained in the form of instantaneous temperatures and rates of heat generation in the thin film heat transfer element.

Since the metal films were in intimate contact with quartz substrates and film temperatures increased rapidly during experimental runs, heat flux to the substrates required consideration. If measurements had been made in steady state, the substrates low thermal conductivity would have caused most of the heat to be transferred to the water pool. But in transient experiments the conduction of sensible heat to a substrate was far from negligible.

Heat Conduction to the Substrate

To develop an expression for heat conduction to the substrate, certain assumptions were required. First, edge

effects were neglected, and the temperature of the front of the substrate was taken equal to the measured film temperature. Thus, the heat conduction case examined was an infinitely wide plate of thickness L, with a front side temperature equal to the film temperature and back side temperature equal to the water temperature (the system initial temperature). Second, the front-side temperature was assumed to increase as a linear function of time. Plots of film temperature versus time are shown for each test in Appendix III, and this assumption appears to be reasonable for the purpose of estimating slide heat flux. Errors introduced by using a linear function of time to express temperature were small when errors from other sources were considered.

Carslaw and Jaeger (55) discuss the use of Laplace transformation methods for solving problems of heat conduction in linear flow. Using their methods the following expression for heat conduction from a thin film to a glass substrate can be developed:

$$\left(\frac{q}{A}\right)_s = - k \left.\frac{d\theta}{dx}\right|_{x=0,t} = \frac{2kC(t)^{\frac{1}{2}}}{\sqrt{\alpha}} \sum_{n=0}^{\infty} \left[i\,\mathrm{erfc}\,\frac{nL}{\sqrt{\alpha t}} + i\,\mathrm{erfc}\,\frac{(n+1)L}{\sqrt{\alpha t}} \right]. \qquad (13)$$

This derivation is shown in Appendix I for the system speci-

fied here, along with an alternate derivation for the special case of short run duration. Variables are defined in Appendix I, and equation (13) has been set up there in a table to aid computation.

It is instructive to examine the temperature profile in a quartz slide after a run has begun. Jakob (56) gives a table from which temperature profiles in a flat plate can be calculated when the temperature of both surfaces is changing linearly with time. This table applies to an infinitely wide plate of finite thickness. If the cool side of the quartz slide is placed at the midplane of the plate, an accurate picture of the temperature profiles in the slide can be obtained until the cool-side temperature appears to rise.

The temperature profiles for a case typical of short-duration tests in this study are plotted in Figure 20. In this example the surface temperature increased at a rate of 210°F per second and burnout occurred at about 1.25 seconds. From Figure 20 it is seen that the temperature at the cool side of the slide is not affected by conditions at the hot side until about one second has elapsed. Thus, the heat flux to the slide is the same as that to a semi-infinite solid for about the first second in runs of this type.

Similar plots of the temperature profiles for a run of about 20 seconds duration lead to the observation that the semi-infinite solid model would adequately describe the tem-

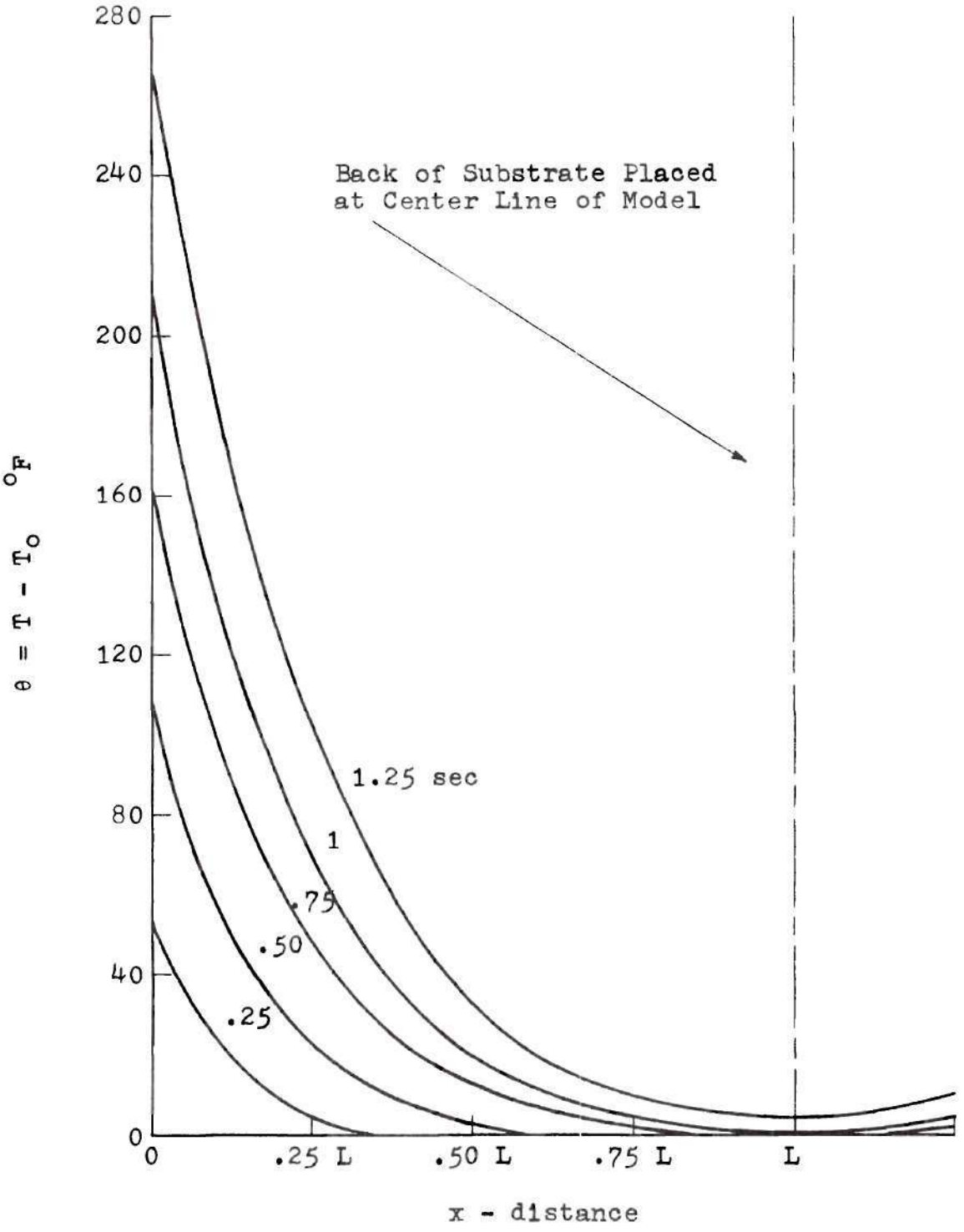

Figure 20. Temperature Distributions in an Infinitely Wide Plate of Finite Thickness with Surface Temperatures Increasing Linearly with Time.

perature in the slide, and thus the heat flux, for about two seconds.

Heat flux to the substrate was calculated by the analytical method summarized here and described in Appendix I until the film temperature ceased to rise linearly with time. In short-duration tests (Nickel Films 18, 20, 22, 34) the film temperature was approximately a linear function of time throughout the run. In longer-duration tests, however, this approximation held only until nucleate boiling began. Then the film temperature appeared to drop a few degrees and afterward increased slowly until burnout occurred.

If the film temperature changes slowly during nucleate boiling, heat flux through the substrate will approach a steady-state condition. Heat generation in the film at this time was 75,000 to 100,000 Btu/hr-ft^2 and the steady-state value of slide heat flux was 10,000 to 12,000 Btu/hr-ft^2. Since heat flux to the water was given by

$$\left(\frac{q}{A}\right)_w = \left(\frac{q}{A}\right)_f - \left(\frac{q}{A}\right)_s \qquad (14)$$

a relatively large error in estimating $\left(\frac{q}{A}\right)_s$ could be tolerated before its effect on $\left(\frac{q}{A}\right)_w$ became important.

The effect of assuming steady-state heat flux through a substrate when nucleate boiling begins should be examined. Consider the behavior of the temperature profile in a quartz

slide after the surface temperature has ceased to rise and remains for several seconds at some constant temperature. After a sufficiently long time the system will reach steady state, and the temperature profile will be linear through the slide. In a typical long experiment the surface temperature reached a steady value of 275°F at a time equal to 3.75 seconds. At this instant the temperature was given by equation (15), which is developed in Appendix I:

$$\theta_{x,t} = Ct \sum_{n=0}^{\infty} \left[4\, i^2 \operatorname{erfc} \frac{x + 2nL}{2\sqrt{\alpha t}} - 4\, i^2 \operatorname{erfc} \frac{(n+1)2L - x}{2\sqrt{\alpha t}} \right] \qquad (15)$$

where C = slope of temperature plot = 49.3 °F/sec,

t = time to incidence of nucleate boiling = 3.75 sec,

and other variables are as defined in Appendix I. The terms in the sum are tabulated as a function of the argument by Carslaw and Jaeger (57). The temperature profile at this time is represented by the heavy line in Figure 21.

Since the problem of observing the change in this temperature profile by analytical techniques would be quite formidable, a graphical method was used. The Schmidt technique as described by Kreith (58) and Jakob (59) is suitable for

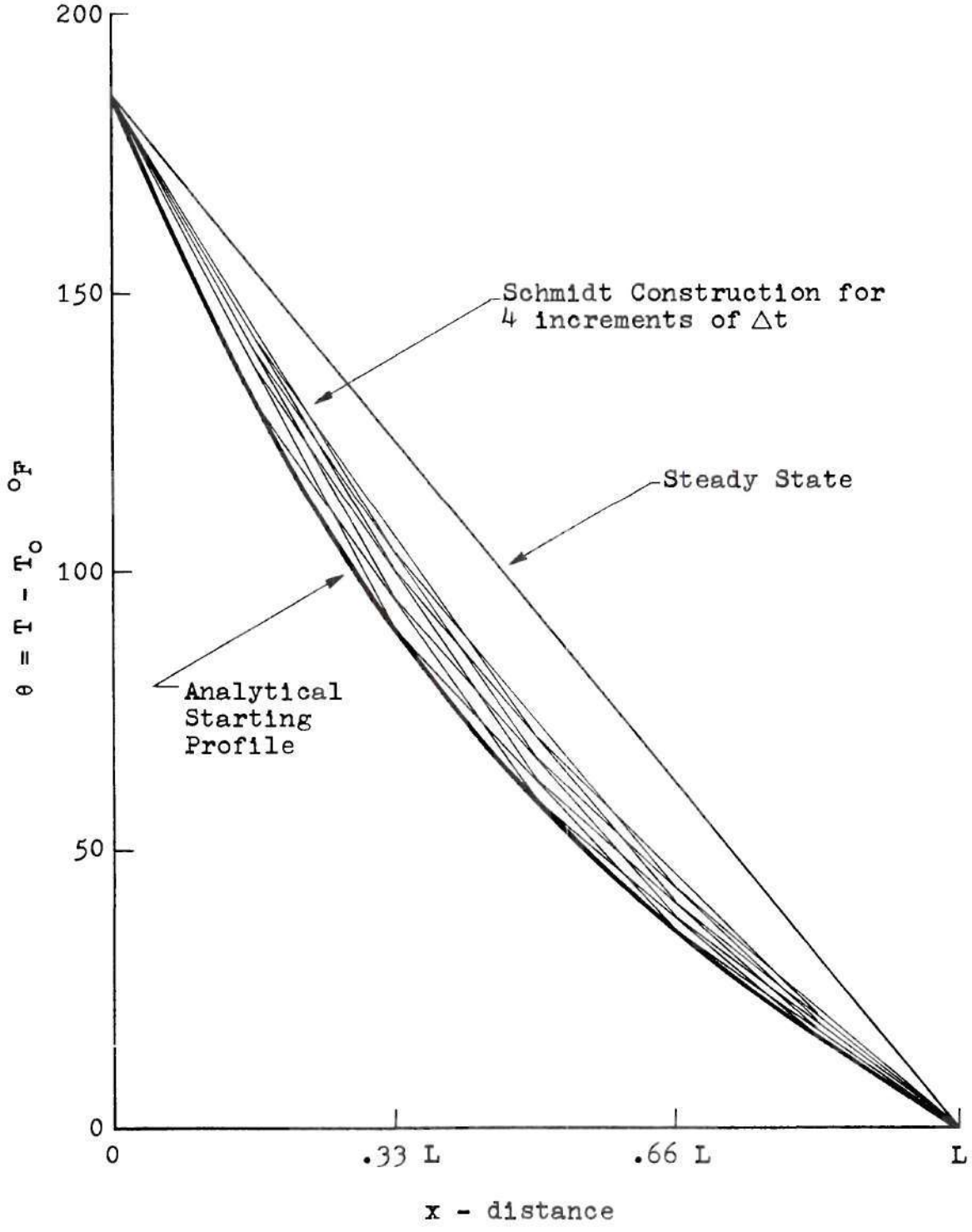

Figure 21. Behavior of Substrate Temperature Profile After Nucleate Boiling Begins.

this purpose. Increments of distance (Δx) and time (Δt) are chosen for convenience so that

$$\frac{(\Delta x)^2}{2\,\alpha\,\Delta t} = 1.$$

Six increments of x were taken, and $\Delta x = \frac{L}{6} = 0.00173$ foot. Then

$$\Delta t = \frac{(\Delta x)^2}{2\alpha} = 0.154 \text{ second.}$$

The averaging of temperatures can be done graphically or arithmetically. A graphical construction for four increments of time is shown in Figure 21.

It is evident that $\frac{d\theta}{dx}$ and heat flux approach their steady-state values asymtotically, and Figure 21 shows that after three or four increments of Δt they have accomplished half this transition. Thus, within one-half second after the front side has reached a "steady" temperature the slide heat flux has approached half way to the steady-state value.

Experimental measurements indicated that during extended runs (longer than five seconds) the film temperature reached a maximum and dropped ten degrees or more before rising again. There would be a corresponding drop in heat flux to the slide superimposed on the effect just discussed. Decrease of the surface temperature would accelerate the

approach to a "steady state" condition by reducing the surface temperature gradient. In any case, the heat flux to the slide at this stage in the run was less than 20 per cent of the rate of heat input to the metal film. An error of 20 per cent in estimating the heat flux to the slide would result in an error of less than 5 per cent in estimating heat flux to the water.

Since a more elaborate technique appeared unwarranted in view of the errors involved, the heat flux to the slide on extended tests was calculated as follows:

(1) During the early part of the test a surface temperature rise linear with time was assumed, and the heat flux was given by equation (13), as with short runs.

(2) From the time that the surface temperature reached a maximum, the heat flux to the slide was given by

$$\left(\frac{q}{A}\right)_s = k \frac{T_f - T_o}{L}$$

Experimental Heat Transfer Measurements

Data for each heat transfer experiment are tabulated in Appendix II and plotted in Appendix III.

Heat Flux versus Temperature Data

Figures 22, 23, 24, and 25 summarize the heat flux curves for the experiments of this study. Results are grouped in each figure according to similarities in experimental conditions, e.g., film orientation, type of power, and test dura-

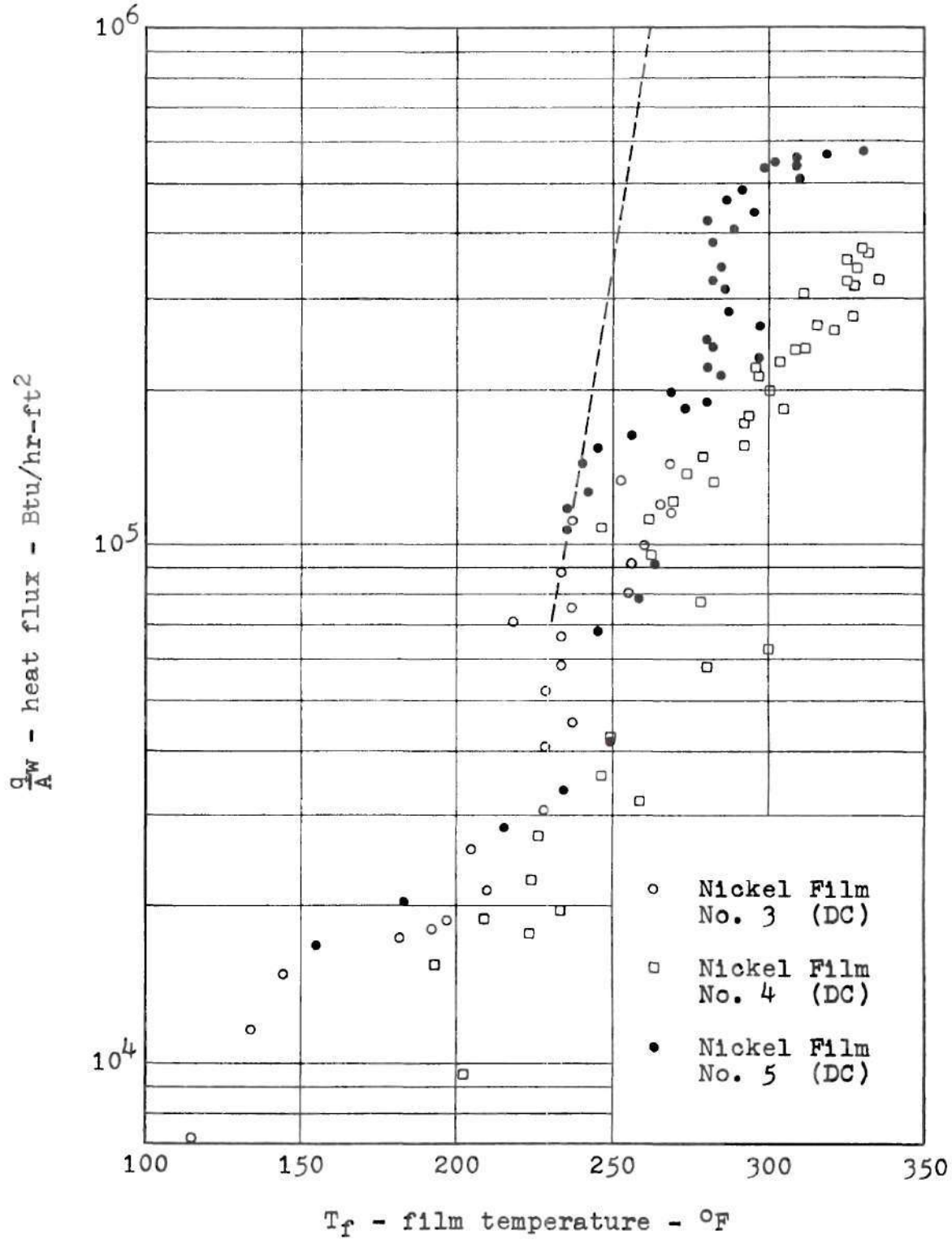

Figure 22. Heat Flux Curves for Horizontal Heat Transfer Films in Long-Duration Tests. (Dotted line taken for reference from Figure 26.)

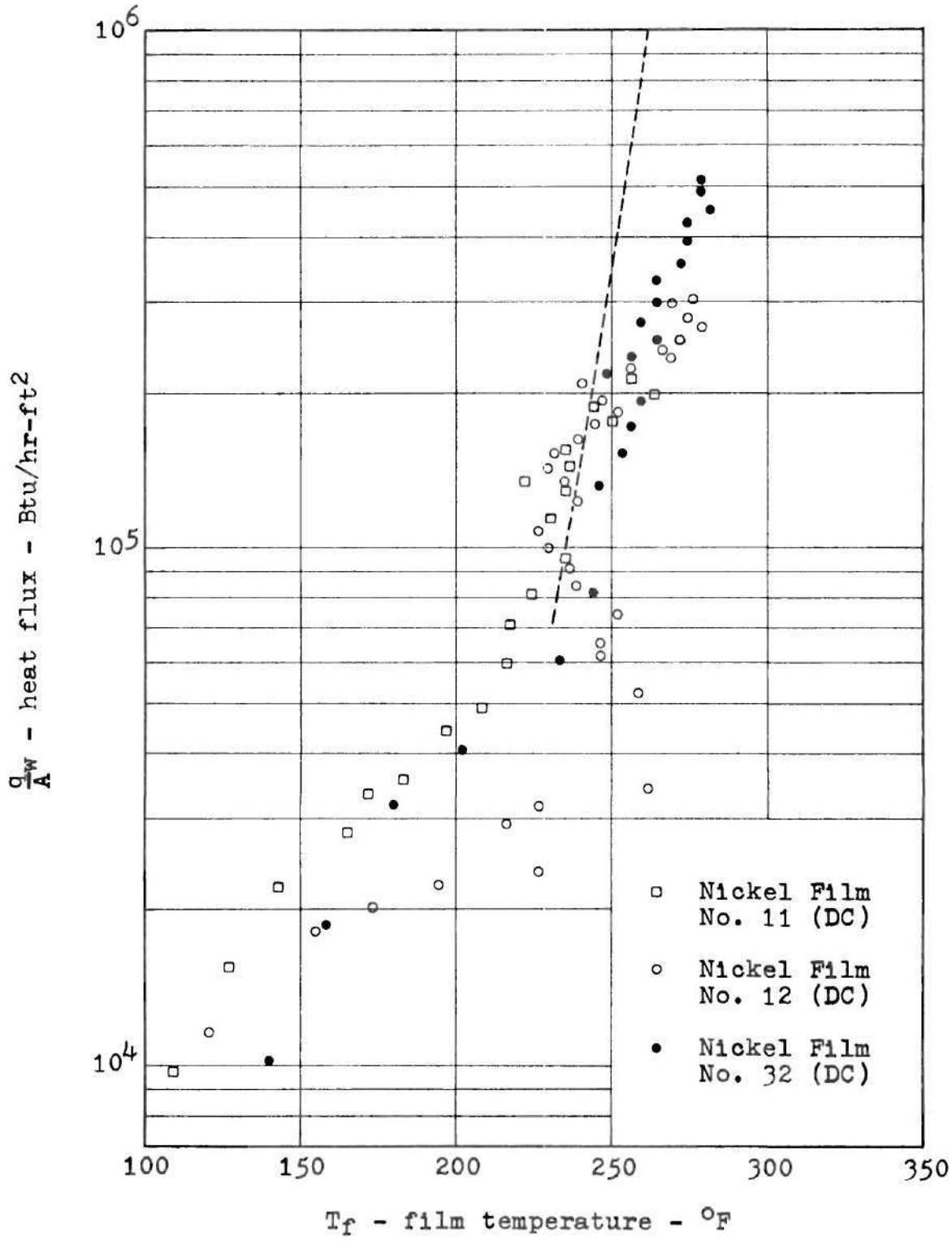

Figure 23. Heat Flux Curves for Vertical Heat Transfer Films in Long-Duration Tests. (Dotted line taken for reference from Figure 26.)

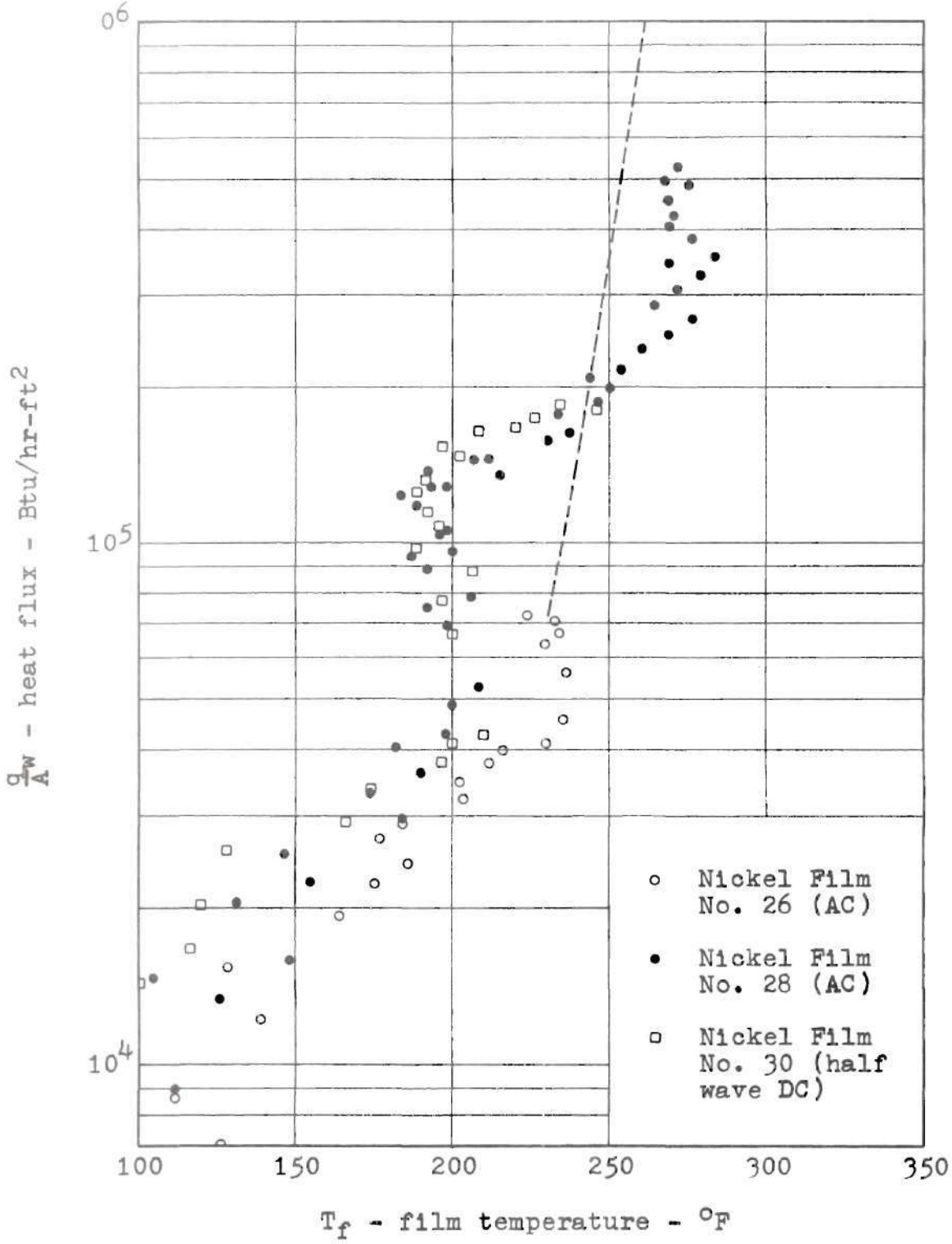

Figure 24. Heat Flux Curves for Horizontal Heat Transfer Films in Long-Duration Tests Using AC and Half-Wave DC. (Dotted line taken for reference from Figure 26.)

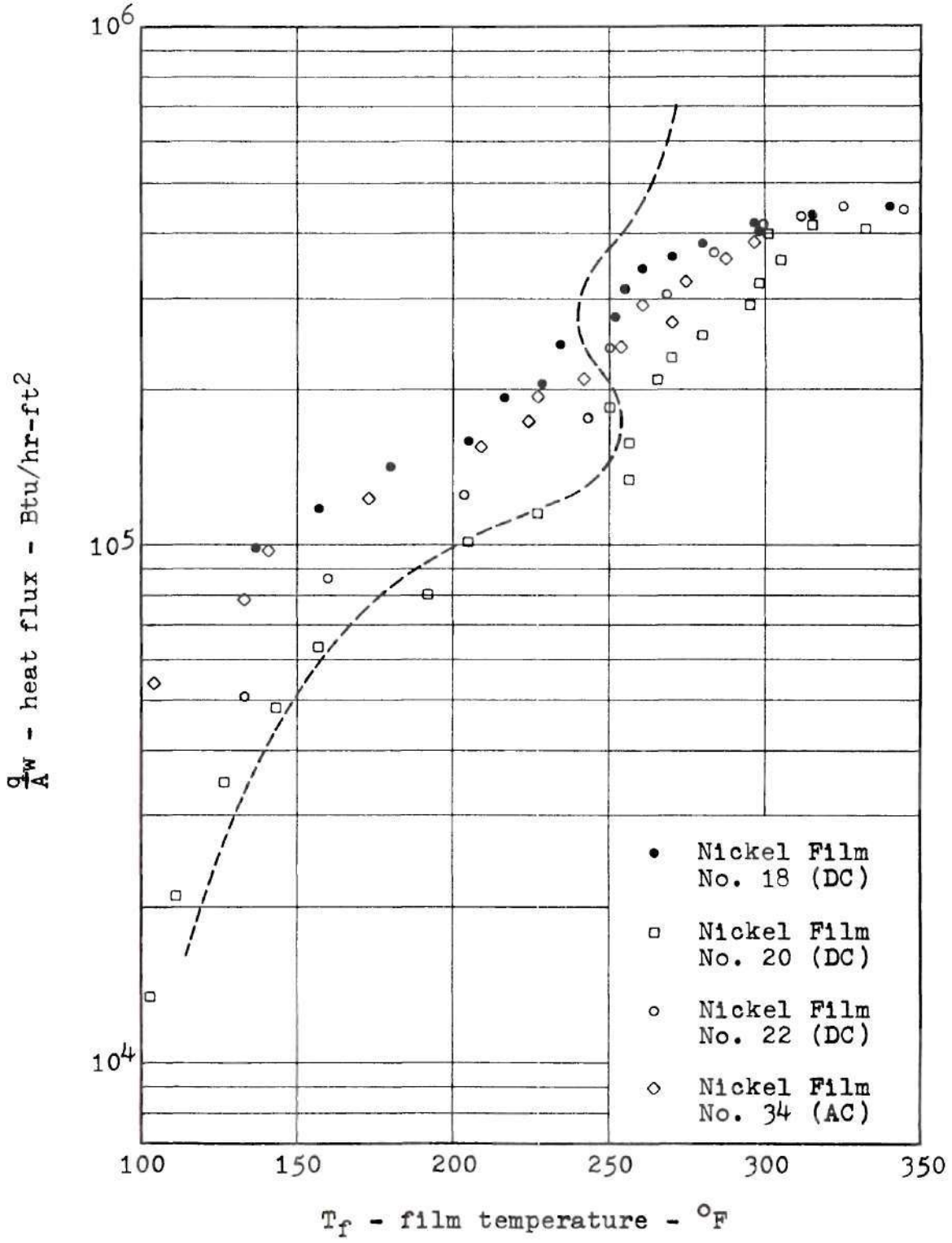

Figure 25. Heat Flux Curves for Horizontal Heat Transfer Films in Short-Duration Tests. (Dotted line taken for reference from Figure 26.)

tion (rate of increase in power). Distilled water at ambient temperature was used in all experiments. Bulk temperatures ranged from 68 to 85°F, but were mostly between 70 and 80°F. Subcooling can be considered essentially constant.

Heat flux versus temperature data for boiling in the literature are ordinarily plotted on logarithmic scales. This practice was not followed in this report because a linear temperature scale provided a clearer picture of the experimental points. The scatter in the data was such that preparation of a general correlation of heat flux and temperature for these experiments was considered inadvisable.

Figure 26 shows published experimental data used for comparison. The data of Gunther and Kreith (25) and Bergles and Rohsenow (41) are for steady-state pool boiling on horizontal ribbons and tubes, respectively, at bulk water temperatures less than 100°F. These data were taken from published curves and therefore are influenced by uncertainties inherent in reading the authors' plots. Duke and Schrock (42) give experimental points as shown in Figure 26 for steady pool boiling of water at a bulk temperature of 90°F on a horizontal plate. A curve through their points is shown for reference in Figures 22, 23, and 24. The transient pool boiling curve of Johnson et al. (17) represents data for a horizontal platinum ribbon when the power level was increasing exponentially with a period of about 90 milliseconds. The bulk water temperature was 100°F and the rate of increase in power was

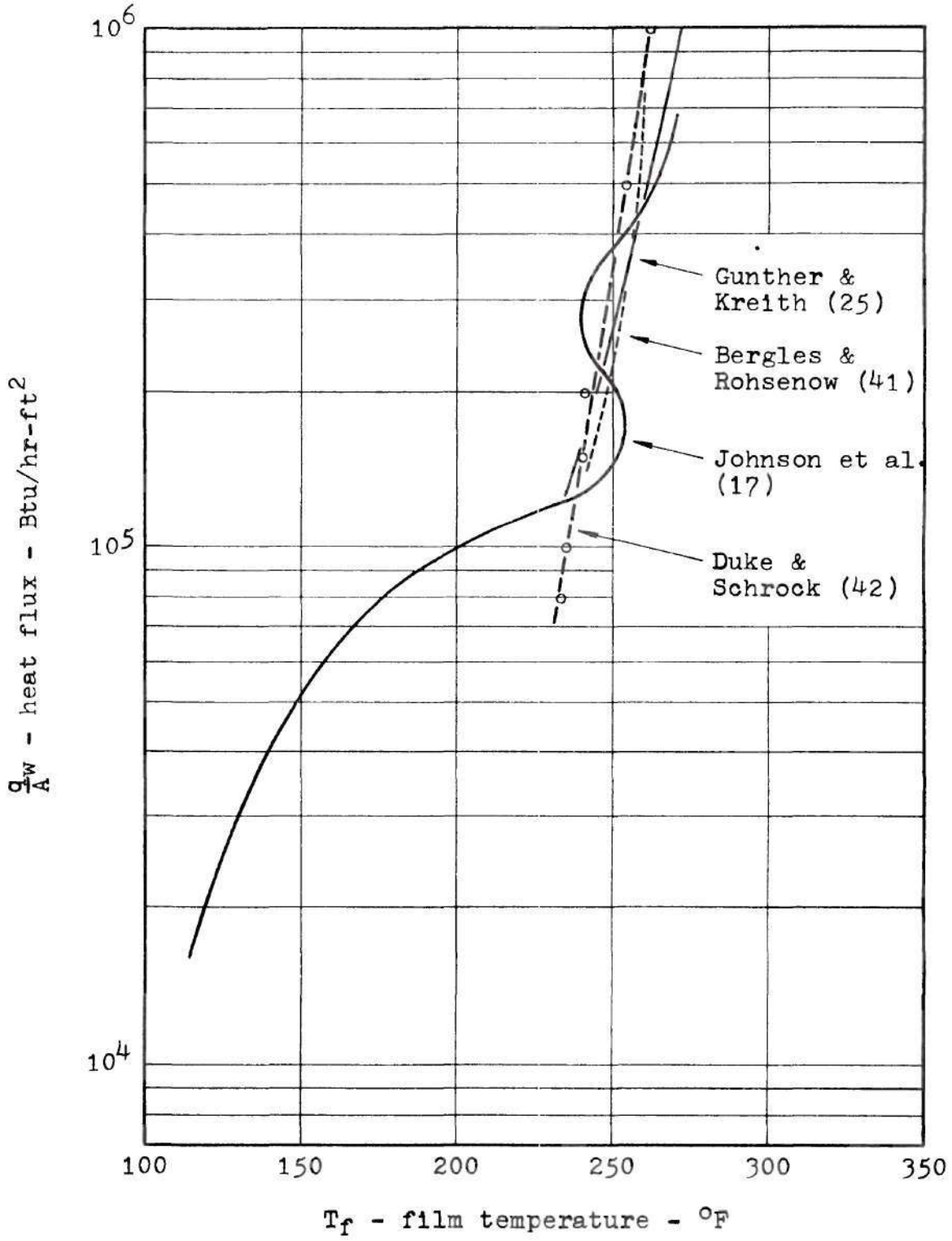

Figure 26. Heat Flux Curves from Literature for Subcooled Pool Boiling.

roughly twice that used for transient experiments in this study. These data, like those of Gunther and Kreith and Bergles and Rohsenow, were taken from curves published by the authors. The curve of Johnson et al. is shown for reference in Figure 25.

Figures 22 and 23 show the results of tests in which the heat transfer films were oriented horizontally and vertically, respectively. The power level was increased slowly (by the standards of this study) until burnout occurred. Film temperature was seen to increase with heat flux until the incidence of nucleate boiling, when it dropped a few degrees, then increased slowly until the film burned out. There was considerable scattering of temperatures within individual experiments, but this must have been caused by uncertainties in determining temperature rather than actual temperature fluctuation. Temperature fluctuations of 30°F have been measured at individual nucleation sites (30)(60), but it is most unlikely that fluctuations of this magnitude could occur on a surface as large as a heat transfer film. The fairly large systematic temperature difference among some runs was also most likely caused by errors in temperature determination. Nickel Films 3 and 4 were the first useable experiments in this study. Their exceptionally wide scatter should probably be attributed to lack of experience on the part of the investigator.

An unexpected phenomenon was found in Figure 24, which shows the heat flux curves for tests using ac and half-wave dc heating. In Nickel Films 28 and 30 the film temperature appeared to drop well below the boiling point of water at heat fluxes clearly indicating the presence of nucleate boiling. The data points followed trends typical of long-duration tests in this study, but at lower temperatures than expected. The tape recording of test 28 was rephotographed and calculations were performed twice with no significant difference in results. As will be discussed later, temperature fluctuations were detected which might account for boiling heat transfer with an average film temperature below the boiling point. Rather large errors in calibration of the recording system may have been responsible for these results. However, experiments made before and after the test of Figure 24 did not reflect such unexpected behavior and the agreement among tests in Figure 24 was better than average. Thus they could not be easily dismissed as containing large calibration errors.

Figure 25 shows the results of the short-duration or rapid-transient tests of this study. Alternating and direct current heating were used. These lasted from 0.67 to 1.20 seconds and agreed fairly well among themselves. They did not, however, display the prominent temperature "overshoot" reported by Johnson et al. (17) in the referenced boiling curve.

The general tendency of heater temperatures to "overshoot" the boiling point in subcooled transient boiling has been observed by Johnson et al. (17), Rosenthal (44), and Lurie and Johnson (45). The overshoot occurs with the initiation of nucleate boiling and is more pronounced with increased subcooling. It becomes less pronounced as the rate of power increase becomes smaller. The overshoot phenomenon was clearly visible in most of the long-duration tests of this study. With the exception of Nickel Film 20 it was seen only as a sudden change of slope in the fast transient runs.

In the reference curve of Figure 25 the time between the maximum and minimum temperatures during the overshoot period was about 25 milliseconds. The corresponding time for test 20 was 50 to 100 milliseconds. The experimental points in Figure 25 were photographed from the oscilloscope screen at intervals of five seconds, equivalent to intervals of 25 milliseconds in the heat transfer runs. Since the overshoot phenomenon occurred over a time interval of the same order of magnitude as the time between data points, it is possible that the maximum and minimum temperatures were simply missed by the camera when data were photographed. The sweep time of the oscilloscope was about two seconds, and every second sweep was photographed, so it is also possible that the temperature maxima and minima were in the photographs but masked by power supply ripple.

In all the experiments of this study, heater temperature increased with heat flux more rapidly than in the reference curves. The reason for this may be seen in Figure 27 which shows a sequence of photographs made during a long experimental test. The pictures clearly show that in the late stages, boiling was not uniform over the area of the metal film. A similar series of pictures revealed the same behavior in another test, and it is thought to have been typical of all tests of this study. The film-thickness uniformity measurements described in Chapter IV show that substantial non-uniformity existed in the nickel heat-transfer films. Since power dissipation from an area of film is inversely proportional to the square of thickness, the local heat flux in a thin area may be far higher than the average heat flux.

In calculating heat transfer parameters from raw experimental data, there is no way to identify the "active area" of a thin film. Calculations must be based on the total film area of assumed uniform thickness. The use of other metals which can give more uniform evaporated films increases the difficulty of measuring temperature accurately, because other candidate metals have lower temperature coefficients of resistivity. Probably the best approach is to try to prepare more uniform nickel films by other methods, such as vapor phase deposition or the use of "liquid bright" metals.

Burnout

The burnout conditions for the experiments are listed

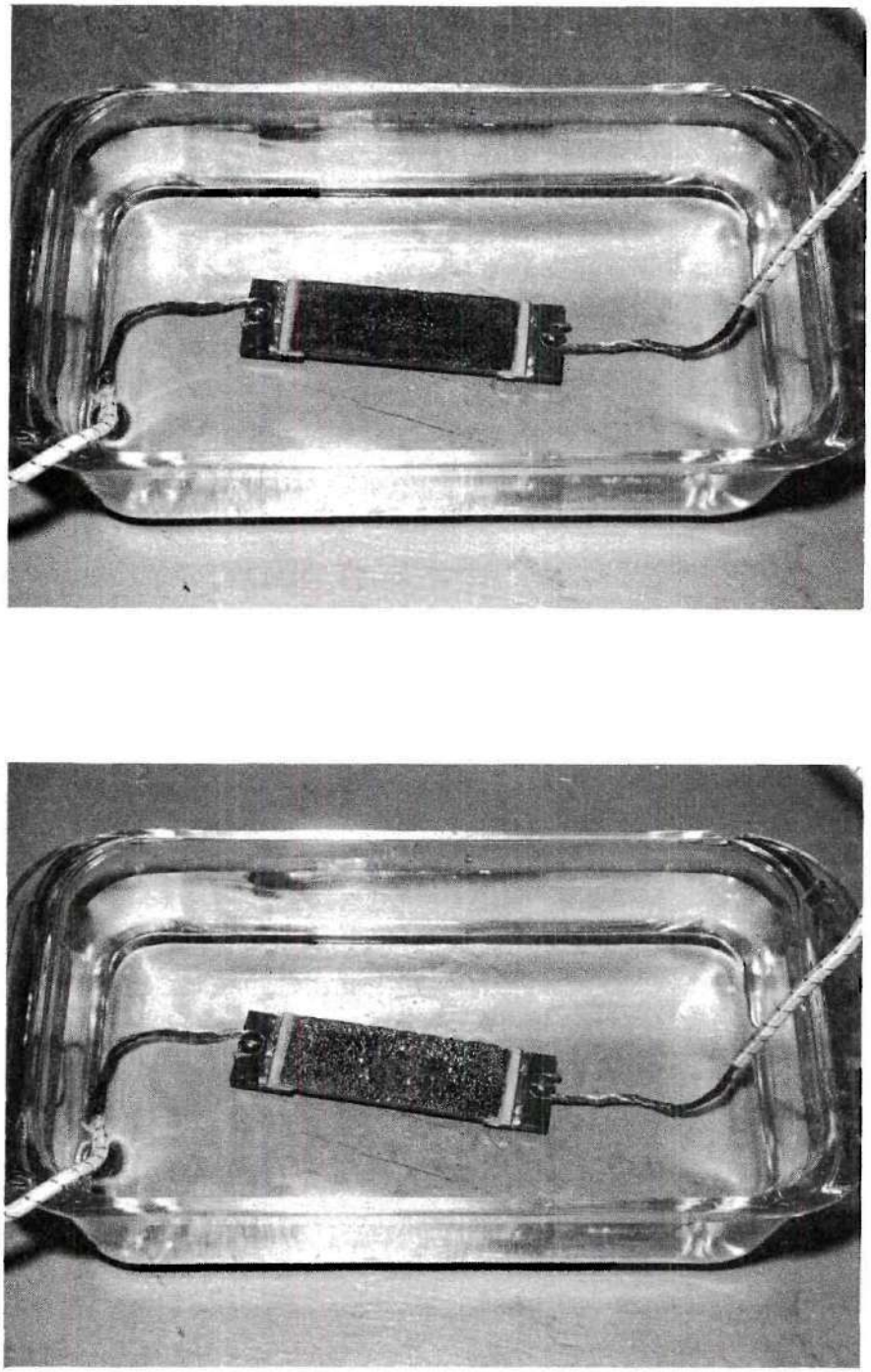

Figure 27. Photographic Sequence Showing Heat Transfer Film During and After Experiment.

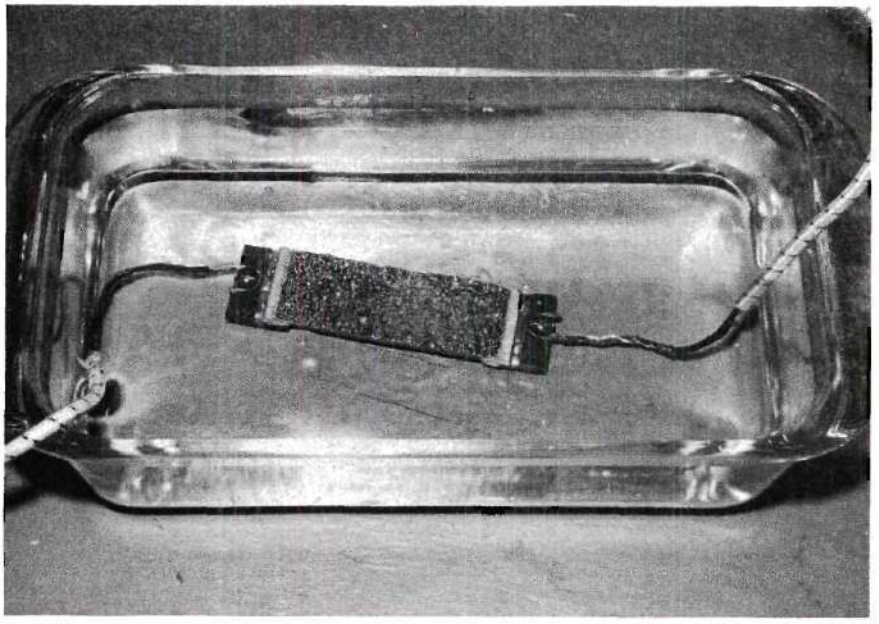

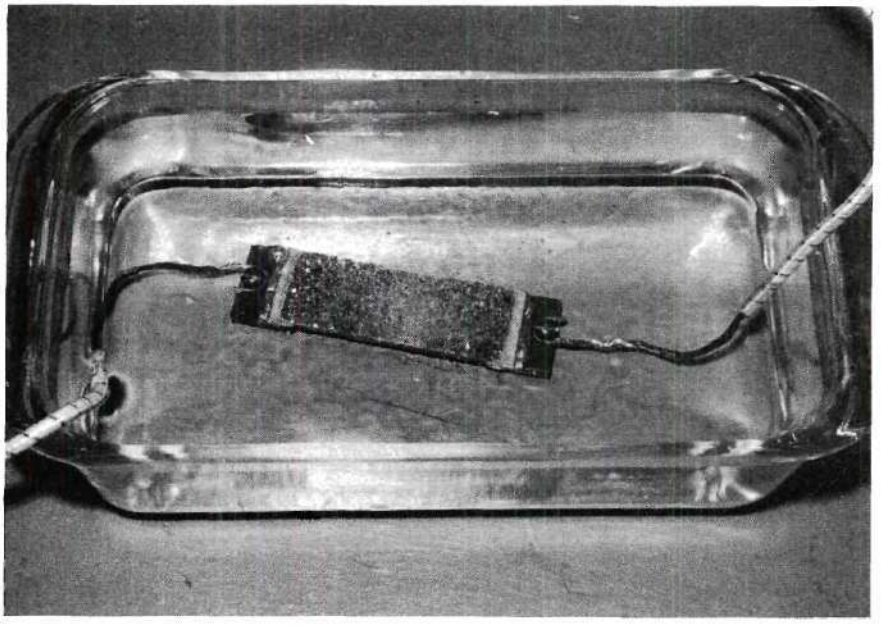

Figure 27. (Continued) Photographic Sequence Showing Heat Transfer Film During and After Experiment.

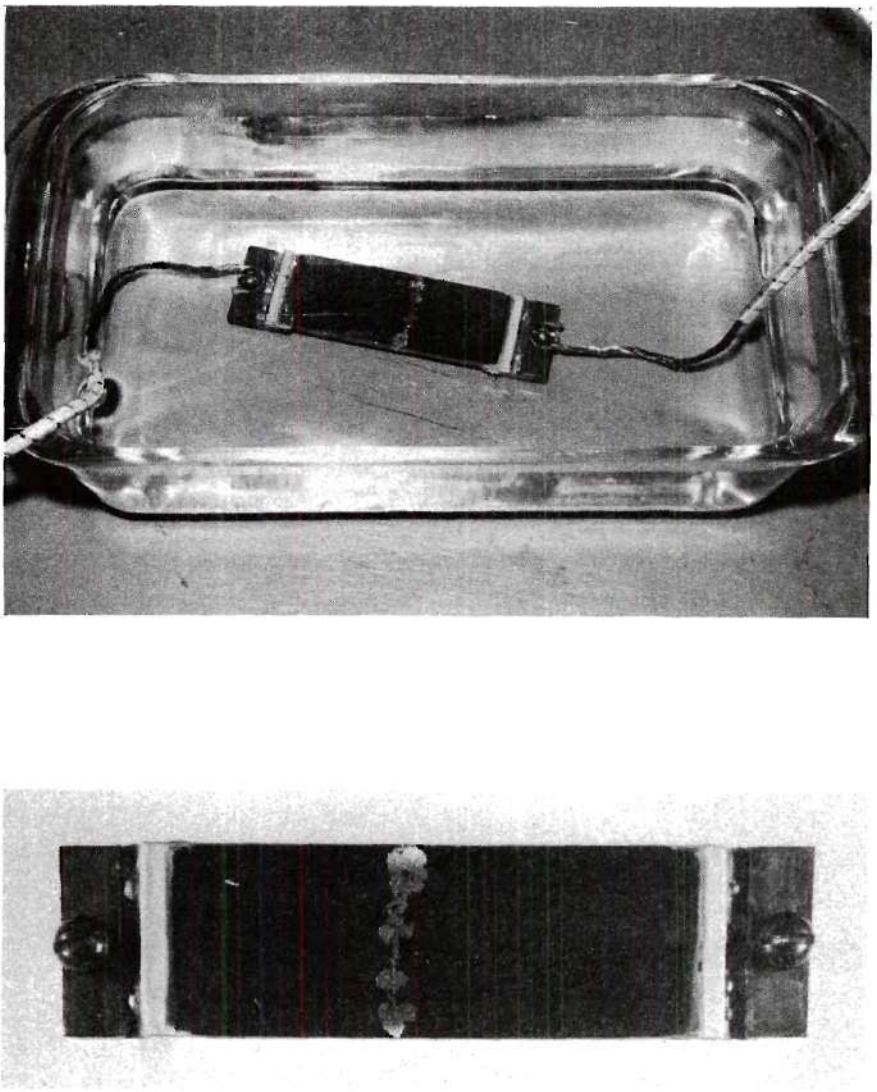

Figure 27. (Continued) Photographic Sequence Showing Heat Transfer Film During and After Experiment.

in Table 1. At least one test in each group reached a maximum water heat flux of more than 450,000 Btu/hr-ft^2. Tests with maximum water heat fluxes of less than 400,000 Btu/hr-ft^2 probably burned out prematurely because of severe thickness non-uniformity, flaws in the metal film, or imperfect end connections.

The several correlations of burnout heat fluxes discussed in Chapter I predict values of about 2,000,000 to 3,000,000 Btu/hr-ft^2 for pool boiling at the level of subcooling used in this investigation. The burnout heat fluxes in this study are seen in Table 1 to have varied rather widely with a maximum of 575,000 Btu/hr-ft^2. These low apparent values were partly caused by film non-uniformity effects as discussed in the previous section.

Bernath (46) explains the mechanism determining peak heat flux with boiling from wires as follows:

> When the diameter of the heater is of the same order of magnitude as the mean diameter of the bubbles formed on the surface, the number of "coincident" bubbles--those generated within a period less than the mean lifetime of bubbles on the surface--required to form a coherent vapor film is relatively small. And the larger the diameter of the heater, the larger is the number of coincident bubbles required to blanket the surface and consequently the higher is the heat flux at burnout.

Bernath further states that the effects of thickness of the boiling film and of the heater wall are combined in the Biot modulus: $N_B = hR/k$ for wires and $N_B = hL/k$ for plates or thin films, where L is the plate thickness. In a boiling liquid, the thickness of the boiling film is proportional to

Table 1. Summary of Experimental Heat Transfer Data

Nickel Film Number	Type of Power	Test Duration (sec)	Maximum Heat Flux to Water $(\frac{Btu}{hr\ ft^2})$	Film Temp at $(\frac{q}{A})_{wmax}$ (^oF)	Location of Failure
	Long-Duration Tests		(horizontal - Figure 22)		
3	DC	17.0	144,000	268	middle
4	DC	22.65	377,000	330	end
5	DC	22.3	575,000	330	middle
	Long-Duration Tests		(vertical - Figure 23)		
11	DC	13.0	213,000	256	end
12	DC	18.5	304,000	276	end
32	DC	6.5	518,000	278	end
	Long-Duration Tests		(horizontal - Figure 24)		
26	AC	9.6	73,900	223	end
28	AC	23.15	524,000	272	middle
30	half-wave DC	8.25	187,000	234	end
	Short-Duration Tests		(horizontal - Figure 25)		
18	DC	1.10	453,000	340	middle
20	DC	1.20	416,000	315	end
22	DC	0.67	453,000	325	middle
34	AC	1.12	388,000	296	middle

$\frac{1}{h}$, and the Biot modulus is a measure of the ratio of wall thickness to boiling film thickness.

It has been shown experimentally by McAdams (12) and others that peak heat fluxes increase with wire diameter to an asymptotic value at a wire diameter of about 0.1 inch. If an analogy based on Biot numbers can be drawn between boiling from wires and plates, then there must be some plate thickness at which peak heat flux approaches an asymptotic value. The metal films used as heaters in this study were on the order of a few hundred molecular layers thick, certainly analogous to small diameter wires. If thin metal films are sufficiently isolated from their substrates because of the substrates' low thermal conductivity, then the films are inherently incapable of reaching the asymptotic peak heat fluxes expected of thick heaters. This must of course be considered in designing heat transfer experiments for simulation of actual operating systems.

The data of this study were not sufficiently precise to support any conclusions regarding the effect of film orientation on burnout heat flux. Bernath reports that the ratio of vertical to horizontal heat flux is about 0.75, when long vertical heaters are used. A thicker boiling film is formed at the top of a vertical heater than at the bottom, leading to early failure at the top of the heater. A heater length of about eight inches is required for the effect to be established. Since the vertical length of heaters in this

study was only one inch, no appreciable difference in burnout heat flux between vertical and horizontal films should be expected.

Apparent film temperatures at burnout varied considerably but seemed to be somewhat higher for fast transient than for slower tests. Similar variation in burnout film temperatures was reported by Johnson et al. in transient boiling studies (17).

Discussion of Experimental Errors

The tendency of some tests to exhibit temperatures consistently different from others in Figures 22 through 25 indicated the presence of systematic error, particularly in the determination of film temperatures. An error of 1 per cent in measuring film resistance corresponded to an error of 5 to $8^{\circ}F$ in temperature.

The potentiometer, Wheatstone bridge, standard cell, and standard shunt resistor used for film and recording system calibration were in good working order, and it is improbable that significant error was introduced from these sources.

The tape recorder and oscilloscope were claimed by their manufacturers to have responses linear to within 1 per cent. Problems were encountered with the tape recorder several times, however, and because of its complexity the manufacturer's specifications may have been a bit optimistic.

This investigator believes that most of the error was

caused by difficulty in reading the photographed data. As stated earlier, ripple from the dc power supply was always a problem; even on ac tests, three-phase rectified dc was used to calibrate the current recording channel. On a particular test, voltage scale factors from the two calibrations usually agreed within 1 or 2 per cent, but a difference of 3 per cent or more sometimes occurred in current calibration. The combined effect of these relatively small errors could have altered indicated film temperatures 25°F or more. Better precision could be achieved by using ripple-free direct current from storage batteries if a suitable voltage control system could be constructed.

Influence of Cycling Power Inputs

One of the objectives of this study was the investigation of heat transfer from thin films with ac and half-wave dc heating. The heat flux curves for long-duration tests in these modes are shown in Figure 24. It was mentioned in the discussion accompanying Figure 24 that calculated film temperatures were lower than expected and, in fact, fell below the boiling point of water when nucleate boiling must have been taking place.

Since the driving force for heat transport is temperature difference, it is obvious that heat cannot be transferred from a solid body to a boiling liquid unless the temperature of the solid exceeds the temperature of the boiling liquid.

If the temperature of the solid varies periodically it must at some time during its cycle exceed the boiling point of the liquid if boiling is to occur. While no timed photographs were made during this study to prove that boiling took place while the indicated film temperature was below 212°F, the shape of the heat flux curves and the magnitude of the heat flux during this time overwhelmingly supported this conclusion. Direct current tests in this study showed the same characteristic shapes with temperatures above the boiling point and provided a basis upon which the tests with pulsed power could be judged.

Gunther and Kreith (25) made a photographic study of subcooled boiling with a horizontal, metal ribbon heater. The resulting high-speed motion pictures showed a pronounced 120 cycle per second rhythm in bubble formation when 60 cycle ac was employed for heating. Thus, even when the heating element was as massive as a metal strip, temperature cycling was detected. Admittedly, the temperature fluctuations in the experiments of Gunther and Kreith were probably small; however, in nucleate boiling the heat flux can change substantially with little change in heater temperature.

Attempts were made to read instantaneous voltages and currents at intervals of wt equal to 15 degrees on individual power pulses of tests 28 and 30. Many of the traces contain "noise", probably introduced at some stage in the tape recording and playback, but it was possible to obtain data

for at least a qualitative inspection of the behavior of film temperature during power cycles. These data for two frames each on tests 28 and 30 are shown in Figures 28 and 29. They are plotted as voltage versus current, so that the slope of a curve represents resistance. For a particular film, resistance is approximately a linear function of film temperature.

The curve designated by the shorter time in each figure represents a power pulse near the initiation of boiling; the longer time designates data near the peak heat flux. In Figure 28 the slope of each curve appears to increase, at least slightly, near the peak of the power pulse. Recalling that a 1 per cent increase in resistance represents an increase of 5 to 8°F in film temperature, it may be concluded that the film temperatures did increase significantly above the "calculated values", which correspond to the slopes of the dashed lines. In Figure 29 the variation of film resistance and temperature is seen to be quite large. Determination of slopes in Figures 28 and 29 with sufficient accuracy to estimate quantitatively peak film temperatures appears impossible.

Figure 30 shows plots of power versus wt for an ac and a half-wave dc power pulse compared to an "ideal" pulse in which the resistance remained constant. The "ideal" pulse must be proportional to $\sin^2$ wt, because the power is

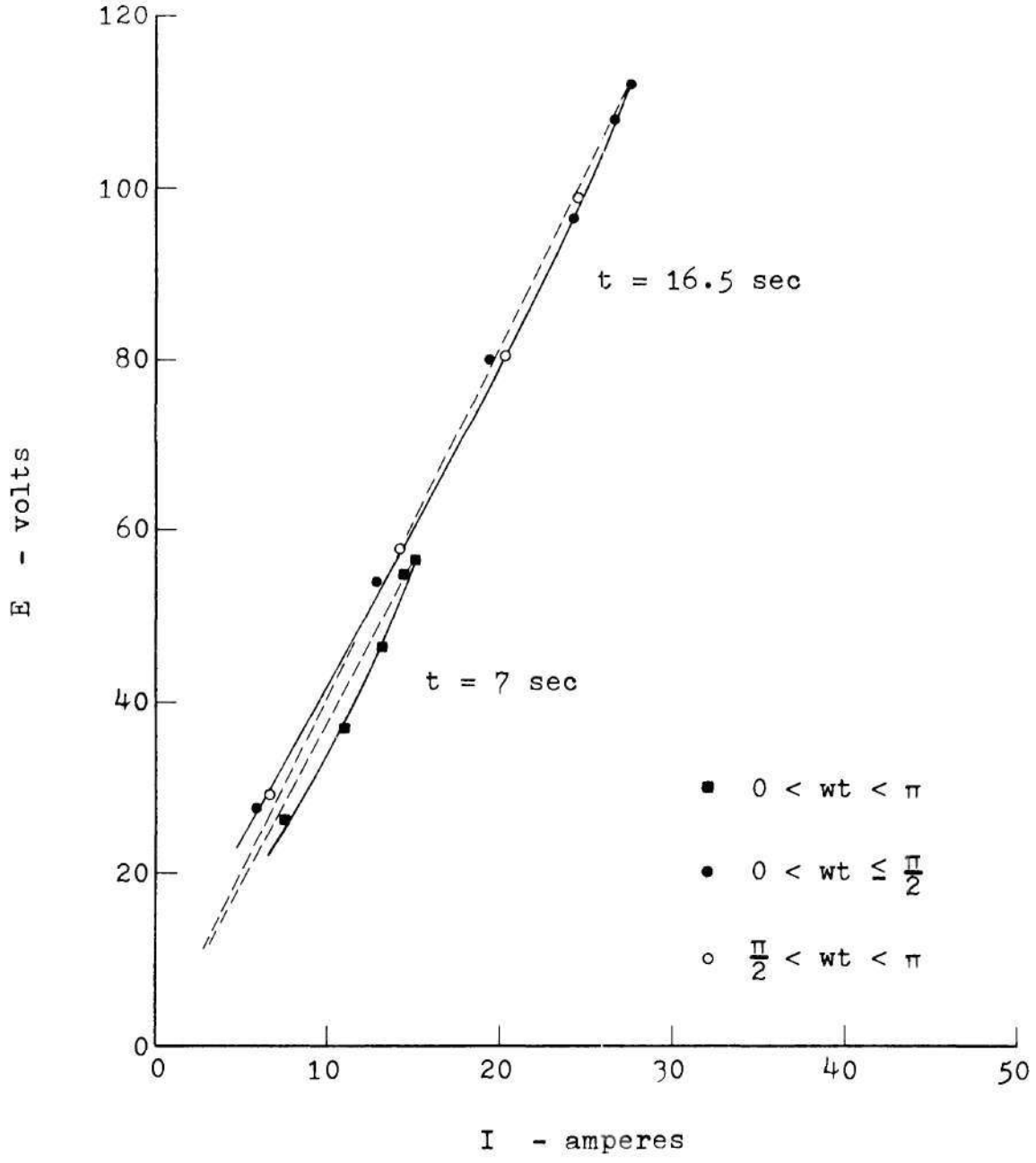

Figure 28. Voltage versus Current Plotted for Individual Power Pulses in Nickel Film No. 28 (AC).

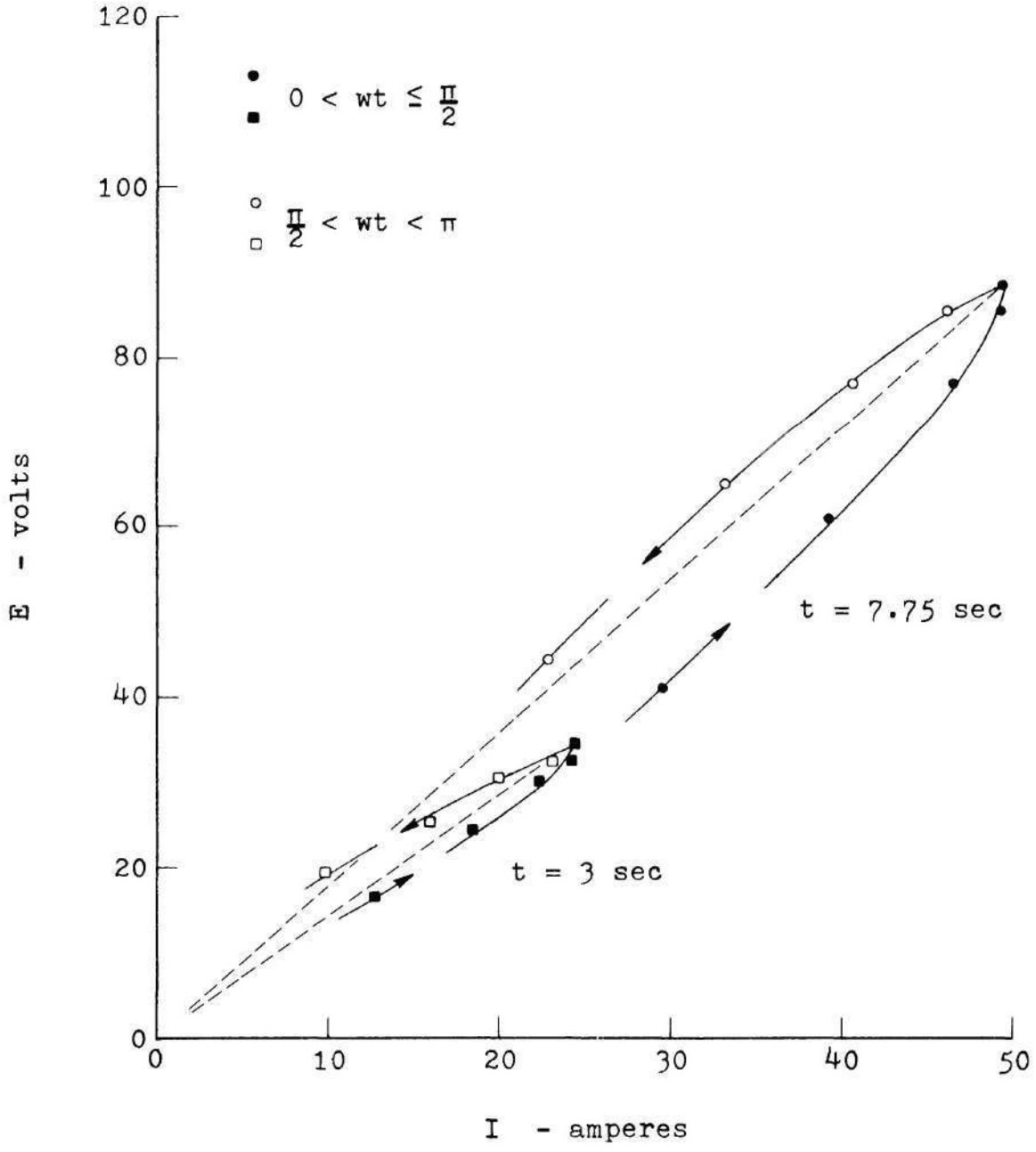

Figure 29. Voltage versus Current Plotted for Individual Power Pulses in Nickel Film No. 30 (half-wave DC).

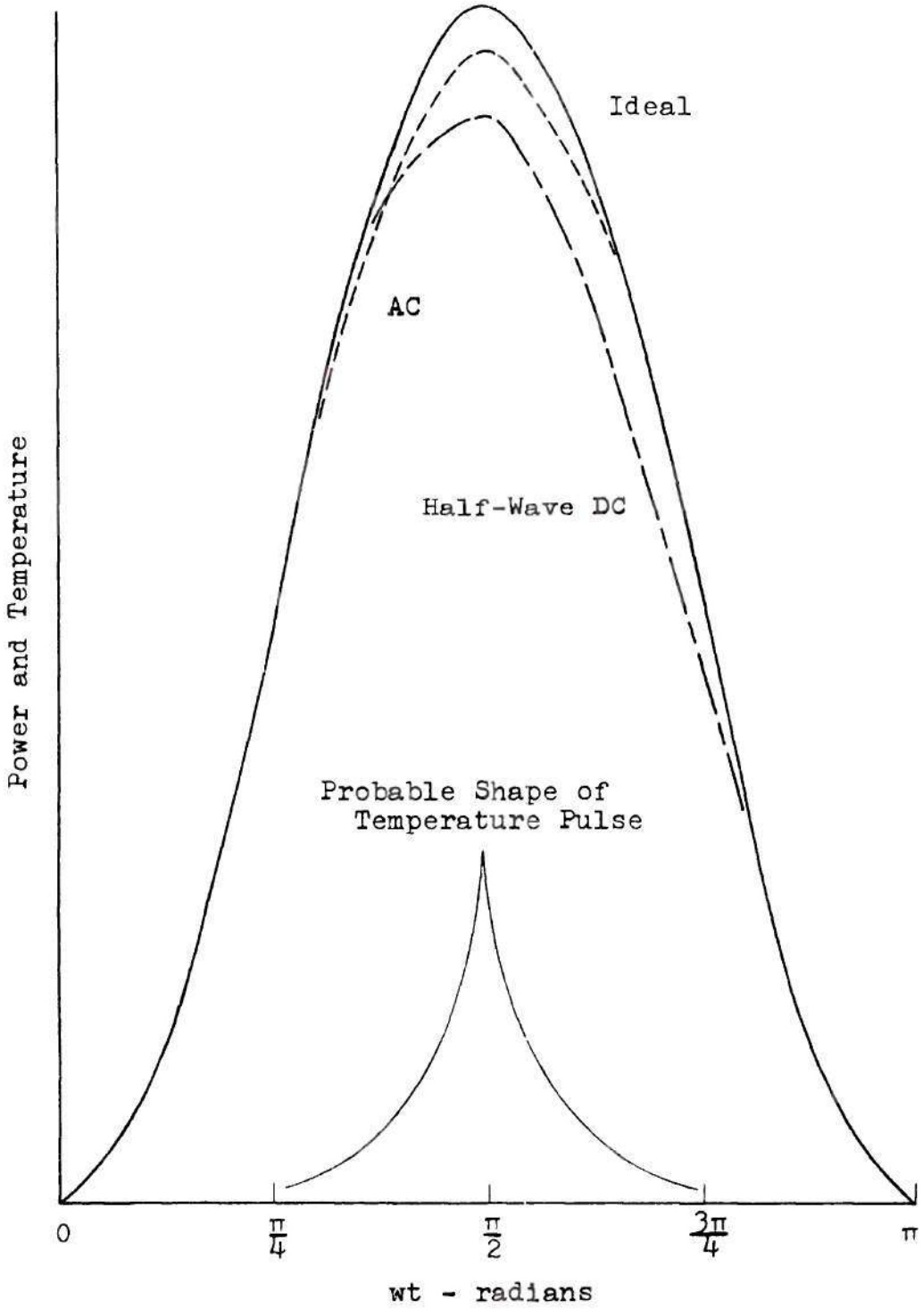

Figure 30. AC, Half-Wave DC and "Ideal" Power Pulses.

given by E^2/R and E is proportional to sin wt. The experimental data for the larger pulses in Figures 28 and 29 were fitted to the ideal curve at values of wt between 0 and $\pi/3$ and between $2\pi/3$ and π. The resulting ac and half-wave dc curves did not reach the peak rate of power generation corresponding to a heater with constant resistance. This further confirms the conclusion that resistance of the metal films increased near the peaks of the power pulses when cycling power was employed. The experimental curves in Figure 30 deviated substantially from the "ideal" only in the interval between $\pi/3$ and $2\pi/3$, indicating that film temperature behaved in a manner described qualitatively by the temperature curve at the bottom of the illustration.

It should be noted that if burnout begins at the peak of a power pulse in ac and half-wave dc heating, then the films heated by alternating current in this study were dissipating almost twice the power shown by the heat-flux curves when burnout began. Nickel Film No. 30 (half-wave dc) was dissipating nearly four times the indicated power, and the film temperature in these cases was far above the calculated value.

Mathematical analysis can give an estimate of the effect of a substrate on film temperature when ac heating is employed. Unless the substrate has zero thermal conductivity, it will have a damping influence on the cycling of film

temperature. Consider a system composed of a metal film operating at steady state with water on one side and a glass substrate on the other side. Assume:

(1) The glass is a semi-infinite solid with an average temperature equal to the film average temperature.

(2) The film is heated by ac power.

(3) The electrical resistance of the film is constant but the temperature can fluctuate.

(4) The rate of heat transfer to the water is steady and, since by assumption (1) there is no net heat loss to the glass, this rate of loss is given by

$$\left(\frac{q}{A}\right)_w = \frac{E_p I_p}{2\pi} \int_0^{2\pi} \sin^2 \text{ wt } d(\text{wt}) = \frac{P_{max}}{2}$$

For the moment also consider a case with the glass completely insulated from the film. A typical nickel film on a one-inch by three-inch glass slide weighs 3.5 milligrams. Then

$m = 3.70 \times 10^{-4}$ lb/ft^2, and

$c_p = 0.103$ Btu/lb.

A heat balance on the film over a differential interval of time gives

$$\left(\frac{q}{A}\right)_{net} = mc_p \frac{dT}{dt} = \left(\frac{q}{A}\right)_f - \left(\frac{q}{A}\right)_{out}$$

and for the moment

$$\left(\frac{q}{A}\right)_{out} = \left(\frac{q}{A}\right)_{water}.$$

Integrating, where t_c = time of one cycle = 1/60 second,

$$mc_p \Delta T = \int_{t_1}^{t_2} \left(P_m \sin^2 \frac{2\pi t}{t_c} - \frac{1}{2} P_m\right) dt$$

$$\Delta T = \frac{P_m}{mc_p} \frac{t_c}{2\pi} \int_{\frac{2\pi t}{t_c}\Big|_1}^{\frac{2\pi t}{t_c}\Big|_2} \left(\sin^2 \frac{2\pi t}{t_c} - \frac{1}{2}\right) d\left(\frac{2\pi t}{t_c}\right)$$

$$\Delta T = \frac{P_m}{mc_p} \frac{t_c}{2\pi} \left[-\frac{1}{4} \sin \frac{4\pi t}{t_c}\right]_{\frac{2\pi t}{t_c}\Big|_1}^{\frac{2\pi t}{t_c}\Big|_2}. \qquad (16)$$

If the integration is begun at $\frac{2\pi t}{t_c}\Big|_1 = 0$, ΔT will have a maximum value when

$$\frac{4\pi t}{t_c} = \frac{\pi}{2}, \frac{3\pi}{2}, \ldots$$

or $$t = 1/480 \text{ sec}, 3/480 \text{ sec}, \ldots$$

Evaluation of ΔT_{max} under these conditions leads to

$$\Delta T_m \ (^oF) = 4.84 \times 10^{-3} \ P_m \ (Btu/hr\text{-}ft^2).$$

At t = 16.5 seconds in Nickel Film 28 (one of the examples in Figure 28) P_m = 532,000 Btu/hr-ft^2. Then $\Delta T_m = 2570^oF$, a value far too high to be realistic.

However, the film temperature is shown to vary as a sine function, with a period of one-half the ac power period. Carslaw and Jaeger (61) give a solution for the temperature distribution in a semi-infinite solid having a surface temperature varying according to the relation $T = A \cos (wt - \lambda)$. This temperature distribution at steady state is given by

$$T = A \ e^{-Kx} \cos (wt - Kx - \lambda)$$

where $$K = (\frac{w}{2\alpha})^{\frac{1}{2}}.$$

Figure 31 shows a plot of temperature profiles in the substrate during the half cycle when surface temperature is decreasing. It should be noted that the surface temperature gradient changes sign twice during each temperature cycle, so that heat is flowing alternately into and out of the substrate. The wavelength of the temperature wave is given by $(\frac{4\pi\alpha}{n})^{\frac{1}{2}}$, where n is the frequency of the surface temperature

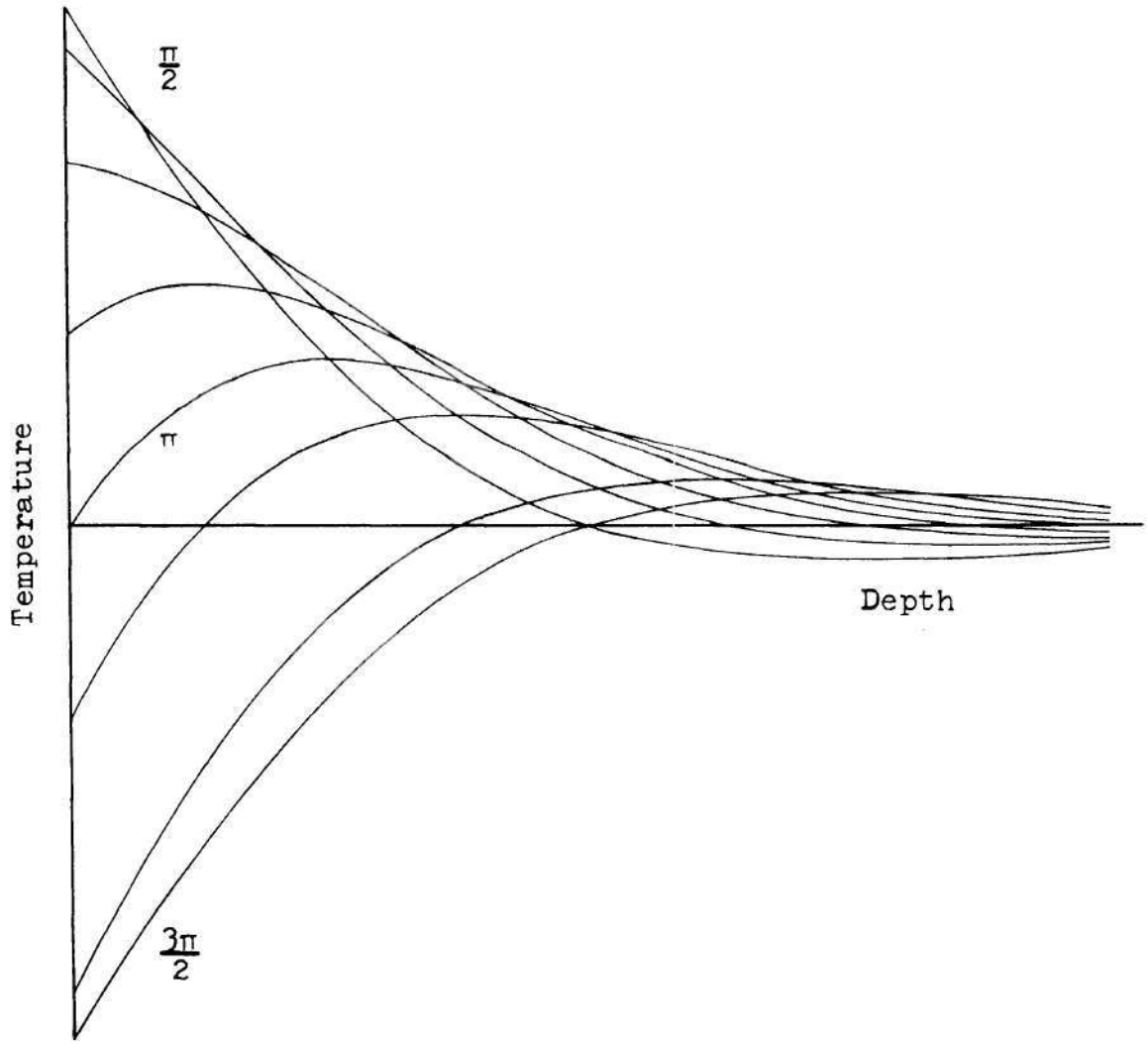

Figure 31. Variation of Temperature with Depth when the Surface Temperature is Decreasing Sinusoidally.

oscillation. In the system under discussion the wavelength would be about 0.012 inch. At a depth of one wavelength the amplitude of the temperature wave is reduced by a factor of $\exp(-2\pi) = 0.0019$. Because of the strong attenuation and short wavelength, the solution for the semi-infinite solid is adequate for this case.

It has been shown that w referred to the ac power frequency is

$$w = 2\left(\frac{2\pi}{t_c}\right) = \frac{4\pi}{t_c} .$$

The rate of heat transfer between the film and substrate is

$$\left(\frac{q}{A}\right)_s = - k \left.\frac{\delta T}{\delta x}\right|_{x=0,t} =$$

$$- k \frac{\delta}{\delta x}\left[\left|\Delta T_m\right| e^{-Kx} \cos\left(\frac{4\pi t}{t_c} - Kx - \lambda\right)\right]_{x=0,t}$$

where $\left|\Delta T_m\right|$ is the maximum positive value of ΔT. Differentiation and substitution of zero for x leads to

$$\left(\frac{q}{A}\right)_s = Kk\left|\Delta T_m\right|\left[\cos\left(\frac{4\pi t}{t_c} - \lambda\right) - \sin\left(\frac{4\pi t}{t_c} - \lambda\right)\right]_t .$$

By a trigonometric identity

$$\left(\frac{q}{A}\right)_s = Kk \left|\Delta T_m\right| \sqrt{2} \left[\cos\left(\frac{4\pi t}{t_c} - \lambda + \frac{\pi}{4}\right)\right] .$$

Integrating with respect to t

$$\left(\frac{Q}{A}\right)_s = Kk \left|\Delta T_m\right| \frac{t_c}{4\pi} \sqrt{2} \left[\sin\left(\frac{4\pi t}{t_c} - \lambda + \frac{\pi}{4}\right)\right]_{\frac{2\pi t}{t_c}\Big|_1}^{\frac{2\pi t}{t_c}\Big|_2}$$

$$\left(\frac{Q}{A}\right)_s = \left[\frac{t_c}{4\pi\alpha}\right]^{\frac{1}{2}} k \left|\Delta T_m\right| \left[\sin\left(\frac{4\pi t}{t_c} - \lambda + \frac{\pi}{4}\right)\right]_{\frac{2\pi t}{t_c}\Big|_1}^{\frac{2\pi t}{t_c}\Big|_2} \quad (17)$$

$\left(\frac{q}{A}\right)_s$ is positive from $\left(\frac{4\pi t}{t_c} - \lambda + \frac{\pi}{4}\right) = -\frac{\pi}{2}$ to $\frac{\pi}{2}$.

From physical reasoning it is observed that when the surface temperature is increasing $\left(\frac{q}{A}\right)_s$ must be positive, or heat is flowing into the substrate. From equation (16) it is seen that this happens when $\frac{d\Delta T}{dt}$ is positive.

$$\frac{d\Delta T}{dt} = -\frac{P_m}{mc_p} \frac{t_c^2}{32\pi^2} \cos\frac{4\pi t}{t_c} .$$

$\frac{d\Delta T}{dt}$ is positive in the range $\frac{4\pi t}{t_c} = \frac{\pi}{2}$ to $\frac{3\pi}{2}$.

Then $\left(\frac{\pi}{2} - \lambda + \frac{\pi}{4}\right) = -\frac{\pi}{2}$ and $\left(\frac{3\pi}{2} - \lambda + \frac{\pi}{4}\right) = \frac{\pi}{2}$

so that $\lambda = \frac{5\pi}{4}$.

Now heat interchange between the film and substrate can be combined with equation (16) in which the substrate was assumed insulated from the metal film. It is noted that

$$mc_p \Delta T = \left(\frac{Q}{A}\right)_f - \left(\frac{Q}{A}\right)_w - \left(\frac{Q}{A}\right)_s .$$

Combining equations (16) and (17) and starting the integration at $\frac{4\pi t}{t_c} = 0$ gives

$$\Delta T = -\frac{P_m t_c}{mc_p 8\pi} \left[\sin \frac{4\pi t}{t_c} \right]_0^{\frac{4\pi t}{t_c}} - \qquad (18)$$

$$\frac{k\left|\Delta T_m\right|}{mc_p} \left[\frac{t_c}{4\pi\alpha}\right]^{\frac{1}{2}} \left[\sin \left(\frac{4\pi t}{t_c} - \pi\right) \right]_0^{\frac{4\pi t}{t_c}} .$$

For convenience several terms are collected into constants, and P_m is taken as 532,000 Btu/hr-ft^2, corresponding to the example considered previously.

$$\frac{P_m t_c}{mc_p 8\pi} = 2570^{\circ}F$$

$$\frac{k}{mc_p}\left[\frac{t_c}{4\pi\alpha}\right]^{\frac{1}{2}} = 69.7 \text{ (dimensionless)}$$

Equation (18) becomes

$$\Delta T = -2570 \sin\frac{4\pi t}{t_c} + 69.7\left|\Delta T_m\right| \sin\frac{4\pi t}{t_c}.$$

ΔT_m will occur at $\frac{4\pi t}{t_c} = \frac{\pi}{2}, \frac{3\pi}{2}, \ldots$

and at $\frac{4\pi t}{t_c} = \frac{\pi}{2}$, ΔT_m is negative by equation (16). Then

$$-\Delta T_m = -2570 \sin\frac{\pi}{2} + 69.7\left|\Delta T_m\right| \sin\frac{\pi}{2}$$

and $$\Delta T_m = 36^{\circ}F.$$

ΔT as a function of time at this power level is given by

$$\Delta T = -36^{\circ}F \sin\frac{4\pi t}{t_c}.$$

The substrate is thus seen to exert a strong damping influence on the film temperature when cycling power inputs are employed.

CHAPTER VI

CONCLUSIONS AND RECOMMENDATIONS

The conclusions reached in this investigation may be stated as follows:

1. Thin metal films can be used simultaneously as resistance thermometers and heaters, and the use of high-speed tape recording systems for determining film temperatures and heat generation rates is practical.

2. The greatest difficulty in experiments of this kind is the determination of film temperature; this difficulty arises in data recording and interpretation rather than in film thermometric calibration.

3. For accurate experimental measurements, a metal film must have the highest possible temperature coefficient of resistance and uniform thickness.

4. In transient, subcooled, pool boiling experiments with thin films, a temperature "overshoot" of 10 to 30°F was observed as boiling commenced, and this effect seemed more pronounced at lower rates of power increase.

5. Thin metal films in subcooled pool boiling exhibited maximum boiling heat fluxes of 500,000 to 600,000 Btu/hr-ft^2 or lower by a factor of three to four than corresponding values reported in the literature.

6. Film temperatures fluctuated when the input power cycled at 60 or 120 pulses per second.

7. The substrate exerts a strong damping effect on film temperature fluctuation when cycling power is used.

Several recommendations can be made concerning future experimental investigations of the type described here.

1. Calibration of the recording system should be accomplished with current from storage batteries or other sources that do not give a cyclic variation of voltage with time.

2. Precision in gathering data from the tape recorder could be improved by reducing line widths on the graphic recording. This would be accomplished by reducing the spot and grid brightness on the oscilloscope screen, and photographing data on higher speed film. Improvement might be achieved by playing the tape recording into a strip chart or similar recorder to place the graphic recording on paper rather than photographic film. This method would also provide a continuous recording.

3. Care must be taken to select the optimum scale factors during data recording so that the recorder capacity can be used advantageously. Sufficient data have been collected in the present study to permit an informed guess at a film's maximum voltage and current to be made prior to an experiment.

4. In fast, transient experiments, a power supply

having an output that could be programmed before the run would be very useful.

5. The most uniform film thickness possible is a requisite for heat transfer experiments using thin films simultaneously as heaters and thermometers. Very uniform nickel films might be produced by vapor deposition of the metal onto smooth opaque substrates.

Useful extensions of this study could include investigation of the effects of subcooling and studies of fluid boundary conditions in flowing systems. Significant improvement in film thickness uniformity would be required before the results of these studies could be assumed generally representative of boiling processes, however.

APPENDIX I

DERIVATION OF EXPRESSION FOR SLIDE HEAT FLUX

Carslaw and Jaeger (55) discuss the use of Laplace transformation methods for solving problems of heat conduction in linear flow. Using their techniques an expression for the heat flux from a metal film to a glass substrate is developed as follows:

Assume

$\theta_o = 0$ = initial uniform slab temperature

$\theta_{x=0} = Ct$ = front side slab temperature

$\theta_{x=L} = 0$ = constant back side slab temperature

negligible edge effects

where

$\theta = T - T_o$

T = temperature at x and t

T_o = initial temperature

t = time

x = length

L = thickness of slab

α = thermal diffusivity.

The basic conduction equation for an infinitely wide plate of thickness L is:

$$\frac{\delta^2\theta}{\delta x^2} - \frac{1}{\alpha}\frac{\delta\theta}{\delta t} = 0 \qquad 0 < x < L$$

which leads to the subsidiary equation

$$\frac{d^2\bar{\theta}}{dx^2} - \frac{p}{\alpha}\bar{\theta} = -\frac{1}{\alpha}\theta_o(x)$$

with boundary conditions

$$\theta_o = 0 \quad \text{for} \quad t = 0,\ 0 < x < L$$

$$\bar{\theta} = 0 \qquad t > 0,\ x = L$$

$$\bar{\theta} = \frac{C}{p^2} \qquad t > 0,\ x = 0.$$

The subsidiary equation becomes

$$\frac{d^2\bar{\theta}}{dx^2} - q^2\bar{\theta} = 0 \qquad 0 < x < L$$

where $$q^2 = \frac{p}{\alpha} .$$

From Murphy (62) the solution can be found by taking roots of the auxiliary equation

$$r^2 - q^2 = 0 \qquad r = +q,\ -q .$$

The solution has the form

$$\bar{\theta} = C_1 \cosh(qx) + C_2 \sinh(qx) .$$

From the third boundary condition

$$\frac{C}{p^2} = C_1 \frac{1}{2} (2) + C_2 \frac{1}{2} (0) \quad \text{and} \quad C_1 = \frac{C}{p^2} .$$

From the second boundary condition

$$0 = \frac{C}{p^2} \cosh (qL) + C_2 \sinh (qL)$$

and

$$C_2 = - \frac{C}{p^2} \frac{\cosh (qL)}{\sinh (qL)} .$$

Then

$$\bar{\theta} = \frac{C}{p^2} \left[\cosh (qx) - \coth (qL) \sinh (qx)\right]$$

$$\bar{\theta} = \frac{C}{p^2} \sinh (qx) \left[\coth (qx) - \coth (qL)\right]$$

$$\bar{\theta} = \frac{C}{p^2} \left[- \frac{\sinh (qx - qL)}{\sinh (qL)}\right] .$$

To transform this to a solution for θ, the above expression must be written in the exponential form and expressed as the sums of series.

$$\bar{\theta} = - \frac{C}{p^2} \left[\frac{e^{q(x-L)} - e^{-q(x-L)}}{e^{(qL)} \quad e^{-(qL)}}\right]$$

$$\bar{\theta} = - \frac{C}{p^2} \frac{(e^{q(x-L)} - e^{-q(x-L)})}{e^{(qL)}(1 - e^{-(2qL)})}$$

$$\bar{\theta} = - \frac{C}{p^2} \frac{(e^{q(x-2L)} - e^{-(qx)})}{(1 - e^{-(2qL)})}$$

$$\bar{\theta} = \frac{C}{p^2} \left[e^{-(qx)} - e^{q(x-2L)}\right] \sum_{n=0}^{\infty} e^{-n(2qL)}$$

$$\bar{\theta} = \frac{C}{p^2} \left[\sum_{n=0}^{\infty} e^{-q(2nL+x)} - \sum_{n=0}^{\infty} e^{-q(2nL+2L-x)} \right].$$

From Carslaw and Jaeger, Appendix V

$$\theta = C \left[\sum_{n=0}^{\infty} (4t)^{\frac{1}{2}m} \, i^m \, \operatorname{erfc} \frac{x + 2nL}{2\sqrt{\alpha t}} - \right.$$

$$\left. \sum_{n=0}^{\infty} (4t)^{\frac{1}{2}m} \, i^m \, \operatorname{erfc} \frac{(n + 1)2L - x}{2\sqrt{\alpha t}} \right]$$

and in the present case $m = 2$, so that

$$\theta = 4Ct \sum_{n=0}^{\infty} \left[i^2 \operatorname{erfc} \frac{x + 2nL}{2\sqrt{\alpha t}} - i^2 \operatorname{erfc} \frac{(n + 1)2L - x}{2\sqrt{\alpha t}} \right].$$

In order to use this expression for temperature as a function of time and distance to calculate the heat flux at the surface $x = 0$, the quantity $\frac{\delta\theta}{\delta x}\Big|_{x=0,t}$ must be evaluated. The derivative of a definite integral is given by

$$\frac{d}{dx}\left[\int_a^x f(u)\,du\right] = f(x)$$

and $i^n \operatorname{erfc} x = \int_x^\infty i^{n-1} \operatorname{erfc} u\,du \qquad n = 1, 2, \ldots$

Then $$\frac{d}{dx}\left[i^2 \operatorname{erfc} x\right] = -\, i \operatorname{erfc} x\,dx$$

$$\frac{\delta\theta}{\delta x}\Big|_{x,t} = -\frac{2Ct}{\sqrt{\alpha t}} \sum_{n=0}^{\infty}\left[i \operatorname{erfc} \frac{x + 2nL}{2\sqrt{\alpha t}} + i \operatorname{erfc} \frac{2(n+1)L - x}{2\sqrt{\alpha t}}\right]$$

$$\frac{\delta\theta}{\delta x}\Big|_{x=0,t} = -\frac{2Ct}{\sqrt{\alpha t}} \sum_{n=0}^{\infty}\left[i \operatorname{erfc} \frac{nL}{\sqrt{\alpha t}} + i \operatorname{erfc} \frac{(n+1)L}{\sqrt{\alpha t}}\right].$$

Heat flux to the slide is given by the Fourier conduction equation which becomes

$$\left(\frac{q}{A}\right)_s = -\,k \frac{\delta\theta}{\delta x}\Big|_{x=0,t} = \frac{2kC(t)^{\frac{1}{2}}}{\sqrt{\alpha}} \sum_{n=0}^{\infty} \qquad (19)$$

$$\left[i \operatorname{erfc} \frac{nL}{\sqrt{\alpha t}} + i \operatorname{erfc} \frac{(n+1)L}{\sqrt{\alpha t}}\right].$$

This result must agree with the semi-infinite solid case for sufficiently short times. If the sum of the series is taken for n = 0, 1, 2, 3:

$$\left(\frac{q}{A}\right)_s = \frac{2kC(t)^{\frac{1}{2}}}{\sqrt{\alpha}} \left[i \text{ erfc } 0 + 2\, i \text{ erfc } \frac{L}{\sqrt{\alpha t}} + 2\, i \text{ erfc } \frac{2L}{\sqrt{\alpha t}} + 2\, i \text{ erfc } \frac{3L}{\sqrt{\alpha t}} \right]. \tag{20}$$

For the quartz substrates in this study at times of one second or less

$$\frac{L}{\sqrt{\alpha t}} = \frac{(.0104 \text{ ft})}{\sqrt{(.0350 \text{ ft}^2/\text{hr})(1 \text{ sec})/(3600 \text{ sec/hr})}} = 3.335$$

Using values for i erfc x in Carslaw and Jaeger, Appendix II, the first term in the brackets in equation (20) is 0.5642 and all subsequent terms are less than 0.0001. To four places, $\frac{1}{\sqrt{\pi}}$ is 0.5642 and equation (20) becomes

$$\left(\frac{q}{A}\right)_s = \frac{2kC(t)^{\frac{1}{2}}}{\sqrt{\pi\alpha}} \tag{21}$$

which agrees with the expression obtained later in this Appendix for a substrate acting as a semi-infinite solid.

Calculation of the slide heat flux for each of the

numerous experimental data points taken in this study was greatly facilitated by constructing a table expressing heat flux as a function of time and the slope C, of the experimental temperature versus time plot. The following assumptions were required:

1. Thermal properties of the clear fused quartz slides were constant. These quantities were taken from a report by Fleming (63), and values were chosen at a mean temperature of 160°F.

$$k = 0.82 \text{ Btu/hr-ft-}^{\circ}\text{F} \quad \text{(p. 105)}$$

$$c_p = 0.170 \text{ Btu/lb-}^{\circ}\text{F} \quad \text{(p. 109)}$$

$$d = 2.205 \text{ gm/cm}^3 = 137.7 \text{ lb/ft}^3 \quad \text{(p. 84)}$$

$$\alpha = \frac{k}{dc_p} = 0.0350 \text{ ft}^2/\text{hr}$$

2. The slide thickness was 0.125 inch or 0.0104 foot and the back surface always remained at the starting temperature. Since the entire slide was immersed in water this assumption is a good approximation. Even in the longest tests, the water became only warm to the touch. Immediately after burnout there were noticeable temperature gradients in the water, and the back of the slide remained cool in comparison to the front and the water near the heating surface.

3. Edge and end effects associated with the slides were negligible. Since the slides were only one-eighth inch thick, the area of the ends and edges was about 25 per cent of the plated area. Most of the heat generated in the metal

film was transferred to the water, and the heat that entered the slide and passed out through the edges could have been only a small fraction of the total. Other uncertainties far outweighed this effect and it was neglected in the calculations.

4. The temperature rise in the film was directly proportional to time. For purposes of estimating heat loss to the slide this is seen experimentally to be an adequate approximation for the entire test if the time is short (Nickel Films 18, 20, 22, and 34). It is less good, but still an adequate approximation for longer tests up to the time that the film temperature levels off and nucleate boiling begins. After this time another technique was required to estimate heat losses to the slide. To establish the slope C for a heat flux calculation, a straight line was fitted visually to the film temperature versus time plot. In most cases the line did not pass through ambient temperature at zero time.

The following form of equation (19) was used to construct Table 2:

$$\left(\frac{q}{A}\right)_s = \frac{kC(t)^{\frac{1}{2}}}{\sqrt{\alpha}} \sum_{n=0}^{\infty} \left[2\ i\ \text{erfc}\ \frac{nL}{\sqrt{\alpha t}} + 2\ i\ \text{erfc}\ \frac{(n+1)L}{\sqrt{\alpha t}} \right]. \quad (22)$$

The arguments of the complementary error functions were tabulated at the desired intervals of time and the sum in equa-

Table 2. Parameters for Calculating Slide Heat Flux

$$\left(\frac{q}{A}\right)_s \frac{\text{Btu}}{\text{hr-ft}^2} = C \frac{^\circ\text{F}}{\text{sec}} \; f(t) \frac{\text{Btu-sec}}{\text{hr-ft}^2\text{-}^\circ\text{F}}$$

$$f(t) = \frac{k(t)^{\frac{1}{2}}}{\sqrt{\alpha}} \sum_{n=0}^{\infty} \left[2 \; i \; \text{erfc} \frac{nL}{\sqrt{\alpha t}} + 2 \; i \; \text{erfc} \frac{(n+1)L}{\sqrt{\alpha t}} \right]$$

Time (sec)	f(t)	Time (sec)	f(t)	Time (sec)	f(t)
0.05	66.5	1.20	325	6.75	825
0.10	93.8	1.25	332	7.00	845
0.15	115	1.50	364	7.25	865
0.20	133	1.75	393	7.50	884
0.25	148	2.00	420	7.75	904
0.30	163	2.25	446	8.00	924
0.35	176	2.50	470	8.25	944
0.40	188	2.75	494	8.50	963
0.45	199	3.00	517	8.75	983
0.50	210	3.25	539	9.00	1002
0.55	220	3.50	561	9.25	1021
0.60	230	3.75	582	9.50	1042
0.65	239	4.00	603	9.75	1062
0.70	248	4.25	624	10.00	1082
0.75	257	4.50	644	10.25	1102
0.80	265	4.75	664	10.50	1122
0.85	274	5.00	685	10.75	1141
0.90	282	5.25	705	11.00	1161
0.95	289	5.50	725	11.25	1180
1.00	297	5.75	745	11.50	1200
1.05	304	6.00	765	11.75	1220
1.10	311	6.25	785	12.00	1239
1.15	318	6.50	805		

tion (22) obtained. The sum converged to four places with values of n = 0, 1, and 2. The terms

$$\frac{k(t)^{\frac{1}{2}}}{\sqrt{\alpha}} \sum_{n=0}^{\infty} \left[\quad \right] \quad \frac{\text{Btu-sec}}{\text{hr-ft}^2\text{-}^{\circ}\text{F}} \tag{23}$$

were grouped together at each of the tabulated times, so that the slide heat flux at a particular time could be calculated by multiplying expression (23) and the appropriate slope C in units of $^{\circ}$F per second. Values of the function (2 i erfc x) are given by Carslaw and Jaeger (57).

Alternate Derivation for a Semi-Infinite Solid

The following derivation for heat flux to a semi-infinite solid is presented to support the more complex derivation developed earlier in this Appendix.

Consider a semi-infinite solid initially at uniform temperature having a surface temperature at time t = 0 beginning to increase in the manner defined by f(t). The heat conduction equation must be satisfied

$$\frac{\delta\theta}{\delta t} = \alpha \frac{\delta^2\theta}{\delta x^2}$$

with boundary conditions:

$\theta = 0$ at $t = 0$

$\theta = f(t)$ at $x = 0$

where all symbols have the same definition as used in the preceding development.

Carslaw and Jaeger (64) give the following solution for the temperature profile in a semi-infinite solid having a surface temperature that is increasing linearly with time according to the relation $f(t) = Ct$:

$$\theta = Ct \left[\left(1 + \frac{x^2}{2\alpha t}\right) \operatorname{erfc} \left(\frac{x}{2\sqrt{\alpha t}}\right) - \frac{x}{\sqrt{\pi \alpha t}} \exp \left(- \frac{x^2}{4\alpha t}\right) \right] . \quad (24)$$

To facilitate differentiation, these substitutions are made:

$$w = \frac{x}{2\sqrt{\alpha t}}$$

$$\operatorname{erfc} w = 1 - \operatorname{erf} w .$$

Then $$\left.\frac{\delta \theta}{\delta x}\right|_t = \left[\frac{\delta w}{\delta x}\right]_t \left[\frac{\delta \theta}{\delta w}\right]$$

and from equation (24)

$$\left.\frac{\delta \theta}{\delta x}\right|_t = \frac{Ct}{2\sqrt{\alpha t}} \frac{\delta}{\delta w} \left[(1 + 2w^2)(1 - \operatorname{erf} w) - \frac{2}{\sqrt{\pi}} w \exp (-w^2) \right]$$

$$\frac{\delta\theta}{\delta x}\Big|_t = \frac{Ct}{2\sqrt{\alpha t}} \left[(1 + 2w^2)\left[-\frac{2}{\sqrt{\pi}} \exp(-w^2)\right] + \right.$$

$$\left. (1 - \text{erf } w)4w - \frac{2}{\sqrt{\pi}} \exp(-w^2) + \frac{4}{\sqrt{\pi}} w^2 \exp(-w^2)\right]$$

$$\frac{\delta\theta}{\delta x}\Big|_t = \frac{Ct}{2\sqrt{\alpha t}} \left[4w(1 - \text{erf } w) - \frac{4}{\sqrt{\pi}} \exp(-w^2)\right].$$

At the surface x = 0

$$\frac{\delta\theta}{\delta x}\Big|_{x=0,t} = -\frac{2\ Ct}{\sqrt{\pi\alpha t}}$$

and the wall heat flux is given by

$$\left(\frac{q}{A}\right)_s = -k \frac{\delta\theta}{\delta x}\Big|_{x=0,t} = \frac{2kC(t)^{\frac{1}{2}}}{\sqrt{\pi\alpha}} \quad .$$

This result agrees with equation (21) in this Appendix for the special case of short test times. Because it was developed by a procedure different from that used for equation (19), it comfirms the validity of equation (19).

APPENDIX II

HEAT TRANSFER DATA

Table 3. Data for Nickel Film No. 3

Power: dc
Duration of Test: 17.0 sec
Film Orientation: horizontal
Location of Failure: middle (at scratch)
Ambient Temperature: 85°F

Time (sec)	Heat Input ($\frac{Btu}{hr\ ft^2}$)	Slide Heat Flux ($\frac{Btu}{hr\ ft^2}$)	Water Heat Flux ($\frac{Btu}{hr\ ft^2}$)	Film Temp. (°F)	Temp. Diff. (°F)
0.00	-0-	-0-	-0-	-	-
1.00	290	-0-	290	115	30
3.00	7,350	-0-	7,350	95	10
4.00	14,000	7,430	6,570	107	22
4.50	16,300	9,100	7,200	115	30
5.00	22,200	10,500	11,700	134	49
5.50	26,700	11,800	14,900	144	59
6.00	30,300	12,900	17,400	182	97
6.50	32,800	14,000	18,800	197	112
7.00	33,200	15,100	18,100	192	107
7.50	37,900	16,100	21,800	210	125
8.00	43,100	17,100	26,000	205	120
8.50	49,100	18,100	31,000	228	143
9.00	52,200	11,300*	40,900	228	143
9.50	57,800	12,000	45,800	237	152
10.00	63,700	11,300	52,400	228	143
10.50	70,700	11,700	59,000	233	148
11.00	78,500	11,700	66,800	233	148
11.50	81,200	10,500	70,700	218	133
12.00	87,700	12,000	75,700	237	152
12.50	93,700	13,400	80,300	255	170
13.00	100,000	11,700	88,300	233	148
13.50	106,000	13,500	92,500	256	171
14.00	114,000	14,000	100,000	260	175
14.50	124,000	12,000	112,000	237	152
15.00	130,000	14,000	116,000	268	183
15.50	135,000	14,000	121,000	265	180
16.00	146,000	13,000	133,000	252	167
16.50	158,000	14,000	144,000	268	183
17.00	146,000	21,000	125,000	355	270

*Assumed linear temperature drop through slide.

Table 4. Data for Nickel Film No. 4

Power: dc
Duration of Test: 22.65 sec
Film Orientation: horizontal
Location of Failure: end of film
Ambient Temperature: 75°F

Time (sec)	Heat Input ($\frac{Btu}{hr\ ft^2}$)	Slide Heat Flux ($\frac{Btu}{hr\ ft^2}$)	Water Heat Flux ($\frac{Btu}{hr\ ft^2}$)	Film Temp. (°F)	Temp. Diff. (°F)
0.00	-0-	-0-	-0-	-	-
1.00	4,090	7,600	-0-	145	70
2.00	11,000	10,700	300	148	73
2.50	17,400	12,000	5,400	148	73
3.00	22,800	13,200	9,600	202	127
3.50	30,000	14,400	15,600	193	118
4.00	33,100	15,400	17,700	223	148
4.50	35,300	16,500	18,800	209	134
5.00	37,200	17,500	19,700	233	158
5.50	41,200	18,600	22,600	224	149
6.00	46,900	19,600	27,300	226	151
6.50	52,800	20,600	32,200	258	183
7.00	57,600	21,600	36,000	246	171
7.50	64,700	22,600	42,100	248	173
8.50	82,900	24,700	58,200	280	205
9.00	89,000	25,700	63,300	300	225
9.50	94,600	16,000*	78,600	278	203
10.00	111,000	14,700	96,300	262	187
10.50	122,000	13,000	109,000	246	171
11.00	128,000	15,000	113,000	262	187
11.50	136,000	15,000	121,000	269	194
12.00	149,000	16,000	133,000	282	207
12.50	154,000	16,000	138,000	274	199
13.00	166,000	16,000	150,000	278	203
13.50	174,000	17,000	157,000	292	217
14.00	190,000	17,000	173,000	292	217
14.50	197,000	17,000	180,000	293	218
15.00	203,000	18,000	185,000	304	229

*Assumed linear temperature drop through slide.

(Continued)

Table 4 (Continued). Data for Nickel Film No. 4

Time (sec)	Heat Input ($\frac{Btu}{hr\ ft^2}$)	Slide Heat Flux ($\frac{Btu}{hr\ ft^2}$)	Water Heat Flux ($\frac{Btu}{hr\ ft^2}$)	Film Temp. (°F)	Temp. Diff. (°F)
15.50	219,000	18,000	201,000	300	225
16.00	231,000	17,000	214,000	297	222
16.50	238,000	17,000	221,000	296	221
17.00	247,000	18,000	229,000	304	229
17.50	259,000	18,000	241,000	308	233
18.00	262,000	19,000	243,000	312	237
18.50	281,000	19,000	262,000	321	246
19.00	288,000	19,000	269,000	315	240
19.50	300,000	20,000	280,000	327	252
20.00	300,000	20,000	280,000	327	252
20.50	326,000	19,000	307,000	311	236
21.00	341,000	20,000	321,000	327	252
21.25	343,000	20,000	323,000	325	250
21.50	347,000	20,000	327,000	335	260
21.75	367,000	20,000	347,000	328	253
22.00	378,000	20,000	358,000	325	250
22.25	388,000	20,000	368,000	332	257
22.50	397,000	20,000	377,000	330	255
22.65	386,000	22,000	364,000	355	280

Table 5. Data for Nickel Film No. 5

Power: dc
Duration of Test: 22.3 sec
Film Orientation: horizontal
Location of Failure: near middle of film
Ambient Temperature: 72°F

Time (sec)	Heat Input ($\frac{Btu}{hr\ ft^2}$)	Slide Heat Flux ($\frac{Btu}{hr\ ft^2}$)	Water Heat Flux ($\frac{Btu}{hr\ ft^2}$)	Film Temp. (°F)	Temp. Diff. (°F)
0.00	-0-	-0-	-0-	-	-
1.00	435	-0-	435	-	-
2.00	3,690	-0-	3,690	90	18
3.25	18,000	10,400	7,600	90	18
4.00	33,300	16,400	16,900	155	83
4.50	39,700	19,400	20,300	183	111
5.00	50,400	22,000	28,400	215	143
5.50	58,200	24,400	33,800	234	162
6.00	68,600	26,600	42,000	249	177
6.50	82,100	13,600*	68,500	245	173
7.00	94,300	14,700	79,600	258	186
7.50	106,000	15,100	90,900	263	191
8.00	120,000	13,000	107,000	235	163
8.50	132,000	13,000	119,000	235	163
9.00	141,000	13,000	128,000	242	170
9.50	157,000	13,000	144,000	240	168
10.00	169,000	14,000	155,000	245	173
10.50	179,000	15,000	164,000	256	184
11.00	202,000	16,000	186,000	273	201
11.50	207,000	16,000	191,000	280	208
12.00	214,000	15,000	199,000	268	196
12.50	230,000	17,000	213,000	284	212
13.00	237,000	16,000	221,000	280	208
13.50	249,000	18,000	231,000	297	225
14.00	259,000	17,000	242,000	282	210
14.50	267,000	16,000	251,000	280	208
15.00	286,000	18,000	268,000	297	225
15.50	302,000	17,000	285,000	287	215
16.00	330,000	17,000	313,000	286	214

*Assumed linear temperature drop through slide.

(Continued)

Table 5 (Continued). Data for Nickel Film No. 5

Time (sec)	Heat Input ($\frac{Btu}{hr\ ft^2}$)	Slide Heat Flux ($\frac{Btu}{hr\ ft^2}$)	Water Heat Flux ($\frac{Btu}{hr\ ft^2}$)	Film Temp. (°F)	Temp. Diff. (°F)
16.50	343,000	17,000	326,000	282	210
17.00	365,000	17,000	348,000	284	212
18.00	401,000	17,000	384,000	282	210
18.50	419,000	17,000	402,000	288	216
19.00	438,000	16,000	422,000	280	208
19.50	458,000	18,000	440,000	295	223
20.00	484,000	17,000	467,000	286	214
20.50	502,000	17,000	485,000	291	219
21.00	526,000	19,000	507,000	310	238
21.25	553,000	18,000	535,000	298	226
21.50	570,000	18,000	552,000	302	230
21.75	565,000	19,000	546,000	308	236
22.00	579,000	19,000	560,000	308	236
22.25	587,000	19,000	568,000	318	246
22.30	595,000	20,000	575,000	330	258
22.30	495,000	28,000	467,000	432	360

Table 6. Data for Nickel Film No. 11

Power: dc
Duration of Test: 13.0 sec
Film Orientation: vertical
Location of Failure: end
Ambient Temperature: 75°F

Time (sec)	Heat Input ($\frac{Btu}{hr\ ft^2}$)	Slide Heat Flux ($\frac{Btu}{hr\ ft^2}$)	Water Heat Flux ($\frac{Btu}{hr\ ft^2}$)	Film Temp. (°F)	Temp. Diff. (°F)
0.00	-0-	-0-	-0-	-	-
0.50	930	-0-	930	80	5
1.00	2,600	-0-	2,600	68	-
1.25	4,220	3,340	880	78	3
1.50	6,150	4,750	1,400	78	3
1.75	7,600	5,810	1,790	90	15
2.00	9,650	6,710	2,940	103	28
2.50	14,200	8,220	5,980	110	35
3.00	19,200	9,490	9,710	109	34
3.50	26,100	10,600	15,500	127	52
4.00	33,900	11,700	22,200	143	68
4.50	40,900	12,700	28,200	165	90
5.00	47,300	13,600	33,700	172	97
5.50	50,500	14,600	35,900	183	108
6.00	59,800	15,500	44,300	197	122
6.50	66,000	16,400	49,600	208	133
7.00	77,100	17,300	59,800	215	140
7.50	89,500	18,200	71,300	217	142
8.00	100,000	19,100	80,900	224	149
8.50	116,000	20,000	96,000	235	160
9.00	126,000	12,000*	114,000	230	155
9.50	143,000	13,000	130,000	235	160
10.00	146,000	12,000	134,000	222	147
10.50	158,000	13,000	145,000	237	162
11.00	170,000	13,000	157,000	235	160
11.50	190,000	14,000	176,000	250	175
12.00	200,000	13,000	187,000	244	169
12.50	214,000	15,000	199,000	263	188
13.00	227,000	14,000	213,000	256	181

*Assumed linear temperature drop through slide.

Table 7. Data for Nickel Film No. 12

Power: dc
Duration of Test: 18.5 sec
Film Orientation: vertical
Location of Failure: end
Ambient Temperature: 80°F

Time (sec)	Heat Input ($\frac{Btu}{hr\ ft^2}$)	Slide Heat Flux ($\frac{Btu}{hr\ ft^2}$)	Water Heat Flux ($\frac{Btu}{hr\ ft^2}$)	Film Temp. (°F)	Temp. Diff. (°F)
0.00	-0-	-0-	-0-	-	-
0.50	2,650	-0-	2,650	116	36
1.00	5,650	-0-	5,650	113	33
1.50	11,200	7,560	3,640	123	43
2.00	17,200	10,700	6,500	107	27
2.50	24,800	13,100	11,700	121	41
3.00	33,300	15,100	18,200	155	75
3.50	37,100	16,900	20,200	173	93
4.00	41,000	18,600	22,400	194	114
4.50	44,000	20,200	23,800	226	146
5.00	51,200	21,700	29,500	216	136
5.50	55,200	23,200	32,000	226	146
6.00	59,300	24,700	34,600	262	182
6.50	66,400	14,000*	52,400	258	178
7.00	75,200	13,200	62,000	247	167
7.50	79,100	13,200	65,900	247	167
8.00	87,900	13,600	74,300	252	172
8.50	96,900	12,500	84,400	238	158
9.00	104,000	12,300	91,700	236	156
9.50	112,000	12,000	100,000	229	149
10.00	120,000	12,000	108,000	226	146
10.50	137,000	13,000	124,000	238	158
11.00	146,000	12,000	134,000	234	154
11.50	155,000	12,000	143,000	229	149
12.00	166,000	12,000	154,000	232	152
12.50	176,000	13,000	163,000	238	158
13.00	188,000	13,000	175,000	244	164
13.50	197,000	14,000	183,000	252	172
14.00	207,000	13,000	194,000	247	167

*Assumed linear temperature drop through slide.

(Continued)

Table 7 (Continued). Data for Nickel Film No. 12

Time (sec)	Heat Input ($\frac{Btu}{hr\ ft^2}$)	Slide Heat Flux ($\frac{Btu}{hr\ ft^2}$)	Water Heat Flux ($\frac{Btu}{hr\ ft^2}$)	Film Temp. (^oF)	Temp. Diff. (^oF)
14.50	222,000	13,000	209,000	240	160
15.00	236,000	14,000	222,000	256	176
15.50	250,000	15,000	235,000	268	188
16.00	260,000	15,000	245,000	266	186
16.50	271,000	15,000	256,000	272	192
17.00	285,000	16,000	269,000	278	198
17.50	295,000	15,000	280,000	274	194
18.00	314,000	15,000	299,000	268	188
18.50	319,000	15,000	304,000	276	196
18.50	207,000	26,000	181,000	410	330

Table 8. Data for Nickel Film No. 18

Power: dc
Duration of Test: 1.10 sec
Film Orientation: horizontal
Location of Failure: near middle of film
Ambient Temperature: 75°F

Time (sec)	Heat Input ($\frac{Btu}{hr\ ft^2}$)	Slide Heat Flux ($\frac{Btu}{hr\ ft^2}$)	Water Heat Flux ($\frac{Btu}{hr\ ft^2}$)	Film Temp. (°F)	Temp. Diff. (°F)
0.00	-0-	-0-	-0-	-	-
0.05	6,900	-0-	6,900	-	-
0.10	16,800	-0-	16,800	-	-
0.15	38,200	-0-	38,200	75	0
0.20	58,400	-0-	58,400	87	12
0.25	78,300	20,300	58,000	87	12
0.30	102,000	28,700	73,300	92	17
0.35	134,000	35,200	98,800	137	62
0.40	160,000	41,000	119,000	157	82
0.45	187,000	45,000	142,000	180	105
0.50	210,000	50,000	160,000	205	130
0.55	247,000	54,000	193,000	216	141
0.60	264,000	58,000	206,000	228	153
0.65	307,000	61,000	246,000	234	159
0.70	344,000	64,000	280,000	252	177
0.75	381,000	67,000	314,000	255	180
0.80	413,000	70,000	343,000	261	186
0.85	435,000	73,000	362,000	270	195
0.90	460,000	76,000	384,000	280	205
0.95	482,000	79,000	403,000	298	223
1.00	498,000	81,000	417,000	297	222
1.05	523,000	84,000	439,000	315	240
1.10	539,000	86,000	453,000	340	265

Table 9. Data for Nickel Film No. 20

Power: dc
Duration of Test: 1.20 sec
Film Orientation: horizontal
Location of Failure: end
Ambient Temperature: 74°F

Time (sec)	Heat Input ($\frac{Btu}{hr\ ft^2}$)	Slide Heat Flux ($\frac{Btu}{hr\ ft^2}$)	Water Heat Flux ($\frac{Btu}{hr\ ft^2}$)	Film Temp. (°F)	Temp. Diff. (°F)
0.00	-0-	-0-	-0-	-	-
0.05	1,580	-0-	1,580	68	-
0.10	6,000	-0-	6,000	137	63
0.15	12,300	-0-	12,300	95	21
0.20	20,300	-0-	20,300	85	11
0.25	28,000	17,300	10,700	93	19
0.30	37,900	24,400	13,500	103	29
0.35	51,100	29,900	21,200	112	38
0.40	69,500	34,600	34,900	127	53
0.45	87,000	38,500	48,500	143	69
0.50	106,000	42,400	63,600	157	83
0.55	126,000	45,800	80,200	192	118
0.60	150,000	49,000	101,000	205	131
0.65	168,000	52,000	116,000	227	153
0.70	189,000	55,000	134,000	257	183
0.75	215,000	57,000	158,000	257	183
0.80	245,000	60,000	185,000	250	176
0.85	272,000	62,000	210,000	265	191
0.90	296,000	65,000	231,000	270	196
0.95	322,000	67,000	255,000	280	206
1.00	360,000	69,000	291,000	295	221
1.05	394,000	71,000	323,000	298	224
1.10	431,000	73,000	358,000	305	231
1.15	475,000	75,000	400,000	301	227
1.20	493,000	77,000	416,000	315	241
1.20	488,000	77,000	411,000	332	258

Table 10. Data for Nickel Film No. 22

Power: dc
Duration of Test: 0.67 sec
Film Orientation: horizontal
Location of Failure: near middle of film
Ambient Temperature: 68°F

Time (sec)	Heat Input ($\frac{Btu}{hr\ ft^2}$)	Slide Heat Flux ($\frac{Btu}{hr\ ft^2}$)	Water Heat Flux ($\frac{Btu}{hr\ ft^2}$)	Film Temp. (°F)	Temp. Diff. (°F)
0.00	-0-	-0-	-0-	-	-
0.05	10,000	-0-	10,000	68	0
0.10	25,500	-0-	25,500	70	2
0.15	60,800	33,800	27,000	93	25
0.20	98,600	47,700	50,900	133	65
0.25	145,000	58,400	86,600	160	92
0.30	193,000	68,000	125,000	203	135
0.35	252,000	75,000	177,000	243	175
0.40	325,000	83,000	242,000	250	182
0.45	395,000	89,000	306,000	268	200
0.50	467,000	95,000	372,000	283	215
0.55	505,000	101,000	404,000	299	231
0.60	539,000	107,000	432,000	312	244
0.65	565,000	112,000	453,000	325	257
0.67	558,000	114,000	444,000	344	276

Table 11. Data for Nickel Film No. 26

Power: ac
Duration of Test: 9.6 sec
Film Orientation: horizontal
Location of Failure: end
Ambient Temperature: 80°F

Time (sec)	Heat Input ($\frac{Btu}{hr\ ft^2}$)	Slide Heat Flux ($\frac{Btu}{hr\ ft^2}$)	Water Heat Flux ($\frac{Btu}{hr\ ft^2}$)	Film Temp. (°F)	Temp. Diff. (°F)
0.00	-0-	-0-	-0-	-	-
0.50	1,040	-0-	1,040	86	6
1.00	2,660	-0-	2,660	121	41
1.50	4,480	-0-	4,480	137	57
2.00	6,700	-0-	6,700	86	6
2.25	8,450	-0-	8,450	96	16
2.50	9,220	-0-	9,220	90	10
2.75	11,100	4,000	7,100	98	18
3.00	12,700	5,600	7,100	126	46
3.50	14,800	7,900	6,900	110	30
4.00	18,400	9,700	8,700	112	32
4.50	23,300	11,200	12,100	138	58
5.00	27,900	12,500	15,400	128	48
5.50	33,100	13,800	19,300	164	84
6.00	37,300	15,000	22,300	175	95
6.25	40,200	15,500	24,700	186	106
6.50	43,400	16,100	27,300	177	97
6.75	45,900	16,700	29,200	184	104
7.00	49,800	17,200	32,600	203	123
7.25	52,700	17,700	35,000	202	122
7.50	56,100	18,300	37,800	212	132
7.75	58,800	18,800	40,000	216	136
8.00	60,400	19,000	41,400	229	149
8.50	66,000	20,000	46,000	235	155
8.75	69,000	12,000*	57,000	236	156
9.00	76,400	12,000	64,400	229	149
9.25	79,500	12,000	67,500	233	153
9.50	83,300	12,000	71,300	232	152
9.60	84,900	11,000	73,900	223	143

*Assumed linear temperature drop through slide.

Table 12. Data for Nickel Film No. 28

Power: ac
Duration of Test: 23.15 sec
Film Orientation: horizontal
Location of Failure: middle
Ambient Temperature: 72°F

Time (sec)	Heat Input ($\frac{Btu}{hr\ ft^2}$)	Slide Heat Flux ($\frac{Btu}{hr\ ft^2}$)	Water Heat Flux ($\frac{Btu}{hr\ ft^2}$)	Film Temp. (°F)	Temp. Diff. (°F)
0.00	-0-	-0-	-0-	-	-
1.00	879	-0-	879	-	-
1.25	1,670	-0-	1,670	104	32
1.50	2,710	-0-	2,710	122	50
1.75	3,760	-0-	3,760	105	33
2.00	4,960	-0-	4,960	82	10
2.25	6,660	-0-	6,660	102	30
2.50	9,140	-0-	9,140	84	12
2.75	11,400	4,400	7,000	94	22
3.00	13,400	6,300	7,100	84	12
3.25	17,400	7,700	9,700	94	22
3.50	17,900	8,900	9,000	112	40
3.75	21,800	10,000	11,800	97	25
4.00	24,400	10,900	13,500	126	54
4.25	26,600	11,800	14,800	105	33
4.50	28,600	12,600	16,000	148	76
4.75	33,700	13,400	20,300	132	60
5.00	36,800	14,100	22,700	155	83
5.25	40,400	14,800	25,600	147	75
5.50	45,400	15,500	29,900	184	112
5.75	49,800	16,200	33,600	174	102
6.00	53,600	16,800	36,800	190	118
6.25	57,800	17,500	40,300	182	110
6.50	62,000	18,100	43,900	198	126
6.75	67,600	18,700	48,900	200	128
7.00	72,400	19,300	53,100	208	136
7.25	79,800	9,900*	69,900	198	126
7.50	85,000	9,500	75,500	192	120

*Assumed linear temperature drop through slide.

(Continued)

Table 12 (Continued). Data for Nickel Film No. 28

Time (sec)	Heat Input ($\frac{Btu}{hr\ ft^2}$)	Slide Heat Flux ($\frac{Btu}{hr\ ft^2}$)	Water Heat Flux ($\frac{Btu}{hr\ ft^2}$)	Film Temp. (°F)	Temp. Diff. (°F)
7.75	89,600	10,500	79,100	206	134
8.00	99,100	9,500	89,600	192	120
8.25	104,000	9,100	94,900	187	115
8.50	107,000	10,100	96,900	200	128
8.75	113,000	10,000	103,000	196	124
9.00	117,000	10,000	107,000	198	126
9.25	128,000	9,000	121,000	188	116
9.50	134,000	9,000	125,000	183	111
9.75	141,000	10,000	131,000	193	121
10.00	141,000	10,000	131,000	198	126
10.25	149,000	9,000	140,000	192	120
10.50	149,000	11,000	138,000	215	143
11.00	157,000	11,000	146,000	207	135
11.50	159,000	11,000	148,000	212	140
12.00	172,000	12,000	160,000	230	158
12.50	172,000	12,000	160,000	230	158
13.00	179,000	13,000	166,000	237	165
13.50	193,000	13,000	180,000	233	161
14.00	202,000	14,000	188,000	246	174
14.50	214,000	14,000	200,000	250	178
15.00	222,000	13,000	209,000	243	171
15.50	231,000	14,000	217,000	253	181
16.00	252,000	15,000	237,000	260	188
16.50	266,000	15,000	251,000	268	196
17.00	287,000	16,000	271,000	276	204
17.50	303,000	15,000	288,000	264	192
18.00	325,000	16,000	309,000	272	200
18.50	343,000	16,000	327,000	278	206
19.00	359,000	15,000	344,000	268	196
19.50	373,000	17,000	356,000	283	211
20.00	400,000	16,000	384,000	276	204
20.50	416,000	15,000	401,000	268	196
21.00	440,000	16,000	424,000	270	198
21.50	472,000	15,000	457,000	268	196
22.00	499,000	16,000	483,000	275	203
22.50	512,000	15,000	497,000	267	195
23.00	540,000	16,000	524,000	272	200
23.15	453,000	25,000	428,000	390	318

Table 13. Data for Nickel Film No. 30

Power: half wave dc
Duration of Test: 8.25 sec
Film Orientation: horizontal
Location of Failure: end of film
Ambient Temperature: 70°F

Time (sec)	Heat Input ($\frac{Btu}{hr\ ft^2}$)	Slide Heat Flux ($\frac{Btu}{hr\ ft^2}$)	Water Heat Flux ($\frac{Btu}{hr\ ft^2}$)	Film Temp. (°F)	Temp. Diff. (°F)
0.00	-0-	-0-	-0-	-	-
0.25	200	-0-	200	77	7
0.50	1,140	-0-	1,140	-	-
0.75	2,380	-0-	2,380	80	10
1.00	4,000	-0-	4,000	-	-
1.25	6,550	-0-	6,550	84	14
1.50	9,200	-0-	9,200	68	-
1.75	13,200	-0-	13,200	70	0
2.00	17,100	7,500	9,600	70	0
2.25	22,200	10,700	11,500	95	25
2.50	27,500	13,100	14,400	100	30
2.75	31,900	15,100	16,800	117	47
3.00	37,200	16,900	20,300	120	50
3.25	44,400	18,500	25,900	128	58
3.50	49,600	20,000	29,600	166	96
3.75	54,700	21,400	33,300	174	104
4.00	61,200	22,700	38,500	197	127
4.25	64,700	23,900	40,800	200	130
4.50	68,500	25,100	43,400	210	140
4.75	78,000	10,200*	67,800	200	130
5.00	87,900	10,000	77,900	197	127
5.25	100,000	10,700	89,300	206	136
5.50	108,000	9,300	98,700	188	118
5.75	117,000	10,000	107,000	196	126
6.00	128,000	10,000	118,000	192	122
6.25	135,000	9,000	126,000	188	118
6.50	147,000	10,000	137,000	192	122
6.75	159,000	10,000	149,000	202	132

*Assumed linear temperature drop through slide.

(Continued)

Table 13 (Continued). Data for Nickel Film No. 30

Time (sec)	Heat Input ($\frac{Btu}{hr\ ft^2}$)	Slide Heat Flux ($\frac{Btu}{hr\ ft^2}$)	Water Heat Flux ($\frac{Btu}{hr\ ft^2}$)	Film Temp. (°F)	Temp. Diff. (°F)
7.00	166,000	10,000	156,000	197	127
7.25	178,000	11,000	167,000	208	138
7.50	181,000	12,000	169,000	220	150
7.75	189,000	12,000	177,000	226	156
8.00	200,000	13,000	187,000	234	164
8.25	200,000	14,000	186,000	246	176
8.25	43,500	29,800	13,700	448	378

Table 14. Data for Nickel Film No. 32

Power: dc
Duration of Test: 6.5 sec
Film Orientation: vertical
Location of Failure: end of film
Ambient Temperature: 80°F

Time (sec)	Heat Input ($\frac{Btu}{hr\ ft^2}$)	Slide Heat Flux ($\frac{Btu}{hr\ ft^2}$)	Water Heat Flux ($\frac{Btu}{hr\ ft^2}$)	Film Temp. (°F)	Temp. Diff. (°F)
0.00	-0-	-0-	-0-	-	-
0.50	331	-0-	331	115	35
0.75	6,840	12,200	-0-	125	45
1.00	17,900	17,300	600	120	40
1.25	31,400	21,200	10,200	140	60
1.50	43,400	24,500	18,900	158	78
1.75	59,700	27,400	32,300	180	100
2.00	70,300	30,000	40,300	202	122
2.25	92,800	32,400	60,400	233	153
2.50	117,000	34,700	82,300	244	164
2.75	146,000	13,000*	133,000	246	166
3.00	167,000	14,000	153,000	253	173
3.25	186,000	14,000	172,000	256	176
3.50	208,000	14,000	194,000	259	179
3.75	231,000	13,000	218,000	248	168
4.00	250,000	14,000	236,000	256	176
4.25	267,000	14,000	253,000	264	184
4.50	288,000	14,000	274,000	259	179
4.75	314,000	14,000	300,000	264	184
5.00	347,000	14,000	333,000	264	184
5.25	372,000	15,000	357,000	272	192
5.50	410,000	15,000	395,000	274	194
5.75	443,000	15,000	428,000	274	194
6.00	472,000	16,000	456,000	282	202
6.25	509,000	16,000	493,000	278	198
6.50	534,000	16,000	518,000	278	198
6.50	486,000	22,000	464,000	362	282

*Assumed linear temperature drop through slide.

Table 15. Data for Nickel Film No. 34

Power: ac
Duration of Test: 1.12 sec
Film Orientation: horizontal
Location of Failure: middle
Ambient Temperature: 75°F

Time	Heat Input	Slide Heat Flux	Water Heat Flux	Film Temp.	Temp. Diff.
(sec)	($\frac{Btu}{hr\ ft^2}$)	($\frac{Btu}{hr\ ft^2}$)	($\frac{Btu}{hr\ ft^2}$)	(°F)	(°F)
0.00	-0-	-0-	-0-	-	-
0.05	746	-0-	746	85	10
0.10	2,130	-0-	2,130	74	-
0.15	5,040	-0-	5,040	-	-
0.20	8,540	-0-	8,540	75	0
0.25	14,700	-0-	14,700	-	-
0.30	23,600	-0-	23,600	90	15
0.35	36,300	-0-	36,300	68	-
0.40	47,000	20,000	27,000	92	17
0.45	63,400	28,100	35,300	78	3
0.50	88,800	34,500	54,300	104	29
0.55	119,000	39,900	79,100	133	58
0.60	142,000	44,400	97,600	141	66
0.65	172,000	49,000	123,000	173	98
0.70	209,000	53,000	156,000	209	134
0.75	229,000	56,000	173,000	224	149
0.80	254,000	60,000	194,000	227	152
0.85	273,000	63,000	210,000	242	167
0.90	309,000	66,000	243,000	253	178
0.95	340,000	69,000	271,000	270	195
1.00	363,000	71,000	292,000	261	186
1.05	401,000	74,000	327,000	274	199
1.10	435,000	77,000	358,000	287	212
1.12	466,000	78,000	388,000	296	221
1.12	259,000	78,000	181,000	436	361

APPENDIX III

PLOTS OF HEAT TRANSFER DATA

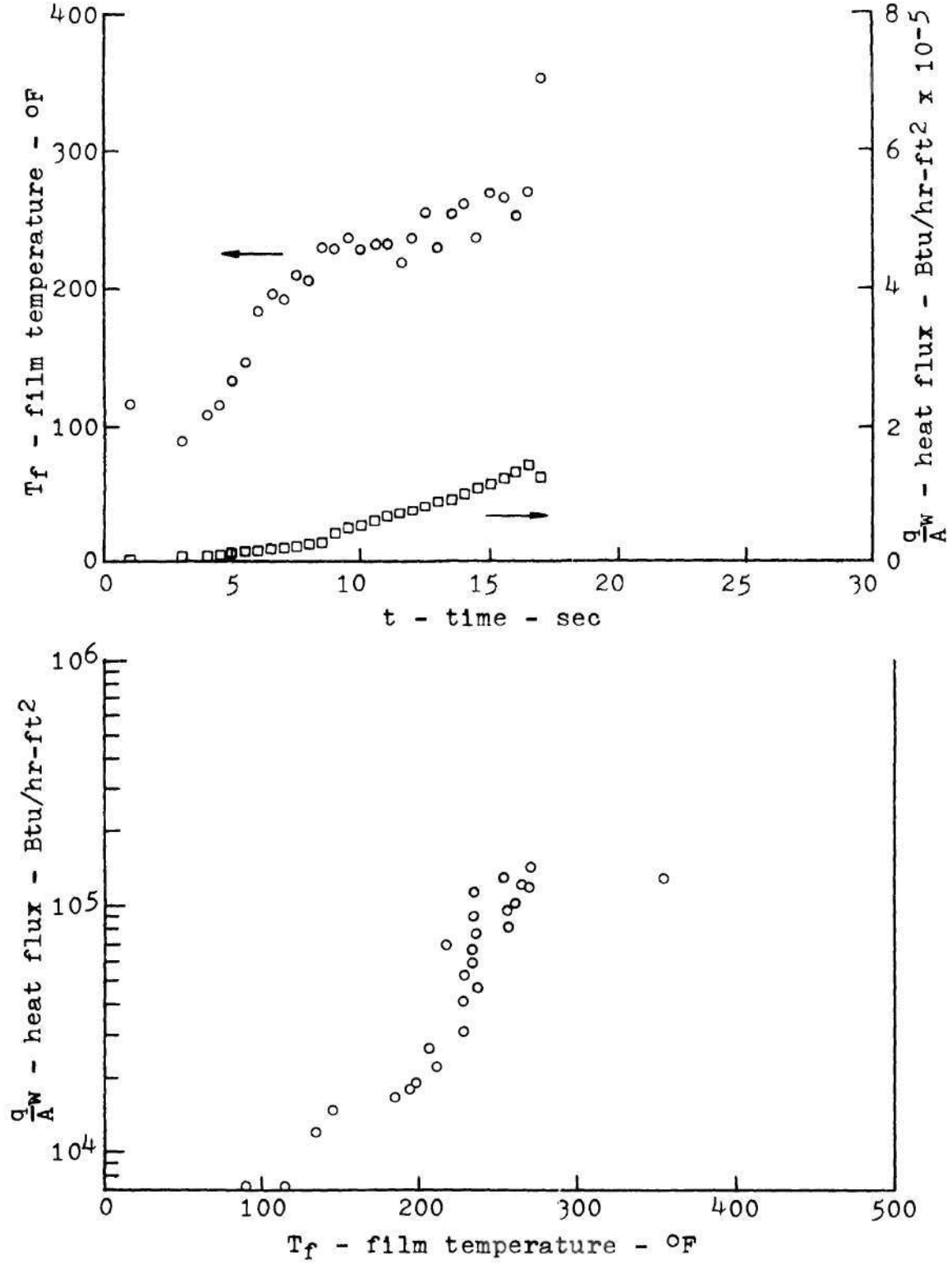

Figure 32. Heat Flux and Film Temperature Curves for Nickel Film No. 3 in Subcooled Water Pool Boiling.

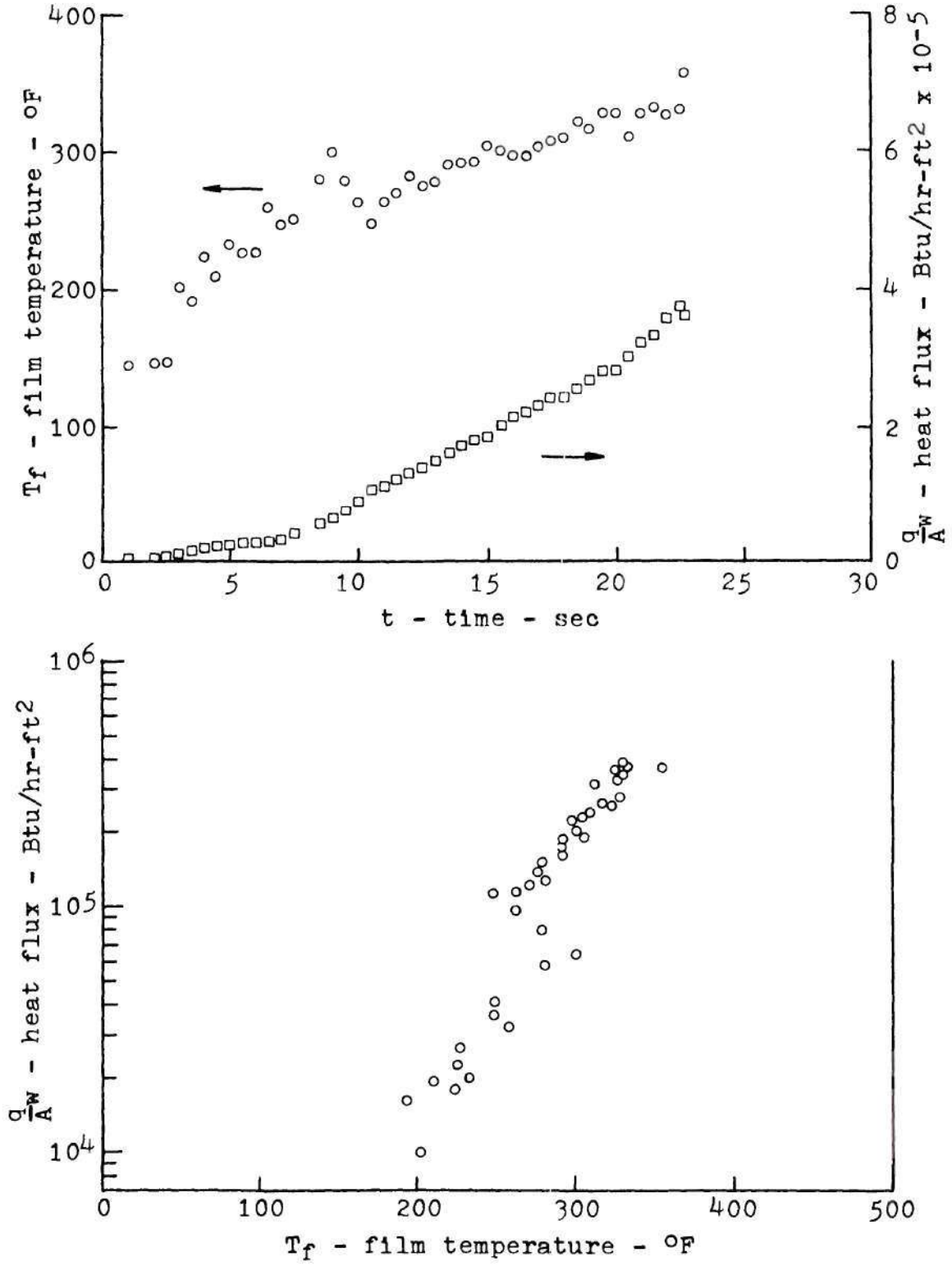

Figure 33. Heat Flux and Film Temperature Curves for Nickel Film No. 4 in Subcooled Water Pool Boiling.

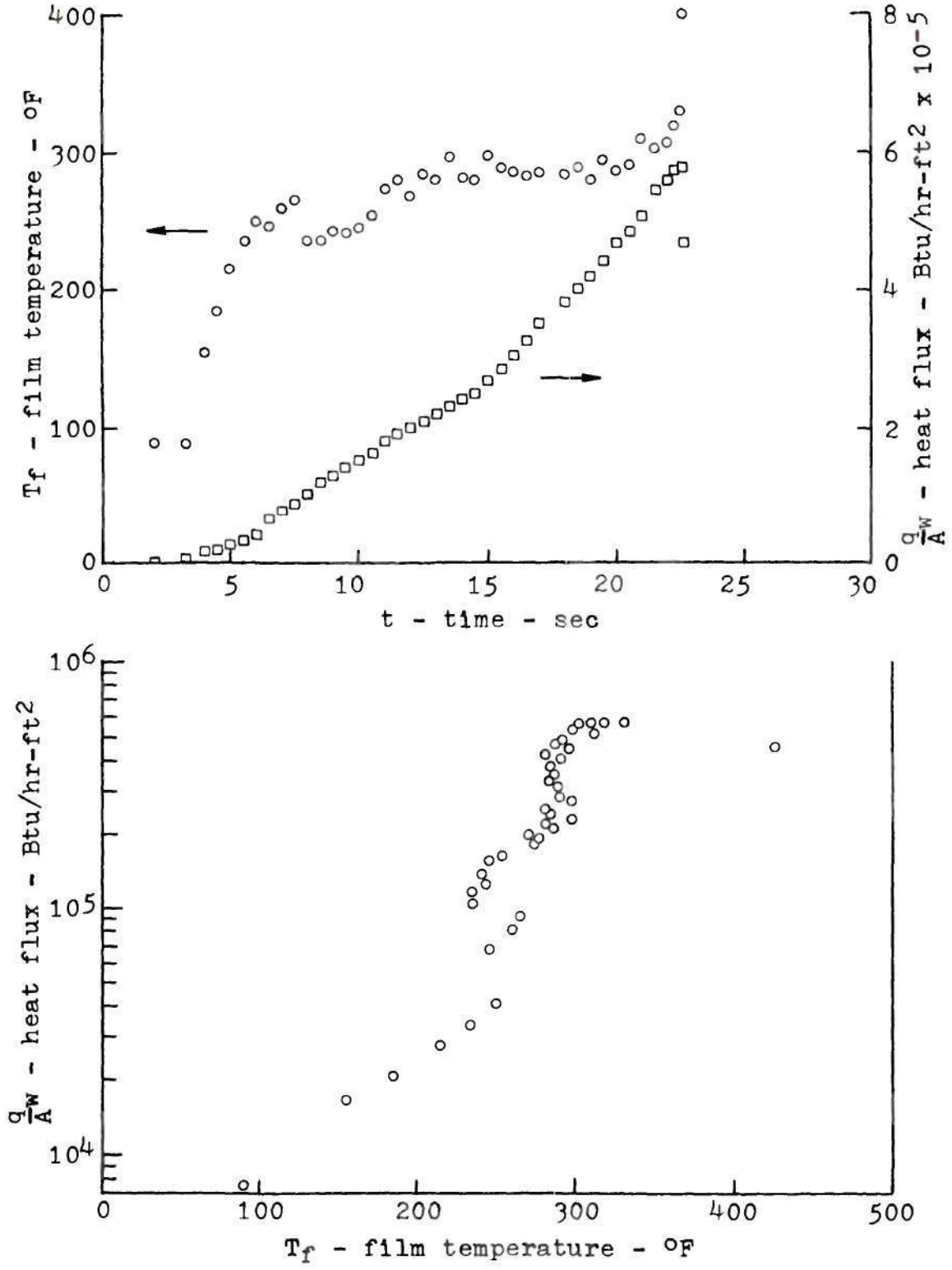

Figure 34. Heat Flux and Film Temperature Curves for Nickel Film No. 5 in Subcooled Water Pool Boiling.

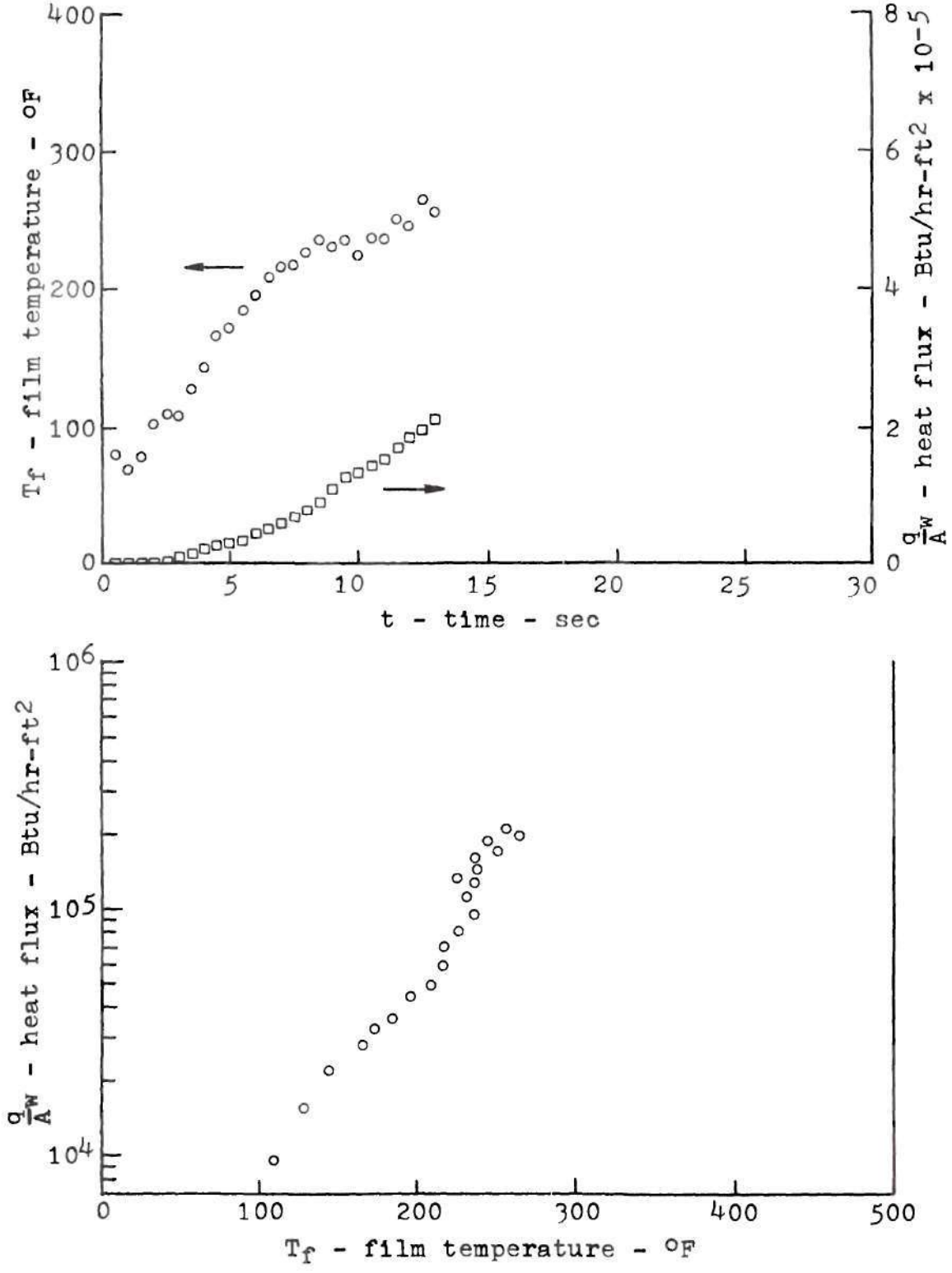

Figure 35. Heat Flux and Film Temperature Curves for Nickel Film No. 11 in Subcooled Water Pool Boiling.

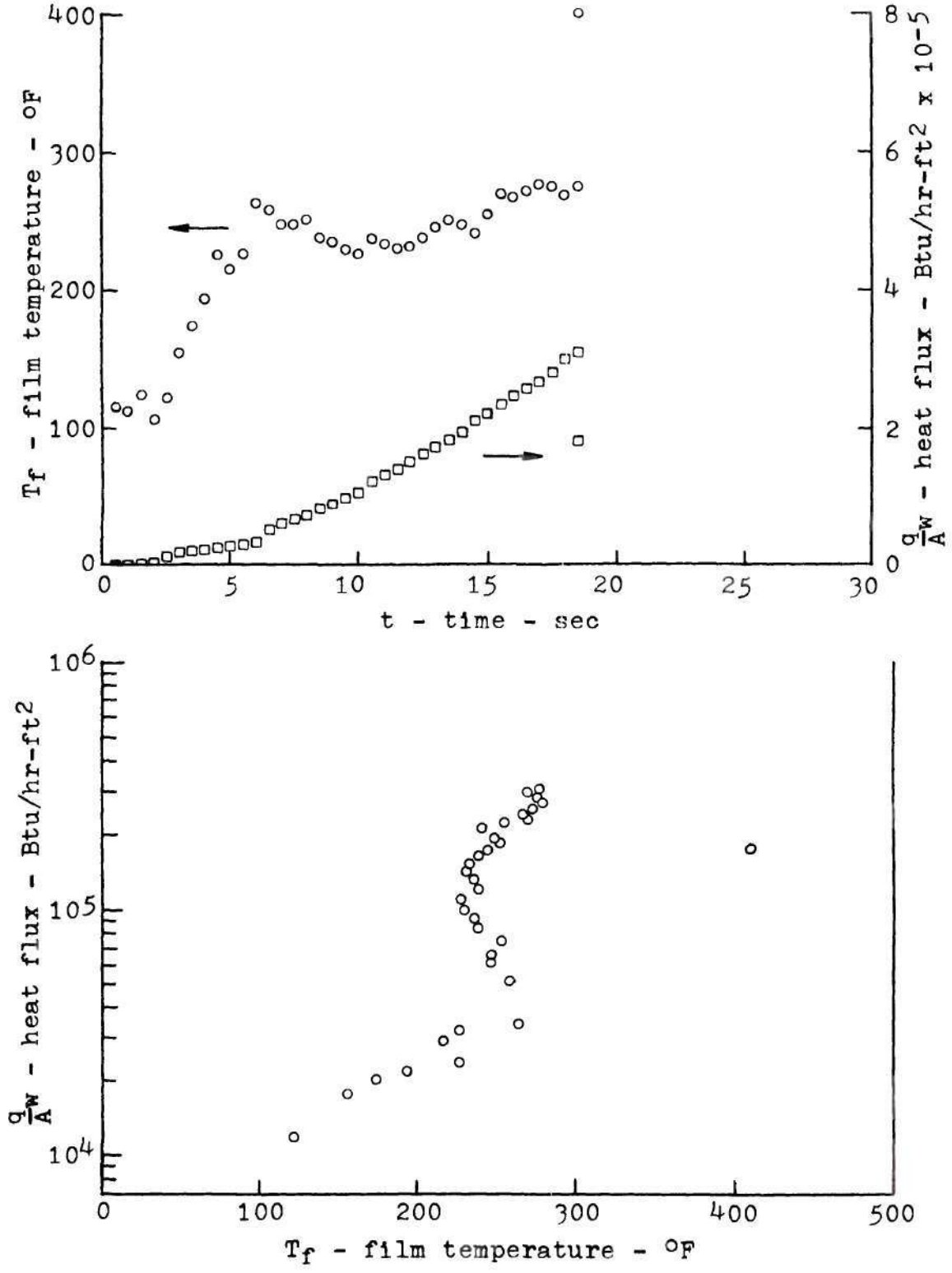

Figure 36. Heat Flux and Film Temperature Curves for Nickel Film No. 12 in Subcooled Water Pool Boiling.

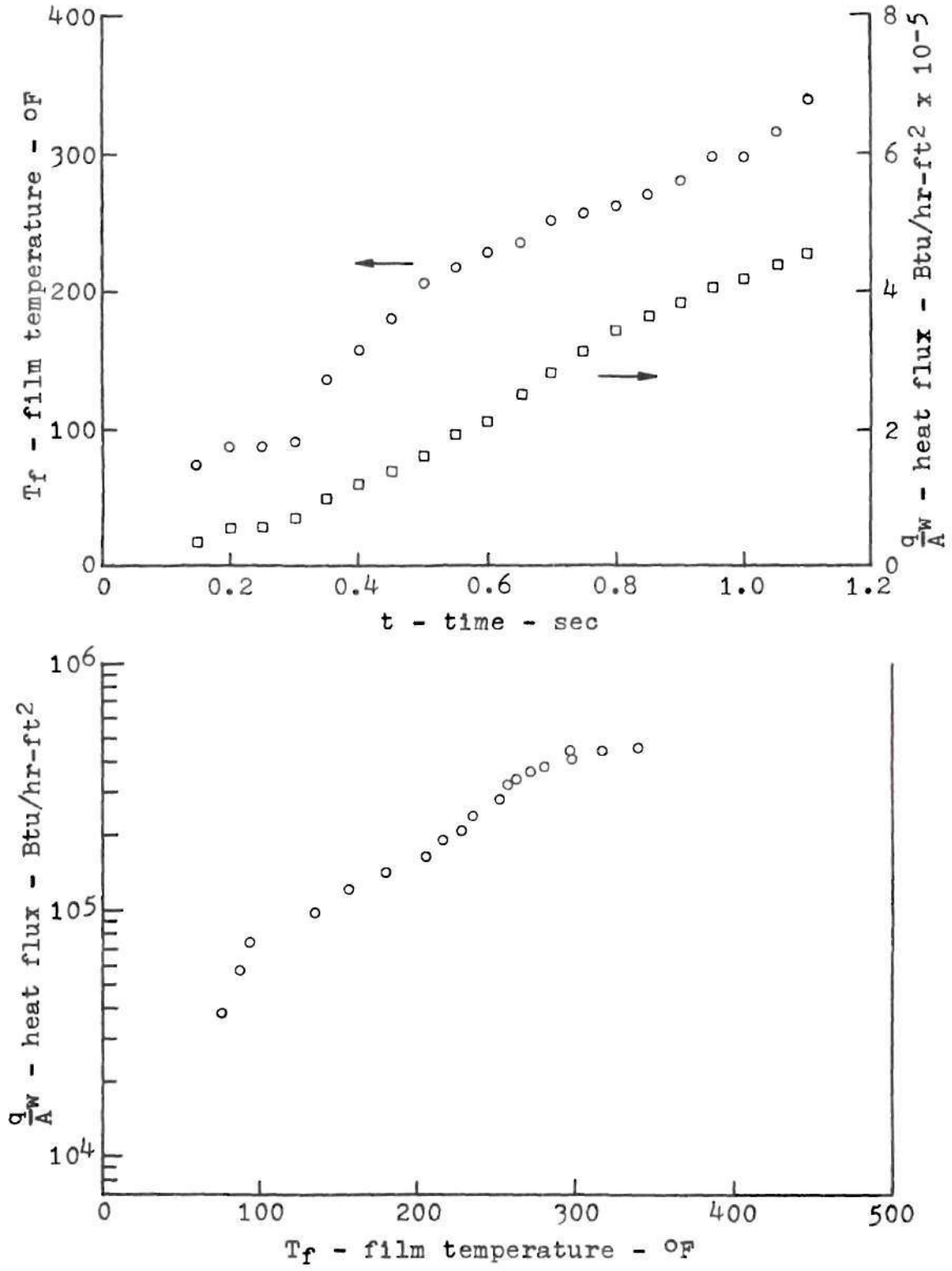

Figure 37. Heat Flux and Film Temperature Curves for Nickel Film No. 18 in Subcooled Water Pool Boiling.

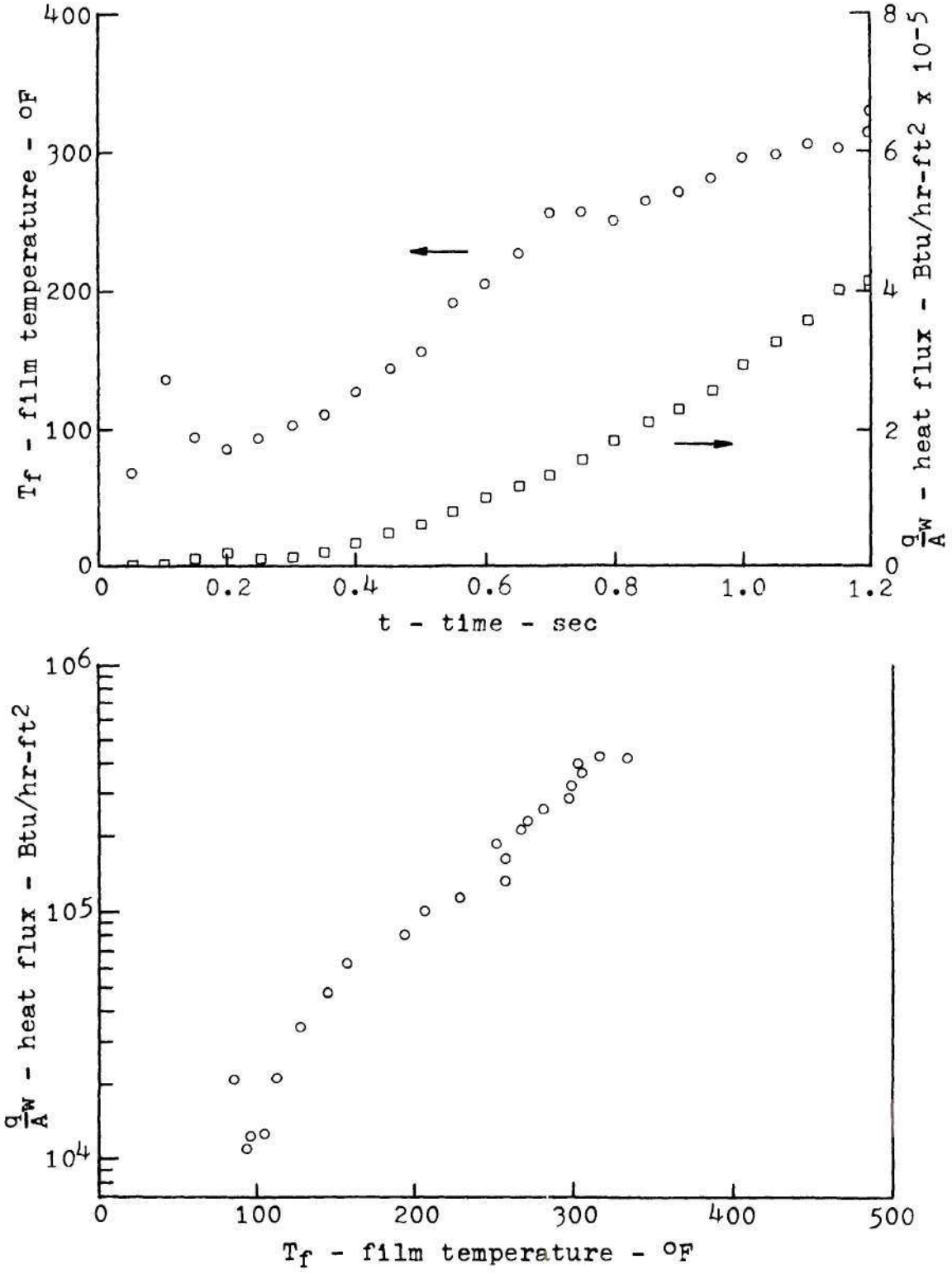

Figure 38. Heat Flux and Film Temperature Curves for Nickel Film No. 20 in Subcooled Water Pool Boiling.

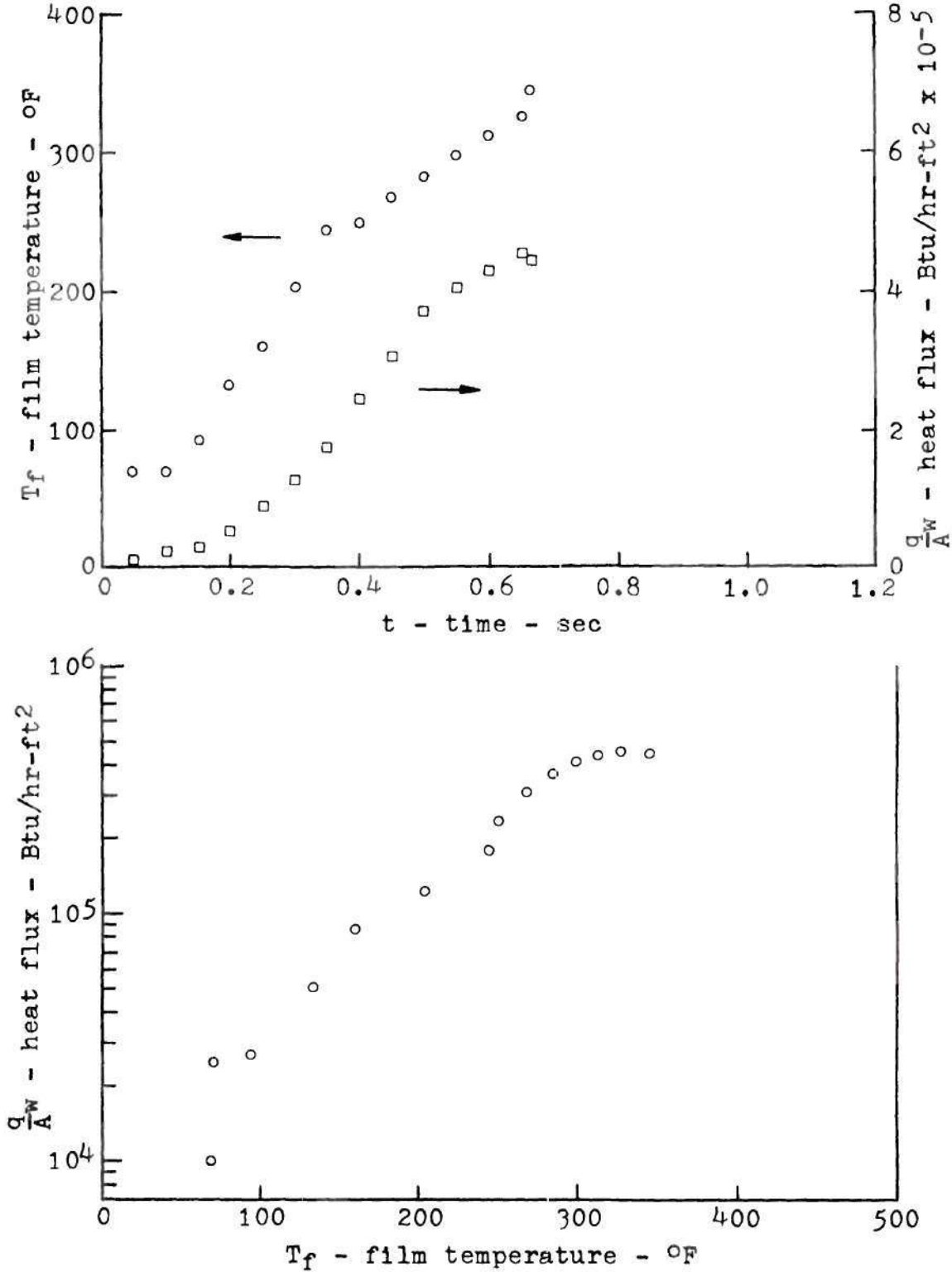

Figure 39. Heat Flux and Film Temperature Curves for Nickel Film No. 22 in Subcooled Water Pool Boiling.

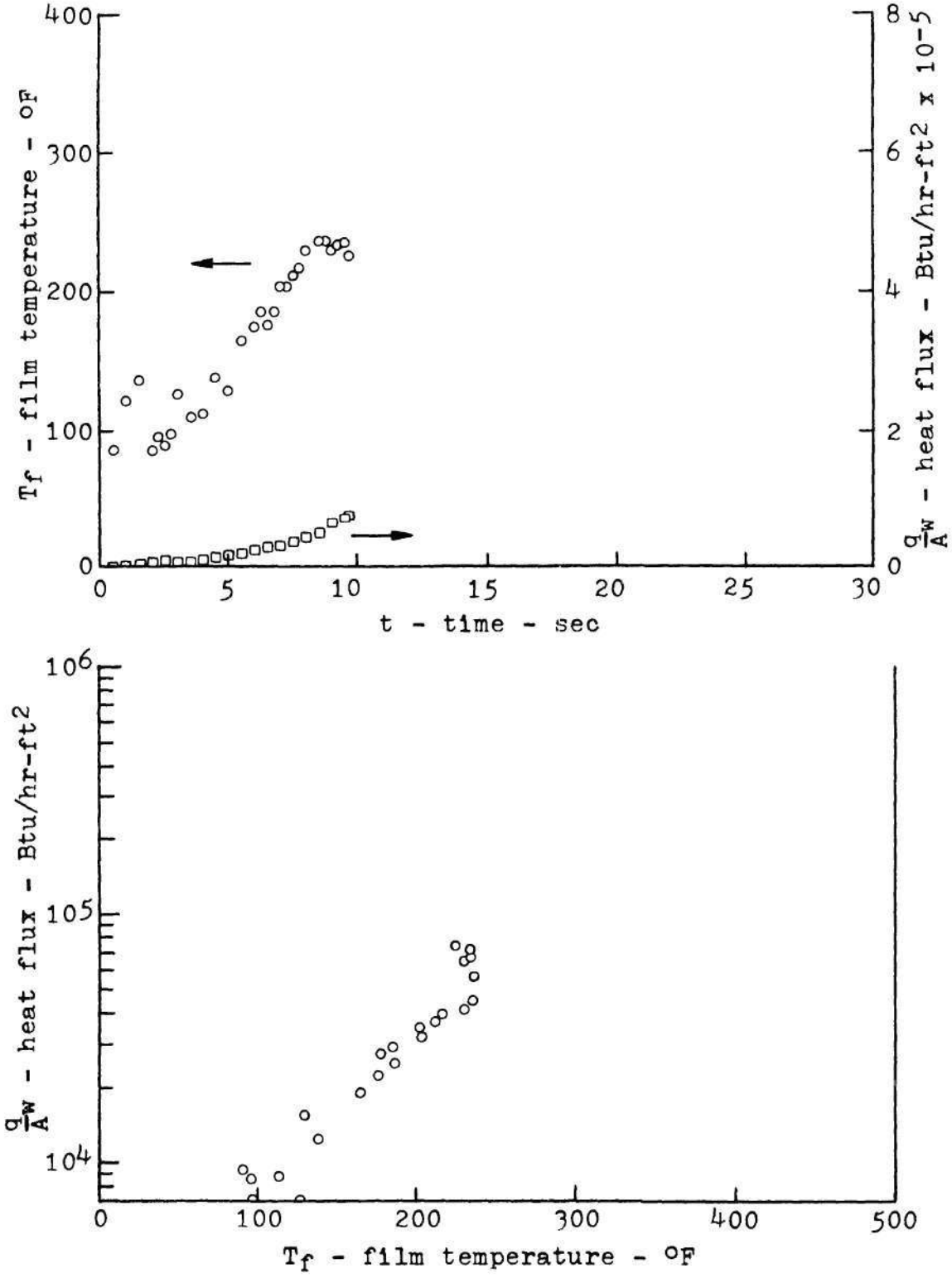

Figure 40. Heat Flux and Film Temperature Curves for Nickel Film No. 26 in Subcooled Water Pool Boiling.

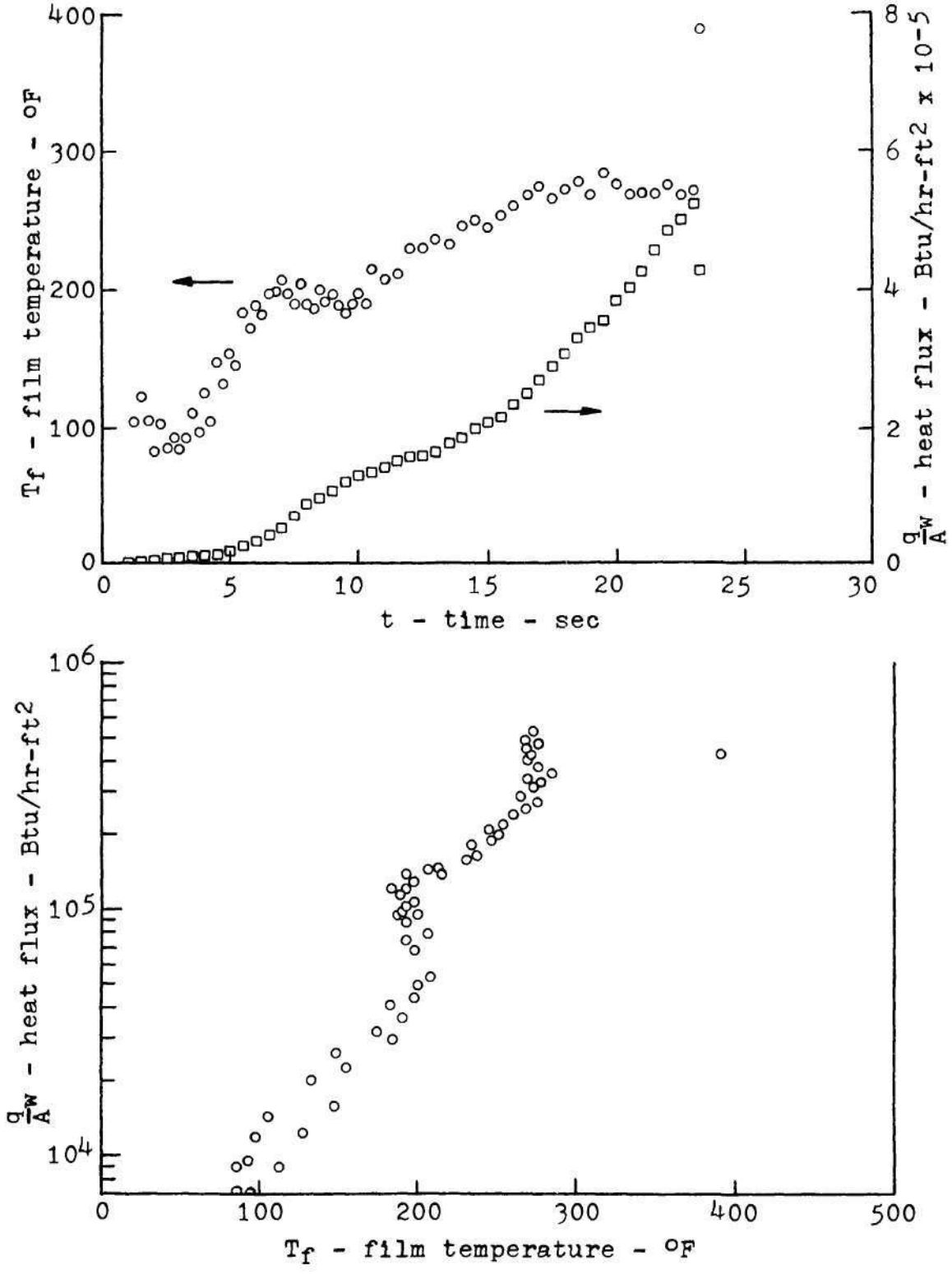

Figure 41. Heat Flux and Film Temperature Curves for Nickel Film No. 28 in Subcooled Water Pool Boiling.

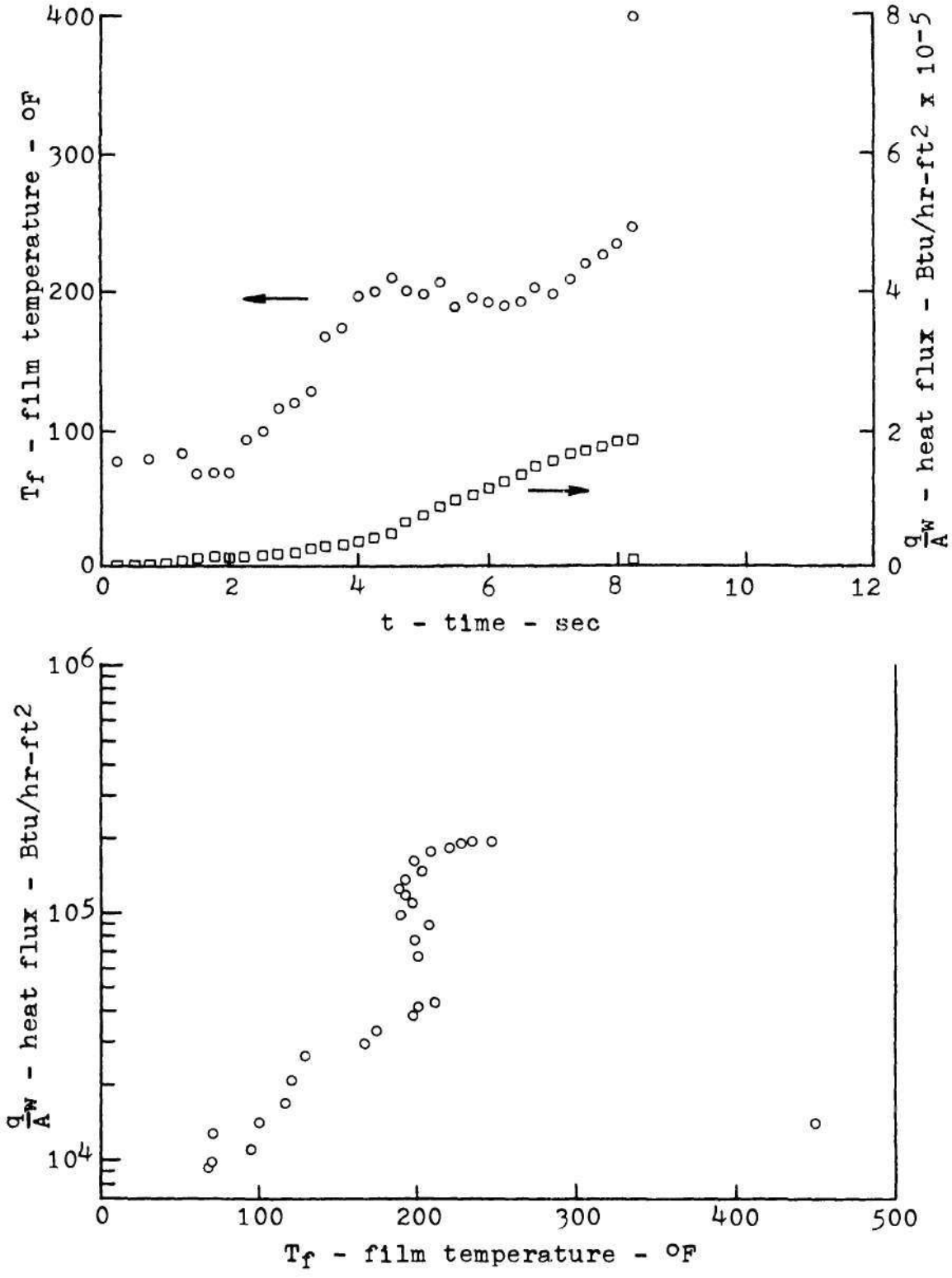

Figure 42. Heat Flux and Film Temperature Curves for Nickel Film No. 30 in Subcooled Water Pool Boiling.

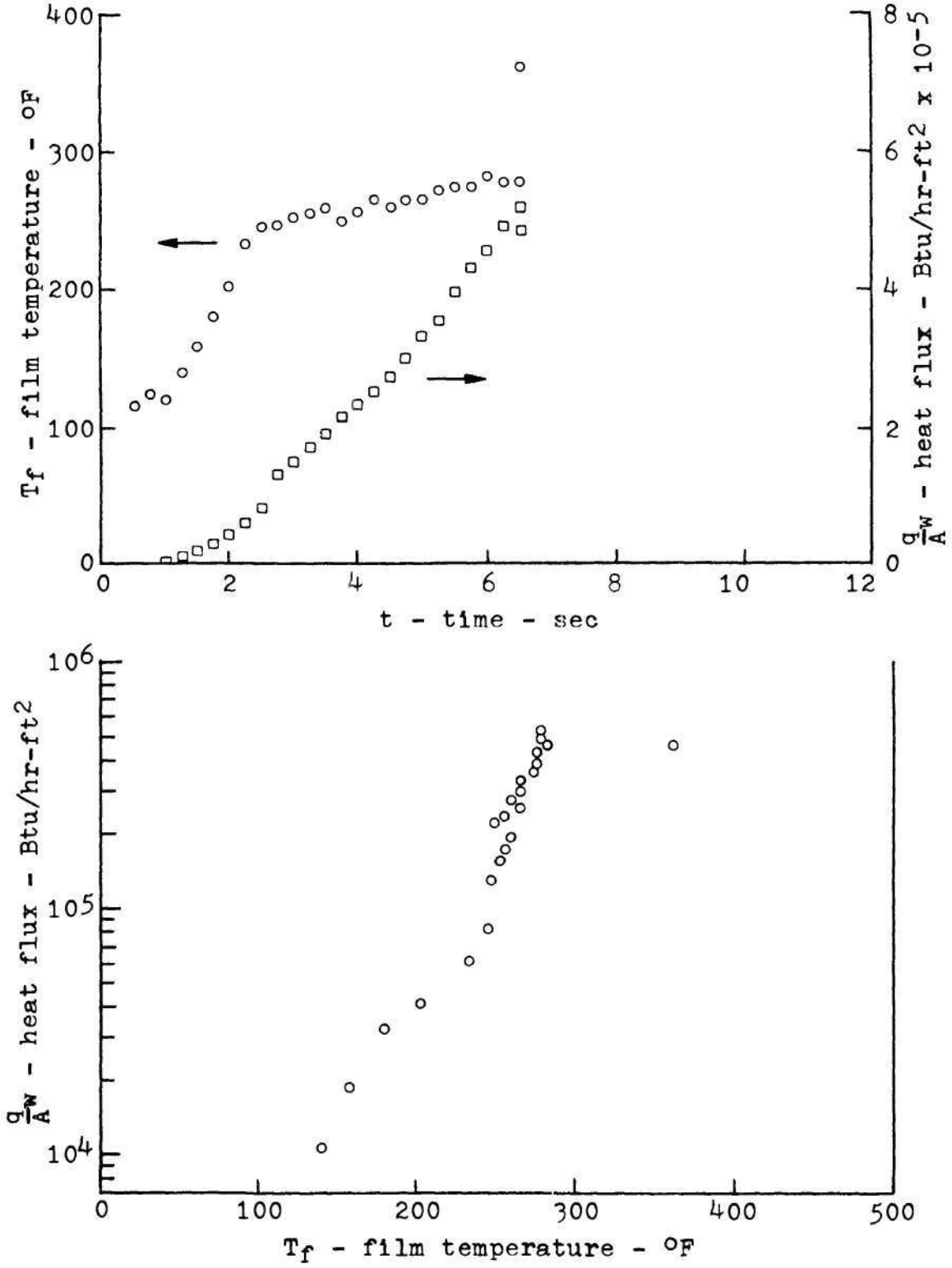

Figure 43. Heat Flux and Film Temperature Curves for Nickel Film No. 32 in Subcooled Water Pool Boiling.

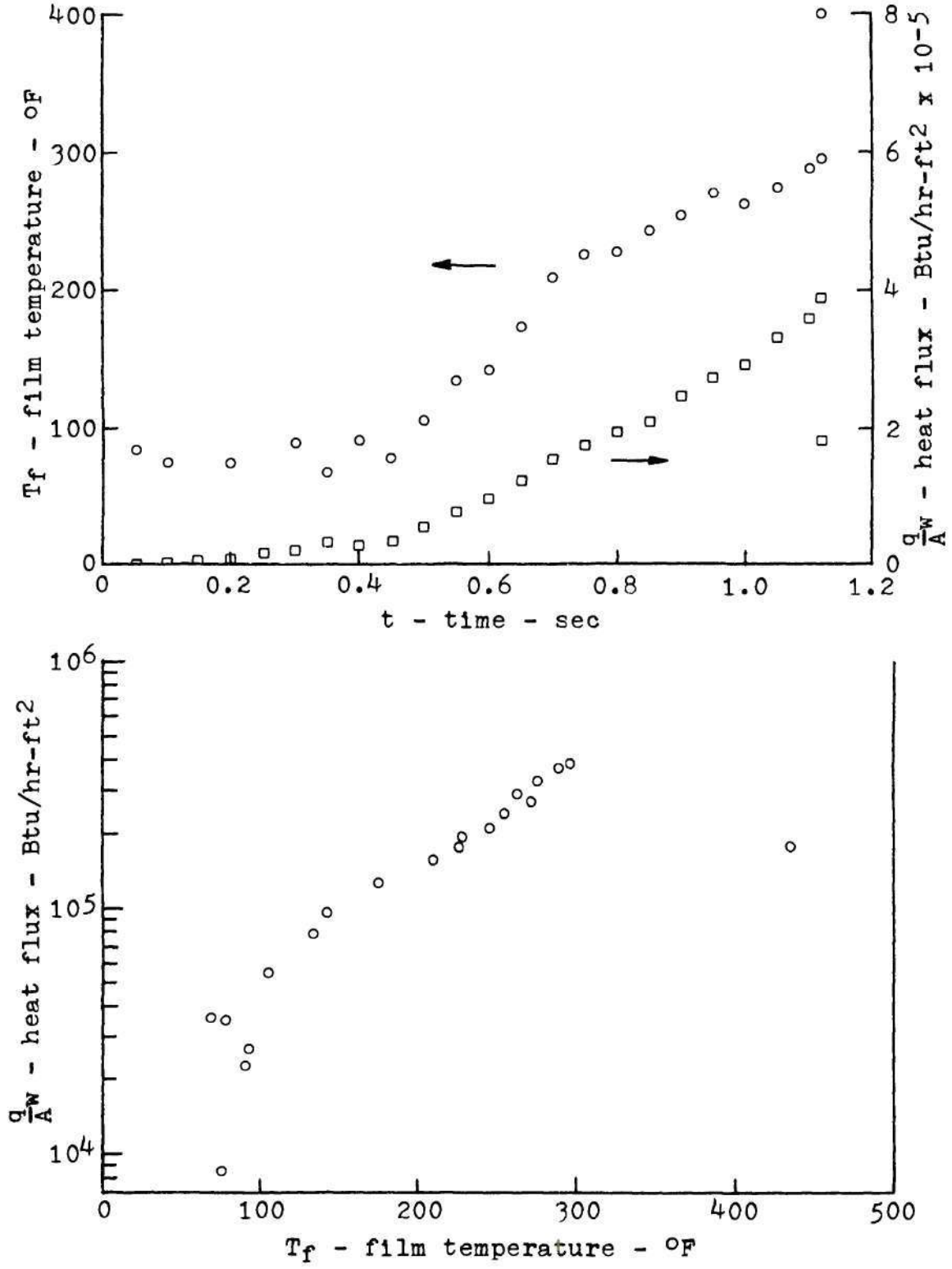

Figure 44. Heat Flux and Film Temperature Curves for Nickel Film No. 34 in Subcooled Water Pool Boiling.

APPENDIX IV

DATA FOR FILM THICKNESS UNIFORMITY STUDIES

Table 16. X-ray Fluorescence Calibration Data for Nickel Uniformity Film No. 1

Sample Number	Weight Before Plating	Sample Area	Film Weight	Average Thickness	Film Peak Area	Blank Peak Area	A_f	A_∞	A_f/A_∞	A_f/A_∞ Average
	(gm)	(cm^2)	(gm)	($\overset{\circ}{A}$)	(in^2)	(in^2)	(in^2)	(in^2)		
1A					4.14	.10	4.04	52.7	.0767	
1B	.84100	3.290	.00067	2290	4.35	.10	4.25	52.7	.0806	.0751
1C					3.80	.10	3.70	54.3	.0681	
2A					4.84	.10	4.74	54.3	.0873	
2B	.83547	3.268	.00075	2580	5.02	.10	4.92	54.3	.0906	.0841
2C					4.26	.10	4.16	56.0	.0743	
3A					5.00	.10	4.90	56.0	.0875	
3B	.79181	3.097	.00071	2570	5.11	.10	5.01	55.4	.0904	.0866
3C					4.64	.10	4.54	55.4	.0819	
4A					4.73	.10	4.63	55.4	.0836	
4B	.87195	3.411	.00074	2440	4.81	.10	4.71	55.4	.0850	.0813
4C					4.23	.10	4.13	54.9	.0752	
5A					4.28	.11	4.17	54.9	.0760	
5B	.83877	3.281	.00064	2190	4.35	.11	4.24	54.9	.0772	.0729
5C					3.82	.12	3.70	56.4	.0656	
6A					3.90	.12	3.78	56.4	.0670	
6B	.76870	3.007	.00052	1940	3.97	.12	3.85	56.4	.0683	.0643
6C					3.45	.12	3.33	57.9	.0575	

Table 17. X-ray Fluorescence Calibration Data for Nickel Uniformity Film No. 2

Sample Number	Weight Before Plating	Sample Area	Film Weight	Average Thickness	Film Peak Area	Blank Peak Area	A_f	A_∞	A_f/A_∞	A_f/A_∞ Average
	(gm)	(cm^2)	(gm)	($\overset{\circ}{A}$)	(in^2)	(in^2)	(in^2)	(in^2)		
1A					4.55	.13	4.42	63.8	.0693	
1B	.76548	2.828	.00061	2420	4.75	.12	4.63	63.8	.0726	.0697
1C					4.40	.12	4.28	63.8	.0671	
2A					4.34	.12	4.22	63.5	.0665	
2B	.82021	3.030	.00068	2520	4.62	.12	4.50	63.5	.0709	.0664
2C					4.04	.11	3.93	63.5	.0619	
3A					4.53	.11	4.42	63.3	.0698	
3B	.81257	3.002	.00061	2280	4.51	.11	4.40	63.3	.0695	.0673
3C					4.07	.11	3.96	63.3	.0626	
4A					4.24	.12	4.12	63.8	.0646	
4B	.96623	3.569	.00067	2110	4.32	.12	4.20	63.8	.0658	.0642
4C					4.08	.12	3.96	63.8	.0621	
5A					4.25	.12	4.13	64.1	.0644	
5B	.94689	3.498	.00066	2120	4.32	.12	4.20	64.1	.0655	.0630
5C					3.90	.12	3.78	64.1	.0590	
6A					4.03	.13	3.90	64.2	.0607	
6B	.92814	3.429	.00061	2000	4.37	.13	4.24	64.2	.0660	.0626
6C					4.06	.13	3.93	64.2	.0612	

Table 18. X-ray Fluorescence Calibration Data for Nickel Uniformity Film No. 3

Sample Number	Weight Before Plating	Sample Area	Film Weight	Average Thickness	Film Peak Area	Blank Peak Area	A_f	A_∞	A_f/A_∞	A_f/A_∞ Average
	(gm)	(cm^2)	(gm)	($\overset{\circ}{A}$)	(in^2)	(in^2)	(in^2)	(in^2)		
1A					4.63	.15	4.48	64.3	.0697	
1B	.82636	3.289	.00064	2190	4.53	.15	4.38	64.3	.0681	.0655
1C					3.92	.15	3.77	64.3	.0586	
2A					5.12	.14	4.98	64.3	.0775	
2B	.84300	3.356	.00063	2110	4.92	.14	4.78	64.3	.0743	.0710
2C					4.05	.12	3.93	64.3	.0611	
3A					3.95	.12	3.83	64.4	.0594	
3B	.81543	3.246	.00046	1590	3.73	.14	3.59	64.4	.0557	.0558
3C					3.51	.15	3.36	64.4	.0522	
4A					3.04	.15	2.89	64.4	.0449	
4B	.78096	3.109	.00035	1270	3.13	.15	2.98	64.4	.0463	.0446
4C					2.90	.16	2.74	64.4	.0425	
5A					3.79	.16	3.63	64.2	.0565	
5B	.76449	3.043	.00047	1740	3.75	.15	3.60	64.2	.0561	.0538
5C					3.28	.14	3.14	64.2	.0489	
6A					4.46	.14	4.32	64.0	.0675	
6B	.83200	3.312	.00058	1970	4.45	.12	4.33	64.0	.0677	.0646
6C					3.87	.12	3.75	64.0	.0586	

Table 19. X-ray Fluorescence Calibration Data for Nickel Uniformity Film No. 5

Sample Number	Weight Before Plating	Sample Area	Film Weight	Average Thickness	Film Peak Area	Blank Peak Area	A_f	A_∞	A_f/A_∞	A_f/A_∞ Average
	(gm)	(cm^2)	(gm)	($\mathring{A}$)	(in^2)	(in^2)	(in^2)	(in^2)		
1A					3.98	.14	3.84	63.2	.0608	
1B	.87477	3.186	.00058	2050	3.82	.15	3.67	63.2	.0581	.0580
1C					3.64	.15	3.49	63.2	.0552	
2A					3.60	.16	3.44	63.2	.0544	
2B	.92915	3.384	.00052	1730	3.65	.16	3.49	63.2	.0552	.0537
2C					3.43	.17	3.26	63.2	.0516	
3A					4.04	.17	3.87	64.6	.0599	
3B	.90858	3.309	.00052	1770	4.08	.17	3.91	64.6	.0605	.0587
3C					3.77	.17	3.60	64.6	.0557	
4A					4.24	.16	4.08	64.6	.0632	
4B	.87268	3.178	.00050	1770	4.32	.16	4.16	64.6	.0644	.0613
4C					3.79	.16	3.63	64.6	.0562	
5A					4.02	.16	3.86	64.7	.0597	
5B	.90122	3.282	.00055	1880	4.13	.16	3.97	64.7	.0614	.0585
5C					3.68	.16	3.52	64.7	.0544	
6A					3.85	.17	3.68	64.7	.0569	
6B	.82828	3.016	.00044	1640	3.79	.17	3.62	64.7	.0560	.0543
6C					3.40	.17	3.23	64.7	.0499	

Table 20. Film Thicknesses as a Function of Position for Nickel Uniformity Films

Substrate Position	Thicknesses (Å) Film No. 1	Film No. 2	Film No. 3	Film No. 5	Theoretical Prediction
1A	2360	2140	2160	1880	2440
1B	2490	2240	2110	1790	2580
1C	2110	2070	1810	1710	2440
2A	2700	2060	2400	1680	2610
2B	2800	2190	2300	1710	2760
2C	2300	1920	1890	1590	2610
3A	2710	2160	1830	1850	2680
3B	2800	2150	1720	1870	2840
3C	2530	1930	1610	1720	2680
4A	2580	1990	1380	1950	2680
4B	2630	2030	1430	1990	2840
4C	2330	1920	1310	1730	2680
5A	2350	1990	1740	1840	2610
5B	2380	2020	1730	1890	2760
5C	2030	1820	1510	1680	2610
6A	2070	1870	2080	1760	2440
6B	2110	2040	2090	1730	2580
6C	1780	1890	1810	1540	2440

LITERATURE CITED

1. J. D. Fleming, Jr., Heat Transfer from Thin Gold Films to Water in Swirling Flow, Ph.D. Thesis, Georgia Institute of Technology, Atlanta, Georgia, 1959.

2. J. G. Leidenfrost, "On the Fixation of Water in Diverse Fire," from A Tract About Some Qualities of Common Water, 1756. Translated by Carolyn Wares, University of Oklahoma, Norman, Oklahoma, 1966; International Journal of Heat and Mass Transfer 9, 1153-1166 (1966).

3. W. H. McAdams, Heat Transmission, 3rd ed., New York: McGraw-Hill Book Company, Inc., 1954. Chapter 14, 368-409.

4. M. Jakob, Heat Transfer, Volume I, New York: John Wiley & Sons, Inc., 1949. Chapter 29, 614-657.

5. M. Jakob, Heat Transfer, Volume II, New York: John Wiley & Sons, Inc., 1957. Supplement to Chapter 29, 580-585.

6. F. Kreith, Principles of Heat Transfer, Scranton, Pa.: International Textbook Company, 1958. Chapter 10, 398-438.

7. J. W. Westwater, "Boiling of Liquids," in Advances in Chemical Engineering, Volume I, ed. by T. B. Drew and J. W. Hoopes, Jr., New York: Academic Press Inc., 1956. 1-76.

8. J. W. Westwater, "Boiling of Liquids," in Advances in Chemical Engineering, Volume II, ed. by T. B. Drew and J. W. Hoopes, Jr., New York: Academic Press Inc., 1958. 1-31.

9. W. M. Rohsenow, "Heat Transfer with Boiling," in Modern Developments in Heat Transfer, ed. by W. Ibele, New York: Academic Press Inc., 1963. 85-158.

10. E. A. Farber and R. L. Scorah, "Heat Transfer to Water Boiling Under Pressure," Transactions of the American Society of Mechanical Engineers 70, 369-384 (1948).

11. Reference 4, pp. 616-618.

12. W. H. McAdams et al., "Heat Transfer from Single Horizontal Wires to Boiling Water," Chemical Engineering Progress 44, 639-646 (1948).

13. W. M. Rohsenow, "A Method of Correlating Heat-Transfer Data for Surface Boiling of Liquids," Trans ASME 74, 969-976 (1952).

14. C. C. Winding, L. Topper, and B. V. Baus, "Metal-Film Resistance Thermometers for Measuring Surface Temperatures," Industrial and Engineering Chemistry 47, 386-392 (1955).

15. T. B. Simpson and C. C. Winding, "Properties of Evaporated Metal Films Related to Their Use for Surface Temperature Measurements," American Institute of Chemical Engineers Journal 2, 113-117 (1956).

16. D. W. Kirby and J. W. Westwater, "Bubble and Vapor Behavior on a Heated Horizontal Plate During Pool Boiling Near Burnout," Chemical Engineering Progress Symposium Series No. 57 61, 238-248 (1965).

17. H. A. Johnson et al., "Transient Pool Boiling of Water at Atmospheric Pressure," International Developments in Heat Transfer, Part II, New York: The American Society of Mechanical Engineers, 1961. 244-254.

18. L. Holland, Vacuum Deposition of Thin Films, London: Chapman and Hall Ltd., 1963.

19. A. J. Laderman, G. J. Hecht, and A. K. Oppenheim, "Thin Film Thermometry in Detonation Research," in Temperature Its Measurement and Control in Science and Industry, Volume 3, Part 2, New York: Reinhold Publishing Corp., 1962. 943 ff.

20. R. A. Hartunian and R. L. Varwig, "On Thin-Film Heat-Transfer Measurements in Shock Tubes and Shock Tunnels," The Physics of Fluids 5, 169-174 (1962).

21. J. J. Ginoux, "A Steady-State Technique for Local Heat-Transfer Measurement and Its Application to the Flat Plate," Journal of Fluid Mechanics 19, 21 ff. (1964).

22. G. S. Ambrok, "Method for Calibrating Thermal Flow Detectors," Measurement Techniques, No. 11, 918 ff. (1964).

23. V. Kmonicek, "The Determination of Unsteady Heat Flow to Wall From the Measurements of Surface Temperature Made with Thin Film Resistance Thermometers," Int J Heat Mass Transfer 9, 199-213 (1966).

24. R. B. Belser and W. H. Hicklin, "Temperature Coefficients of Resistance of Metallic Films in the Temperature Range 25° to 600°C," Journal of Applied Physics 30, 313-322 (1959).

25. F. C. Gunther and F. Kreith, "Photographic Study of Bubble Formation in Heat Transfer to Subcooled Water," Heat Transfer and Fluid Mechanics Institute, New York: The American Society of Mechanical Engineers, 1949. 113-126.

26. F. Kreith and M. Summerfield, "Heat Transfer to Water at High Flux Densities With and Without Surface Boiling," Trans ASME 71, 805-815 (1949).

27. F. C. Gunther, "Photographic Study of Surface-Boiling Heat Transfer to Water With Forced Convection," Trans ASME 73, 115-123 (1951).

28. W. H. McAdams et al., "Heat Transfer at High Rates to Water with Surface Boiling," Ind Eng Chem 41, 1945-1953 (1949).

29. W. M. Rohsenow and J. A. Clark, "A Study of the Mechanism of Boiling Heat Transfer," Trans ASME 73, 609-620 (1951).

30. F. D. Moore and R. B. Mesler, "The Measurement of Rapid Surface Temperature Fluctuations During Nucleate Boiling of Water," AIChE Journal 7, 620-624 (1961).

31. S. G. Bankoff, "A Note on Latent Heat Transport in Nucleate Boiling," AIChE Journal 8, 63-65 (1962).

32. R. F. Gaertner, "Photographic Study of Nucleate Pool Boiling on a Horizontal Surface," Journal of Heat Transfer, Trans ASME, Series C, 84, 17-29 (1965).

33. C. J. Rallis and H. H. Jawurek, "Latent Heat Transport in Saturated Nucleate Boiling," Int J Heat Mass Transfer 7, 1051-1068 (1964).

34. H. K. Forster and N. Zuber, "Dynamics of Vapor Bubbles and Boiling Heat Transfer," AIChE Journal 1, 531-535 (1955).

35. Y. P. Chang, "A Theoretical Analysis of Heat Transfer in Natural Convection and Boiling," Trans ASME 79, 1501-1513 (1957).

36. C. H. Gilmour, "Nucleate Boiling--A Correlation," Chem Eng Prog 54, No. 10, 77-79 (1958).

37. S. Levy, "Generalized Correlation of Boiling Heat Transfer," Journal of Heat Transfer, Trans ASME, Series C, 81, 37 ff. (1959).

38. Y. P. Chang and N. W. Snyder, "Heat Transfer in Saturated Boiling," Chem Eng Prog Symposium Series No. 30 56, 25-38 (1960).

39. K. E. Forster and R. Greif, "Heat Transfer to a Boiling Liquid--Mechanism and Correlations," Journal of Heat Transfer, Trans ASME, Series C, 81, 43-53 (1959).

40. S. G. Bankoff, "On the Mechanism of Subcooled Nucleate Boiling," Chem Eng Prog Symposium Series No. 32 57, 156-172 (1961).

41. A. E. Bergles and W. M. Rohsenow, "The Determination of Forced-Convection Surface-Boiling Heat Transfer," Journal of Heat Transfer, Trans ASME, Series C, 86, 365-372 (1964).

42. E. E. Duke and V. E. Schrock, "Void Volume, Site Density and Bubble Size for Subcooled Nucleate Pool Boiling," Heat Transfer and Fluid Mechanics Institute, Stanford, Calif.: Stanford University Press, 1961. 130-145.

43. P. Grassmann and I. J. Hauser, "Heat Transfer from Wire to Subcooled and Boiling Water," Int J Heat Mass Transfer 7, 211-214 (1964).

44. M. W. Rosenthal, "An Experimental Study of Transient Boiling," Nuclear Science and Engineering 2, 640-656 (1957).

45. H. Lurie and H. A. Johnson, "Transient Pool Boiling of Water on a Vertical Surface With a Step in Heat Generation," Journal of Heat Transfer, Trans ASME, Series C, 84, 217-224 (1962).

46. L. Bernath, "A Theory of Local-Boiling Burnout and Its Application to Existing Data," Chem Eng Prog Symposium Series No. 30 56, 95-116 (1960).

47. Reference 9, p. 148.

48. Reference 6, p. 414.

49. N. Zuber, M. Tribus and J. W. Westwater, "The Hydrodynamic Crisis in Pool Boiling of Saturated and Subcooled Liquids," International Developments in Heat Transfer, Part II, New York: The American Society of Mechanical Engineers, 1961. 230-236.

50. R. D. Enyeart, "Testing Versus Quality Versus Production," Proceedings of the Seventh Annual Conference of the Society of Vacuum Coaters, 5-6 March 1964, 27-34.

51. N. K. Hearn, personal communication.

52. Reference 18, Chapter V, pp. 141-168.

53. Reference 18, p. 178.

54. "How To" Suggestions for Thin Film Deposition, Pamphlet of the Sloan Instruments Corp., Santa Barbara, Calif., 1965, 4 pages.

55. H. S. Carslaw and J. C. Jaeger, Conduction of Heat in Solids, 2nd ed., Oxford: The Clarendon Press, 1959. Chapter 12, 297-326.

56. Reference 4, p. 268.

57. Reference 55, Appendix II, pp. 482-487.

58. Reference 6, pp. 153-156.

59. Reference 4, pp. 383-385.

60. S. T. Hsu and F. W. Schmidt, "Measured Variations in Local Surface Temperatures in Pool Boiling of Water," Journal of Heat Transfer, Trans ASME, Series C, 83, 254-260 (1961).

61. Reference 55, pp. 64-66.

62. G. M. Murphy, Ordinary Differential Equations and Their Solutions, Princeton: D. Van Nostrand Company, Inc., 1960. p. 84.

63. J. D. Fleming, Fused Silica Manual, TID-21312, Georgia Institute of Technology, Engineering Experiment Station, Atlanta, September 1964.

64. Reference 55, p. 63.

VITA

Steve Herren Bomar, Jr. was born December 6, 1936 in Atlanta, Georgia. He attended the public schools of Atlanta, and entered the Georgia Institute of Technology in 1955. In 1959 he was awarded the degree Bachelor of Chemical Engineering and commissioned a Second Lieutenant in the U. S. Army Reserve.

Following graduation, he enrolled in the Graduate Division of the Georgia Institute of Technology and became a Research Assistant at the Engineering Experiment Station of Georgia Tech. In 1961 he was awarded the degree Master of Science in Chemical Engineering.

In 1959 he married Miss Sandra Kay Badger. They have two daughters, Karen Sandra and Jane Marie.

In 1965 he entered active duty in the U. S. Army for two years. He was stationed at Frankford Arsenal in Philadelphia, Pennsylvania, and assigned there to the Pitman-Dunn Research Laboratories as a Chemical Engineer. He attained the rank of Captain while on active duty.